UC San Diego

UC San Diego Electronic Theses and Dissertations

Title

Astrocytic Glypican 5 in the Synaptic Maturation and Stabilization of the Primary Visual Cortex

Permalink

https://escholarship.org/uc/item/1fd731fg

Author

Bosworth, Alexandra

Publication Date

2021

Peer reviewed|Thesis/dissertation

eScholarship.org Powered by the California Digital Library
University of California

UNIVERSITY OF CALIFORNIA SAN DIEGO

Astrocytic Glypican 5 in the Synaptic Maturation and Stabilization of the Primary Visual Cortex

A dissertation submitted in partial satisfaction of the requirements for the degree Doctor of Philosophy

in

Neurosciences

by

Alexandra Paige Bosworth

Committee in Charge:

Professor Nicola Allen, Chair
Professor Gentry Patrick, Co-Chair
Professor Ed Callaway
Professor Stacy Glasgow
Professor Jeffrey Isaacson
Professor Axel Nimmerjahn

2021

Copyright

Alexandra Paige Bosworth, 2021

All rights reserved.

The dissertation of Alexandra Paige Bosworth is approved, and it is acceptable in quality and form for publication on microfilm and electronically.

University of California San Diego

2021

DEDICATION

This dissertation is dedicated to my grandfather Rodger Ewy, who helped me with my first experiments and inspired me with his beautiful imaging techniques.

TABLE OF CONTENTS

LIST OF ABBREVIATIONS

AMPAR	AMPA-type glutamate receptor
cKO	Conditional knock out
EM	Electron microscopy
FISH	Fluorescent in situ hybridization
GluA	AMPA-type glutamate receptor subunit
Gpc	Glypican
IHC	Immunohistochemistry
L	Layer
MD	Monocular deprivation
ME	Monocular enucleation
OD	Ocular dominance
P	Postnatal
V1b	Binocular zone of primary visual cortex
vGluT	Vesicular glutamate transporter
WT	Wildtype

LIST OF FIGURES

ACKNOWLEDGEMENTS

I would like to acknowledge Professor Nicola Allen for her support as the chair of my committee and as a wonderful mentor. It has been an honor to work under such a brilliant and rigorous scientist. I am also grateful for everyone in my lab, both current and past members, for all of their assistance and patience over the years.

I would also like to thank Sammy Weiser Novak and Uri Manor in the Waitt Biophotonics core for their advice and assistance with experiments.

Chapters 1-5, in part, are currently being prepared for submission for publication of the material. Bosworth, AP, Weiser Novak, S, Manor, U, Allen NJ. Astrocytic glypican 5 in the synaptic maturation and stabilization of the primary visual cortex. The dissertation author was the primary investigator and author of this material.

Chapter 1 contains a published figure from Bosworth AP, Allen NJ. The diverse actions of astrocytes during synaptic development. Current Opinions in Neurobiology. 2017 Dec. 47:38-43. The dissertation author was the primary author of this material.

VITA

2015 Bachelor of Science, University of Washington

2021 Doctor of Philosophy, University of California San Diego

PUBLICATIONS

Bosworth AP, Weiser Novak S, Manor U, Allen NJ. Astrocytic glypican 5 in the synaptic maturation and stabilization of the primary visual cortex. *In preparation*

Bosworth AP, Allen NJ. The diverse actions of astrocytes during synaptic development. *Current Opinions in Neurobiology*. 2017 Dec. 47:38-43

FIELDS OF STUDY

Major Field: Neuroscience

Studies in astrocyte biology
Professor Nicola Allen

ABSTRACT OF DISSERTATION

Astrocytic Glypican 5 in the Synaptic Maturation and Stabilization of the Primary Visual Cortex

by

Alexandra Paige Bosworth

Doctor of Philosophy in Neurosciences

University of California San Diego, 2021

Professor Nicola Allen, Chair

Professor Gentry Patrick, Co-chair

The establishment and stabilization of proper synaptic connections is a vital step in the maturation of cortical circuits. The prevention of these processes can lead to downstream developmental delays and unstable connections in the adult. We show that astrocyte expressed glypican 5 (Gpc5) is necessary for the refinement and strengthening of thalamocortical synapses

in the mouse primary visual cortex binocular zone (V1b) during the critical period. Using electron microscopy, we show that in the absence of Gpc5, thalamocortical synapses show distinct structural immaturity, including smaller boutons and weaker synapses during the critical period. This structural immaturity is accompanied by a delay in the developmental incorporation of GluA2-containing calcium impermeable AMPARs at intracortical synapses, as observed using immunohistochemistry. Upon reaching adulthood, mice lacking astrocytic Gpc5 demonstrate intact synaptic composition but exhibit increased levels of ocular dominance plasticity, potentially as a result of destabilized thalamocortical synapses. The work in this thesis suggests that astrocytic Gpc5 is necessary for the stabilization of thalamocortical terminals during development and in the adult.

1 Introduction

1.1 Introduction

The central nervous system is often divided into two main cell types, electrically excitable neurons, and the rest, collectively referred to as glia ('glue', in Greek). Within the label glia, there exists an incredibly diverse group of cells including astrocytes, oligodendrocytes, and macrophages, all of which are necessary for the support and function of neurons. While once ignored as "glue", astrocytes have come to be known as essential for both the structure and connectivity of the central nervous system. Through tiling of the brain, astrocytes are optimally positioned to provide both metabolic support to neurons and maintain the extracellular environment to facilitate synaptic transmission (Bélanger et al., 2011; Sofroniew & Vinters, 2010). They do this by transporting nutrients across the blood brain barrier, supporting neuronal metabolic needs, and buffering the ionic concentration of the extracellular space, allowing neurons to maintain the electrochemical gradient necessary for synaptic signaling (Figure 1.1). Through physical ensheathment of synapses, astrocytes can also play a direct role in the duration of synaptic transmission and the necessary electrochemical gradient (Papouin et al., 2017). For many years, it was believed that the only role of astrocytes was to perform these homeostatic functions, facilitating the synaptic communication of neurons. Astrocyte formation and maturation parallels the timing of synaptic formation and maturation which temporally places them to be involved in these processes (Perez-Catalan et al., 2021; Ullian et al., 2001). The discovery that astrocytes alone are sufficient to induce synapse formation in vitro began a new field of research focused on how astrocytes are able to actually shape synaptic connectivity (Ullian et al., 2001). The complex role that astrocytes play in the central nervous system as well as their impressive spatial heterogeneity has left many unanswered questions regarding the extent of astrocytic involvement

in synaptic for and function. The goal of this dissertation is to add to the body of knowledge regarding how astrocytes are able to regulate synaptic connectivity within the central nervous system.

1.2 Astrocytes: Synaptic form and function

Excitatory synapses within the central nervous system, are predominantly glutamatergic, containing ionotropic α-amino-3-hydroxy-5-methyl-4-isoxazole propionic acid (AMPA), N-methyl-D-aspartate (NMDA), and kainate type glutamate receptors. Multiple astrocytic factors have been identified which regulate the structure of these synapses as well as the presence and composition of the glutamatergic receptors (Figure 1.2) (Allen, 2013). Astrocytic factors have been shown to be sufficient to regulate the structural formation of glutamatergic synapses (Kucukdereli et al., 2011; Singh et al., 2016a). Astrocytes can induce the clustering of both AMPA (Gpc4/6, tumor necrosis factor-α) and NMDA (activity dependent neurotrophic factor) receptors (Allen et al., 2012; Beattie et al., 2002; Blondel et al., 2000; Chung et al., 2015). They are also involved in the stabilization and maintenance of AMPARs at the synapses, through factors such as chordin like 1 (Chrdl1) and chondroitin sulfate proteoglycans (CSPGs) (Blanco-Suarez et al., 2018; Pyka et al., 2011). Aside from regulating the formation and maintenance of synapses, astrocytes have also been implicated in synaptic pruning and refinement via factors such as the secreted transforming growth factor-β3 which triggers the classical complement cascade (Bialas & Stevens, 2013; Schafer & Stevens, 2013). These examples demonstrate that astrocytes are involved with regulating every aspect of synaptic form and function within the central nervous system. It is also important to point out that the action of astrocytes can be restricted to a single area or subset of synapses. For example, the loss of astrocyte-secreted hevin in the visual cortex leads to a loss of thalamocortical synapses but not intracortical synapses (Singh et al., 2016b).

Through the spatial heterogeneity of astrocytic and neuronal protein expression, synaptic circuits can be independently regulated to establish the complex connectivity necessary for normal brain function.

1.3 Astrocytes and plasticity in the visual cortex

It has been well established that astrocytes are necessary for the establishment and maintenance of synaptic connectivity as demonstrated by the examples above. However, the role of astrocytes extends beyond this, as they are also involved in the modification of synapses during learning and experience dependent plasticity. Plasticity within the central nervous system is integral for the formation of cortical circuits during development as well as for learning and memory processes later in life. In the visual cortex, following eye opening, there is a critical period during which experience dependent plasticity is greatly enhanced prior to the maturation of GABAergic circuits and the establishment of perineuronal nets (PNNs) (Coleman et al., 2009; Cooke & Bear, 2014; Fawcett et al., 2019). This period is classically defined as the time during which neurons undergo a shift in ocular dominance following monocular deprivation (Coleman et al., 2009; Espinosa & Stryker, 2012). After this critical period, plasticity is greatly reduced in the adult. The role of astrocytes in visual plasticity is as complex as their role in synaptic formation and function. Astrocyte involvement in visual cortex plasticity was first observed when it was discovered that the implantation of cultured astrocytes into an aged animal was sufficient to reactivate juvenile-like plasticity (CM Müller & J Best, 1989). Ongoing research has discovered that astrocytes secreted factors, such as hevin and SPARC, are necessary for normal plasticity during the critical period (Singh et al., 2016b). Astrocytes are also involved in the closure of the critical period through CSPGs, which are part of PNNs which restrict plasticity through stabilizing AMPARs at the synapse (Céleste-É et al., n.d.; Fawcett et al., 2019). As evidenced by these

examples, it is clear that astrocytes are necessary for the processes of bidirectional plasticity underlying circuit formation and modification.

1.4 Glypicans

Glypicans are a family of heparan sulfate proteoglycans, expressed in the brain and periphery throughout development and adulthood, which were originally identified as regulators of growth factor signaling, and more recently as regulators of synaptic formation and function. These factors are expressed by multiple cell types, including astrocytes, neurons, and oligodendrocyte precursors (Cahoy et al., 2008). They are bound to the plasma membrane via glycosyl-phoshtidylinositol (GPI) anchors which can be released from the cell surface by lipases or endoprotelytic cleavage (Filmus et al., 2008). There are 6 mammalian glypicans (Gpc1-6) which can be divided into two broad groups based upon sequence homology and conservation across species (Filmus et al., 2008; Song & Filmus, 2008). Within the developing brain, expression of Gpc4, 5 and 6 are enriched in cortical astrocytes compared to other cell types, and the three glypicans have distinct temporal expression profiles (Cahoy et al., 2008; Farhy-Tselnicker et al., 2021). Astrocytic Gpc4 and Gpc6 have been shown to be synaptogenic during normal development via inducing nascent synapses containing GluA1 AMPA receptors, correlating with their timing of expression (Allen et al., 2012; Farhy-Tselnicker et al., 2017). Neuronal Gpc4 has also been shown to be synaptogenic, via interactions with the transsynaptic adhesion protein LRRTM4 (Siddiqui et al. 2013). Within humans, glypicans have been implicated in multiple neurological disorders including autism (Gpc4,6), schizophrenia (Gpc4,5,6), Sanfillipo syndrome type B (Gpc5), and Alzheimer's disease (Gpc5) (Gandal et al., 2018; Grubman et al., 2019; Irie et al., 2012; Lau et al., 2020; Potkin et al., 2010; Wang et al., 2012). The involvement of glypicans in these disorders, which all contain some aspect of aberrant

glutamatergic signaling, fits with their known role in the establishment and maintenance of excitatory connectivity. Expression of astrocytic Gpc4 and 6 peaks early during development at P7 and P14 respectively, while Gpc5 expression increases at P14-P28, and remains high through adulthood (Figure 1.4 B&C) (Cahoy et al., 2008; Farhy-Tselnicker et al., 2021). The developmental period during which Gpc5 expression is increased is a time of robust synaptic maturation and refinement as cortical circuits are established during the visual critical period. The timing of Gpc5 expression therefore suggests that it may be involved in the organization of these circuits, as well as their maintenance in the adult.

1.5 Astrocytic Glypican 5

In this dissertation I investigate the role of astrocyte expressed Gpc5 in regulating synaptic properties in the mouse visual cortex. To do this I first investigated when and where Gpc5 is expressed, and then developed a genetic mouse model to specifically remove Gpc5 from astrocytes, which is used in the majority of experiments in subsequent chapters. Previous studies using RNA sequencing have demonstrated that in the mouse cortex, Gpc5 mRNA expression is enriched in both astrocytes and OPCs compared to other cell types, including neurons and microglia (Zhang et al., 2014). Expression of Gpc5 by cortical astrocytes is upregulated between P7 and P14, near the time of eye opening, and remains highly expressed throughout adulthood (P28 and P120) (Figure 1.4 B). This expression pattern is in contrast to other astrocyte-expressed glypican family members, Gpc4 and Gpc6, which peak in expression at P7 and P14 respectively and then decline (Figure 1.4 C) (Farhy-Tselnicker et al., 2021). Additionally, the level of Gpc5 mRNA detected in astrocytes is ~10-fold higher than either Gpc4 or Gpc6 at the peak of expression (Figure 1.4 B&C), demonstrating Gpc5 is the predominant glypican family member expressed by astrocytes. Spatial analysis of Gpc5 mRNA in V1b using single molecule fluorescent

in situ hybridization (smFISH) has demonstrated that Gpc5 is expressed at comparable levels by astrocytes across cortical layers 1-6 throughout postnatal development, showing homogeneous expression (Figure 1.4 A) (Farhy-Tselnicker et al., 2021). Based on the temporal expression of Gpc5 – upregulated at P14 and remaining high into adulthood, and the known role of other glypican family members in regulating synaptic development, we hypothesized that Gpc5 plays a role in regulating synaptic maturation and/or stability.

To ask how astrocyte-expressed Gpc5 regulates synapses we developed an astrocyte-specific Gpc5 knock out line by crossing floxed-Gpc5 mice (Gpc5tm1c(KOMP)Wtsi) to an astrocyte specific GFAP cre recombinase line (B6.Cg-Tg(Gfap-cre)73.12Mvs/J), and compared Gpc5fl/fl cre negative (WT) and Gpc5fl/fl cre positive (cKO) littermate pairs for all experiments.

To determine if Gpc5 expression, in the cKO line, has been reduced specifically in astrocytes across layers 1-6, we used smFISH (RNAscope). The V1b of WT and cKO littermate pairs at P28 was probed for Gpc5 mRNA, along with an astrocyte probe, Glast (Slc1a3), and an OPC probe, Cspg4 (Figure 1.5). Gpc5 expression was analyzed within the boundary of Glast and Cspg4 positive cells. As previously demonstrated, in WT mice we detected widespread expression of Gpc5 throughout V1b, with Gpc5 expressed in both astrocytes and OPCs as shown by colocalization with the respective cell markers (Fraction of each cell type expressing Gpc5 ± SEM: astrocytes=0.93 ± 0.02; OPCs=0.97 ± 0.004) (Figure 1.4 D). In cKO mice, Gpc5 expression is significantly decreased in astrocytes (Threshold area (μm^2) ± SEM, WT=5.51 ± 0.3, cKO=1.96 ± 0.2, p=0.0001) but not OPCs (Threshold area (μm^2) ± SEM, WT=6.09 ± 0.9, cKO=4.97 ± 0.8, p=0.34), demonstrating the specificity of the approach (Figure 1.5). cKO mice retain a significant amount of Gpc5 due to OPC expression (Threshold area (μm^2) norm to WT, WT=1, cKO=0.43 ± 0.03) (Figure 1.4 E). Additionally, we asked whether there is a compensatory response in

astrocytes to knocking out Gpc5 by probing for two other astrocyte-expressed glypicans, Gpc4 and Gpc6. Gpc4 and Gpc6 expression were analyzed within the boundary of Glast positive cells in WT and cKO littermates and showed no significant change for either Gpc4 (Threshold area (μm^2) ± SEM, WT=1.32 ± 0.055, cKO=1.26 ± 0.12, p=0.66) or Gpc6 (Threshold area (μm^2) ± SEM, WT=1.82 ± 0.095, cKO=1.63 ± 0.11, p=0.32) expression (Figure 1.6). This shows that Gpc5 is enriched in glial cells in the mouse visual cortex, and that removing Gpc5 from astrocytes does not cause a compensatory upregulation of Gpc5 in OPCs or Gpc4 and Gpc6 in astrocytes. Utilizing this Gpc5 cKO, we analyzed V1b at two different time points with high Gpc5 expression. We analyzed P28, a period of synaptic and astrocytic maturation during the critical period, as well as P120, when synaptic connectivity is stable and there is minimal baseline plasticity. We focused our study on cortical layers 1 through 4, characterizing both intracortical and thalamocortical connectivity.

Throughout this dissertation, we investigated the role of astrocytic Gpc5 in the maturation of synapses within the primary visual cortex during the critical period and in the adult. Utilizing immunohistochemistry, we found that the absence of Gpc5 delays the incorporation of GluA2 at intracortical synapses rendering these synapses more immature during the critical period. Using serial section electron microscopy, we found that thalamocortical synapses are also structurally immature and less refined during the critical period. Further, in mice lacking astrocyte Gpc5 we found an increase in plasticity in response to a visual deprivation assay in adulthood, but not during the critical period, suggesting Gpc5 as a plasticity restricting factor in adult mice. This data identifies astrocytic Gpc5 as a regulator of synaptic maturation and plasticity, distinct from glypicans 4&6 which regulate synapse initiation, showing diverse roles for these family members in cortical circuit development.

1.6 Methods

Mice: Mice were housed with a 12 hour light/dark cycle in the Salk Institute animal facilities. Mice were provided access to food and water ad libitum. Mice of both genders were used in experiments.

Astrocyte specific Glypican 5 knock out mice: In order to selectively remove Gpc5 from astrocytes, homozygous Gpc5 floxed mice were crossed to the astrocyte specific GFAP cre recombinase line, B6.Cg-Tg(Gfap-cre)73.12Mvs/J (Jax stock number 012886). Gpc5 floxed mice were generated by KOMP/MMRRC/EUCOMM as conditional ready mice. Gpc5 strain was received as the tm1a allele (C57BL/6N-Atm1Brd Gpc5tm1a(KOMP)Wtsi, MMRRC Stock #: 047921-UCD) and crossed with mice expressing the Flp recombinase (B6.129S4-Gt(ROSA)26Sortm1(FLP1)Dym/RainJ, Jax stock number 009086) to generate Gpc5tm1c(KOMP)Wtsi (UC Davis KOMP repository, project ID CSD76974) in which exon 3 is floxed. Upon exposure to cre recombinase, exon 3 is excised, causing a frameshift and premature stop codon, leading to a nonsense mediated decay of the mRNA. All experiments were performed using cre negative WT and cre positive cKO littermate pairs. Mice of both genders were used.

Characterization of glypican 5 conditional knockout

Tissue Collection and Preparation: Mice were anesthetized with an intraperitoneal injection of 100mg/kg Ketamine (Victor Medical Company) and 20 mg/kg Xylazine (Anased) prior to intracardial perfusion. For the collection of fresh frozen tissue used for *in situ* hybridization experiments, mice were transcardially perfused with 10 mls PBS. Collected brains were embedded in OCT (Scigen 4583), frozen in dry ice/ethanol, and stored at -80°C.

Fluorescent *in situ* hybridization: Littermate mice (GFAP Cre x Gpc5 fl/fl WT and KO) were used at age P28 to analyze Gpc5 expression patterns. Fresh frozen, 18 µm coronal sections (3.4

mm posterior to Bregma) were collected using a cryostat (Hacker Industries OTF5000). Fluorescent (FISH) (ACDbio 320850) *in situ* hybridization was performed following manufacturer's instructions for fresh frozen tissue. Slides were briefly frozen at -20C for 20 minutes, followed by 15 minutes in PFA at 4C. Sections then underwent dehydration via 5 minute washes in 50%, 75%, and 100% (x2) ethanol. Following dehydration, sections were incubated with Protease 3 (P28) or Protease 4 (P120) for 15 minutes at room temperature and then washed 2 times in PBS. Slides were incubated with target probes for 2 hours at 40C followed by 3 amplification steps and 1 detection step with RNAscope wash buffer rinses between each step. Sections were mounted with SlowFade gold antifade with DAPI (ThermoFisher Scientific S36939) and applied coverslip (22 mm x 50 mm, 1.5 thickness) was sealed with clear nail polish. Slides were imaged within 1 day or stored at -20C.

Probes used were Gpc4 (ACDbio 442821), Gpc5 (ACDbio 442831), Gpc6 (ACDbio 453301), Slc1a3/GLAST (ACDBio 430781-C2), CSPG4 (ACDbio 404131-C3). A negative 3-plex probe (ACDbio 320871) was used to determine background signal.

Imaging: Probes Gpc4, Gpc5, and Gpc6 were imaged in channel 550, Slc1a3/GLAST was imaged in channel 488, and CSPG4 was imaged in channel 647. In all experiments, a minimum of 5 littermate pairs and 3 sections per animal were imaged. Layer I-VI of the visual cortex were imaged at 20X on Zeiss LSM710 confocal microscope at a resolution of 2048x2048 pixels as 2 µm z-stacks (3 slices). Representative images are maximum intensity projections of the z-stack.

Analysis: Quantification of FISH signal was done using a custom ImageJ macro. Images were made into maximum intensity projections, and layer I-VI was manually cropped out. Astrocytes were identified by the Slc1a3/GLAST signal and OPCs were identified by the CSPG4 signal. An ROI was drawn around the cell body using the Slc1a3/GLAST or CSPG4 signal and the probe of

interest was thresholded consistently across all images. The thresholded area was recorded for each defined ROI. ROIs with no thresholded glypican signal were considered non expressing cells. Total glypican expression was calculated as total glypican 5 thresholded are relative to total ROI area. 5 mice/condition included. Statistics by T-test.

1.7 Acknowledgements

This chapter, in part, is currently being prepared for submission for publication of the material. Bosworth, AP, Weiser Novak, S, Manor, U, Allen NJ. Astrocytic glypican 5 in the synaptic maturation and stabilization of the primary visual cortex. The dissertation author was the primary investigator and author of this material.

Figure 1.2 from Bosworth AP, Allen NJ. The diverse actions of astrocytes during synaptic development. *Current Opinions in Neurobiology*. 2017 Dec. 47:38-43

Figure 1.3 B&C contains data previously published in Farhy-Tselnicker, I., Boisvert, M. M., Liu, H., Dowling, C., Erikson, G. A., Blanco-Suarez, E., Farhy, C., Shokhirev, M. N., Ecker, J. R., & Allen, N. J. (2021). Activity-dependent modulation of synapse-regulating genes in astrocytes. *ELife*, 10. https://doi.org/10.7554/ELIFE.70514.

1.8 Figures

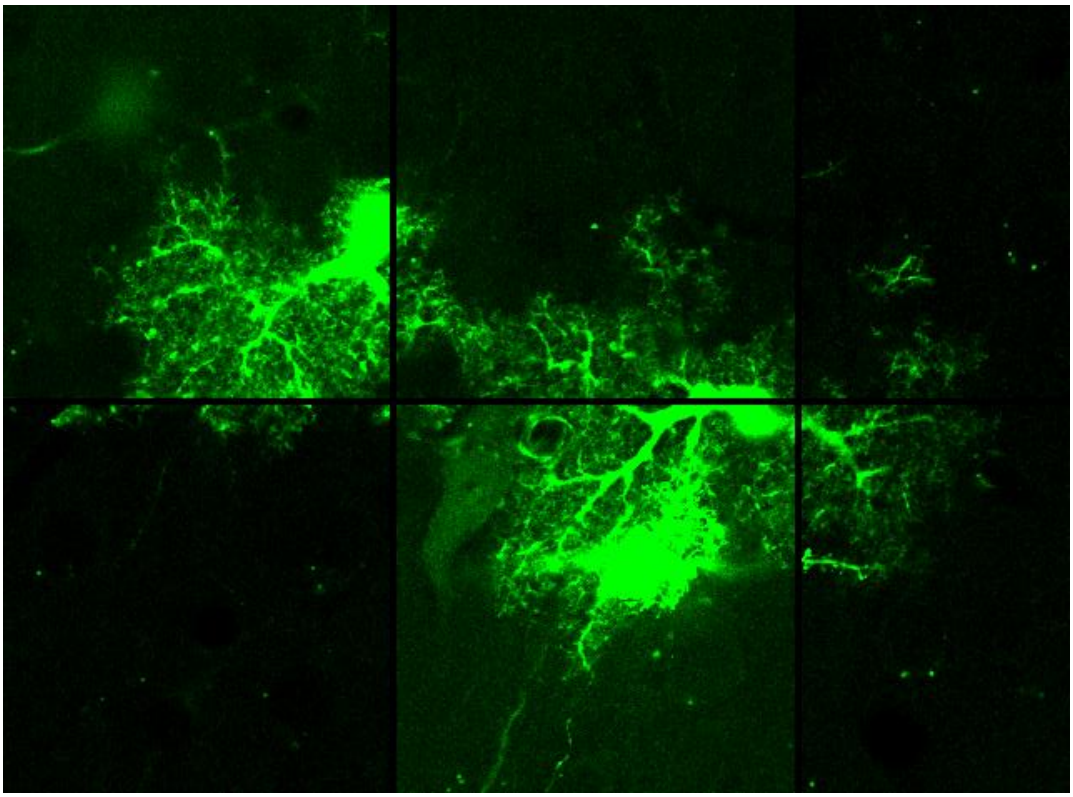

Figure 1.1: Image of cortical astrocytes. Cortical astrocytes in V1b. Astrocyte filled with AF488

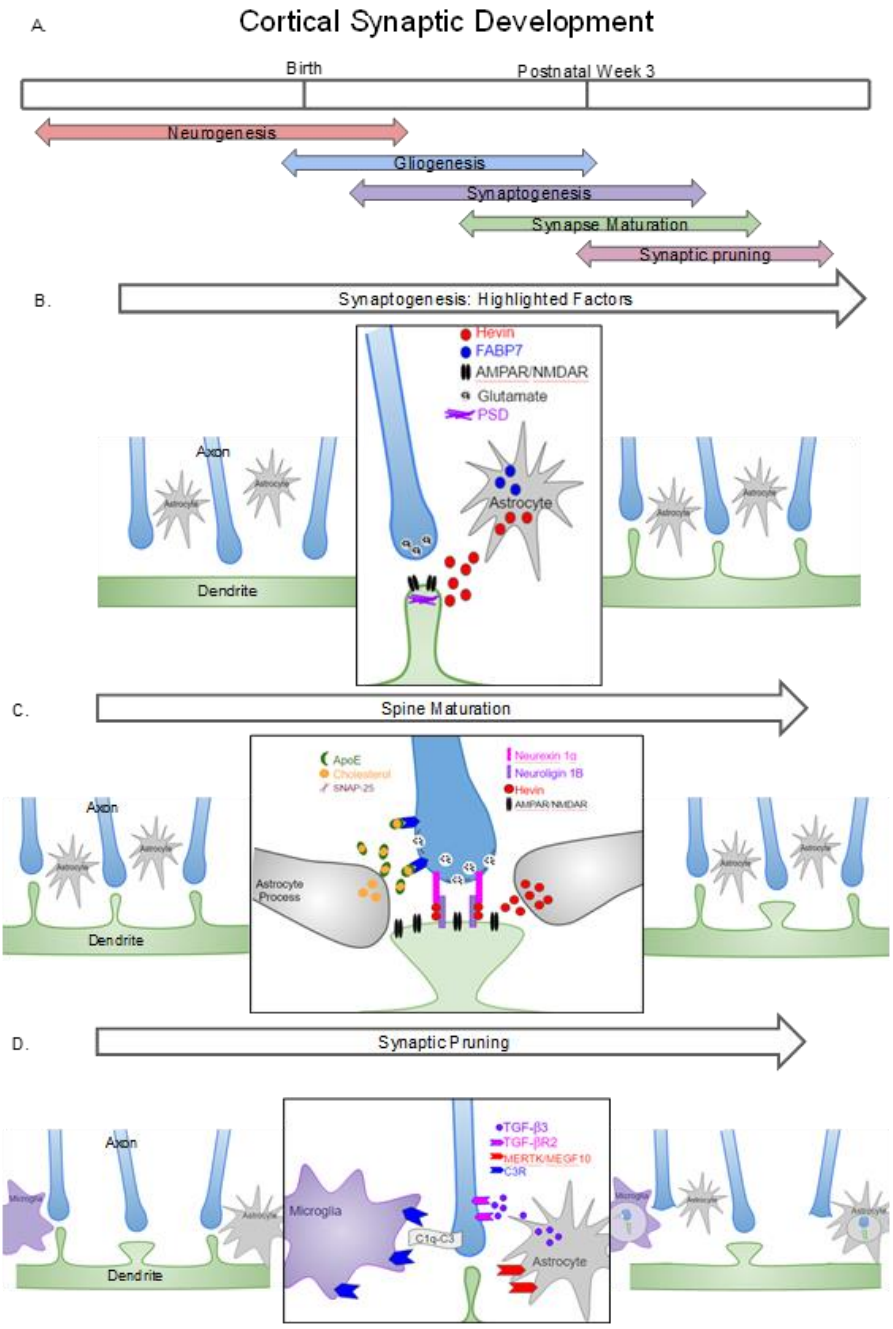

Figure 1.2: Schematic of astrocyte action during cortical development. **A.** Schematic of mouse cortical development. **B.** Astrocytes during synaptogenesis. **C.** Astrocytes during synaptic maturation**. D.** Astrocytes during synaptic pruning. Figure from: **Bosworth AP**, Allen NJ. The diverse actions of astrocytes during synaptic development. *Current Opinions in Neurobiology*. 2017 Dec. 47:38-43

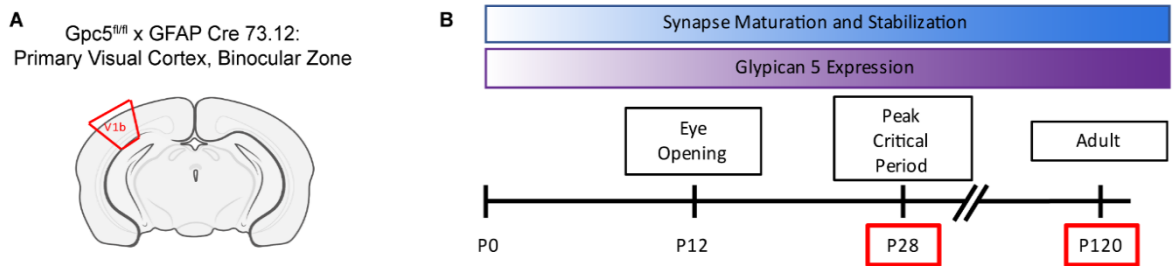

Figure 1.3: Schematic of Experimental Outline. **A.** Schematic of mouse coronal brain slice indicating the binocular zone of the primary cortex which is the focus of this study. Also included in this genetic cross that was used to create an astrocyte specific Gpc5 cKO mouse. **B.** Timeline of experimental design. Synapse maturation and stabilization occur during the period in which Gpc5 expression is upregulated. Timepoints P28 and P120 were selected as periods of enriched astrocytic Gpc5 expression.

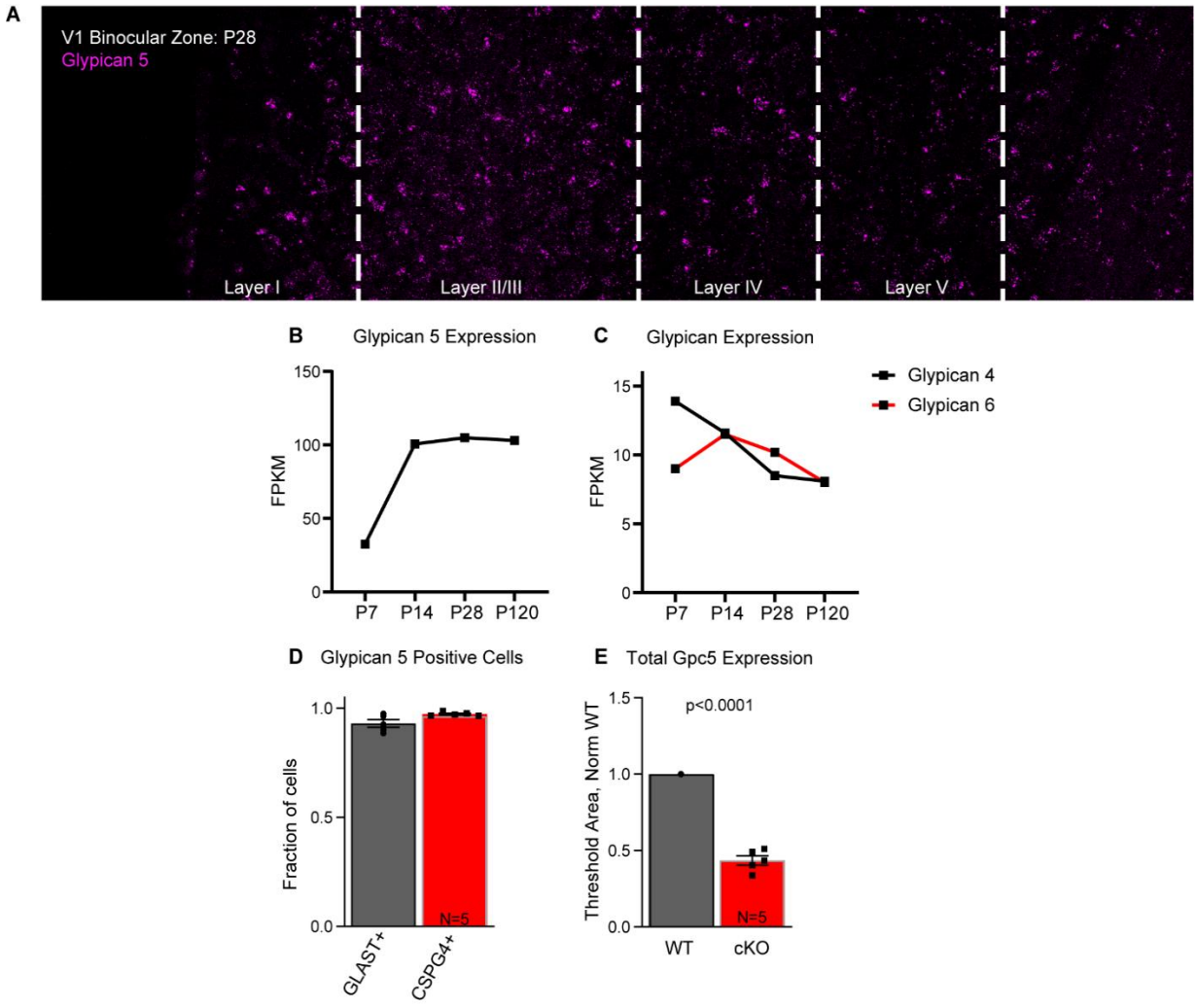

Figure 1.4: Glypican 5 expression throughout V1b. Glypican 5 is expressed uniformly throughout LI-VI in V1b. **A.** Representative image of WT Gpc5 expression as shown via FISH. **B.** Astrocytic glypican 5 expression peaks between P7-P14. Astrocytic glypican 5 expression timeline. Adapted from Farhy-Tselnicker et al. 2021. **C.** Astrocytic glypican 4 and 6 expression timelines. Adapted from Farhy-Tselnicker et al. 2021. **D.** Glypican 5 is expressed by the majority of astrocytes and OPCs within V1b at P28. Quantification of Figure 1D. **E.** Total glypican 5 expression is decreased by 57% in Gpc5 cKO mice. Normalized to WT expression. N=5 mice/condition. Graphs show mean ± SEM. Individual data points representing mice. Statistics by T-test, significance stated on graph.

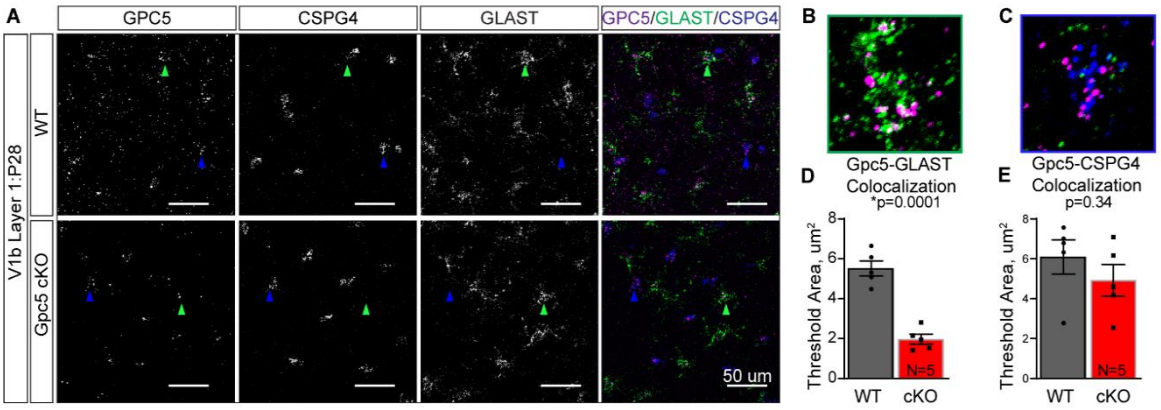

Figure 1.5: Characterization of astrocyte specific Gpc5 cKO mice. Fluorescent *in situ* hybridization to determine the specific removal of Gpc5 from astrocytes but not OPCs. **A.** Representative images of WT and Gpc5 cKO P28 layer 1 V1b Gpc5 expression. Left panel, Gpc5 expression, middle panels, cell marker expression, right panel, merge-Gpc5 (magenta), astrocytes (green), OPCs (blue). **B.** Representative image of Gpc5 and Glast colocalization. **C.** Representative image of Gpc5 and Cspg4 colocalization. **D.** Gpc5 expression is decreased in astrocytes in Gpc5 cKO mice. Quantification of A. Expression of Gpc5 in Glast positive cells. **E.** Gpc5 expression is unchanged in OPCs in cKO mice. Quantification of A. Expression of Gpc5 in Cspg4 positive cells. Scale bar in A: 50µM. N=5 mice/condition. Graphs show mean ± SEM. Individual data points representing mice. Statistics by T-test, significance stated on graph.

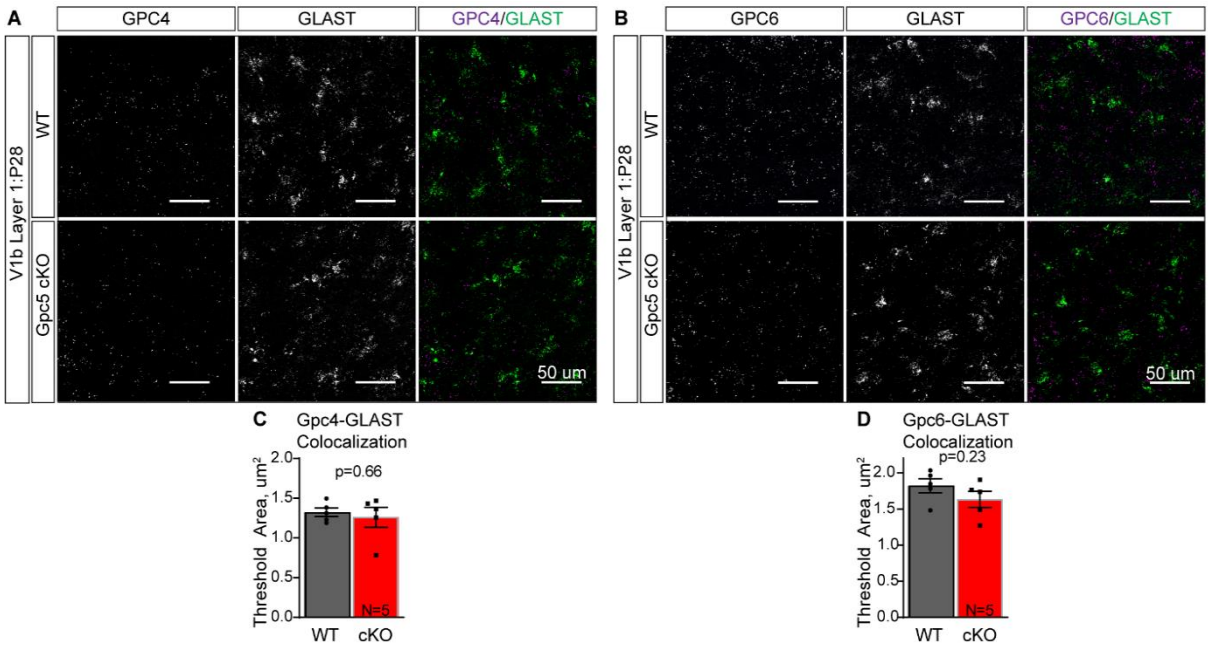

Figure 1.6: Evaluation of glypican compensation in astrocyte specific Gpc5 cKO mice. Expression of astrocyte secreted Gpc4&6 is not upregulated in Gpc5 cKO mice. **A.** Representative images of WT and cKO P28 layer 1 V1b Gpc4 expression. Left panel, Gpc4 expression, middle panel, astrocyte marker expression, right panel, merge-Gpc4(magenta), astrocytes (green). **B.** Representative Images of WT and cKO P28 layer 1 V1b Gpc6 expression. Left panel, Gpc6 expression, middle panel, astrocyte marker expression, right panel, merge-Gpc6(magenta), astrocytes (green). **C,D.** Quantification of A and B respectively. Gpc4 and Gpc6 astrocyte expression is unchanged in cKO mice. Scale bar in A,B: 50μM. N=5 mice/condition. Graphs show mean ± SEM. Individual data points representing mice. Statistics by T-test, significance stated on graph.

1.9 References

Allen, N. J. (2013). Role of glia in developmental synapse formation. In *Current Opinion in Neurobiology* (Vol. 23, Issue 6, pp. 1027–1033). https://doi.org/10.1016/j.conb.2013.06.004

Allen, N. J., Bennett, M. L., Foo, L. C., Wang, G. X., Chakraborty, C., Smith, S. J., & Barres, B. A. (2012). Astrocyte glypicans 4 and 6 promote formation of excitatory synapses via GluA1 AMPA receptors. *Nature*, *486*(7403), 410–414. https://doi.org/10.1038/nature11059

Beattie, E. C., Stellwagen, D., Morishita, W., Bresnahan, J. C., Ha, B. K., Zastrow, M. von, Beattie, M. S., & Malenka, R. C. (2002). Control of Synaptic Strength by Glial TNFα. *Science*, *295*(5563), 2282–2285. https://doi.org/10.1126/SCIENCE.1067859

Bélanger, M., Allaman, I., & Magistretti, P. J. (2011). Brain Energy Metabolism: Focus on Astrocyte-Neuron Metabolic Cooperation. *Cell Metabolism*, *14*(6), 724–738. https://doi.org/10.1016/J.CMET.2011.08.016

Bialas, A. R., & Stevens, B. (2013). TGF-Beta Signaling Regulates Neuronal C1q Expression and Developmental Synaptic Refinement. *Nature Neuroscience*, *16*(12), 1773–1782. https://doi.org/10.1038/nn.3560.TGF-

Blanco-Suarez, E., Liu, T.-F., Kopelevich, A., & Allen, N. J. (2018). Astrocyte-Secreted Chordin-like 1 Drives Synapse Maturation and Limits Plasticity by Increasing Synaptic GluA2 AMPA Receptors. *Neuron*, *100*(5), 1116-1132.e13. https://doi.org/10.1016/J.NEURON.2018.09.043

Blondel, O., Collin, C., McCarran, W. J., Zhu, S., Zamostiano, R., Gozes, I., Brenneman, D. E., & McKay, R. D. G. (2000). A Glia-Derived Signal Regulating Neuronal Differentiation. *Journal of Neuroscience*, *20*(21), 8012–8020. https://doi.org/10.1523/JNEUROSCI.20-21-08012.2000

Cahoy, J. D., Emery, B., Kaushal, A., Foo, L. C., Zamanian, J. L., Christopherson, K. S., Xing, Y., Lubischer, J. L., Krieg, P. A., Krupenko, S. A., Thompson, W. J., & Barres, B. A. (2008). *A Transcriptome Database for Astrocytes, Neurons, and Oligodendrocytes: A New Resource for Understanding Brain Development and Function.* https://doi.org/10.1523/JNEUROSCI.4178-07.2008

Céleste-É, X., Stephany, L., Ikrar, T., Nguyen, C., Xu, X., Aaron, X., & Mcgee, W. (n.d.). *Development/Plasticity/Repair Nogo Receptor 1 Confines a Disinhibitory Microcircuit to the Critical Period in Visual Cortex*. https://doi.org/10.1523/JNEUROSCI.0935-16.2016

Chung, W. S., Allen, N. J., & Eroglu, C. (2015). Astrocytes control synapse formation, function, and elimination. *Cold Spring Harbor Perspectives in Biology*, *7*(9). https://doi.org/10.1101/cshperspect.a020370

CM Müller, & J Best. (1989). Ocular dominance plasticity in adult cat visual cortex after transplantation of cultured astrocytes. *Nature*, *342*(6248), 427–430. https://doi.org/10.1038/342427A0

Coleman, J. E., Law, K., & Bear, M. F. (2009). Anatomical origins of ocular dominance in mouse primary visual cortex. *Neuroscience*, *161*(2), 561–571. https://doi.org/10.1016/j.neuroscience.2009.03.045

Cooke, S. F., & Bear, M. F. (2014). How the mechanisms of long-term synaptic potentiation and depression serve experience-dependent plasticity in primary visual cortex. *Philosophical Transactions of the Royal Society of London. Series B, Biological Sciences*, *369*(1633), 20130284. https://doi.org/10.1098/rstb.2013.0284

Espinosa, J. S., & Stryker, M. P. (2012). Development and plasticity of the primary visual cortex. *Neuron*, *75*(2), 230–249. https://doi.org/10.1016/j.neuron.2012.06.009

Farhy-Tselnicker, I., Boisvert, M. M., Liu, H., Dowling, C., Erikson, G. A., Blanco-Suarez, E., Farhy, C., Shokhirev, M. N., Ecker, J. R., & Allen, N. J. (2021). Activity-dependent modulation of synapse-regulating genes in astrocytes. *ELife*, *10*. https://doi.org/10.7554/ELIFE.70514

Farhy-Tselnicker, I., van Casteren, A. C. M., Lee, A., Chang, V. T., Aricescu, A. R., & Allen, N. J. (2017). Astrocyte-Secreted Glypican 4 Regulates Release of Neuronal Pentraxin 1 from Axons to Induce Functional Synapse Formation. *Neuron*, *96*(2), 428-445.e13. https://doi.org/10.1016/j.neuron.2017.09.053

Fawcett, J. W., Oohashi, T., & Pizzorusso, T. (2019). The roles of perineuronal nets and the perinodal extracellular matrix in neuronal function. *Nature Reviews Neuroscience 2019 20:8*, *20*(8), 451–465. https://doi.org/10.1038/s41583-019-0196-3

Filmus, J., Capurro, M., & Rast, J. (2008). Glypicans. *Genome Biology*, *9*(5), 224. https://doi.org/10.1186/gb-2008-9-5-224

Gandal, M. J., Haney, J. R., Parikshak, N. N., Leppa, V., Ramaswami, G., Hartl, C., Schork, A. J., Appadurai, V., Buil, A., Werge, T. M., Liu, C., White, K. P., Consortium, C., Consortium, P., Group, iPSYCH-B. W., Horvath, S., & Geschwind, D. H. (2018). Shared molecular neuropathology across major psychiatric disorders parallels polygenic overlap. *Science (New York, N.Y.)*, *359*(6376), 693. https://doi.org/10.1126/SCIENCE.AAD6469

Grubman, A., Chew, G., Ouyang, J. F., Sun, G., Choo, X. Y., McLean, C., Simmons, R. K., Buckberry, S., Vargas-Landin, D. B., Poppe, D., Pflueger, J., Lister, R., Rackham, O. J. L., Petretto, E., & Polo, J. M. (2019). A single-cell atlas of entorhinal cortex from individuals with Alzheimer's disease reveals cell-type-specific gene expression regulation. *Nature Neuroscience 2019 22:12*, *22*(12), 2087–2097. https://doi.org/10.1038/s41593-019-0539-4

Irie, F., Badie-Mahdavi, H., & Yamaguchi, Y. (2012). Autism-like socio-communicative deficits and stereotypies in mice lacking heparan sulfate. *Proceedings of the National Academy of Sciences of the United States of America*, *109*(13), 5052. https://doi.org/10.1073/PNAS.1117881109

Kucukdereli, H., Allen, N. J., Lee, A. T., Feng, A., Ozlu, M. I., Conatser, L. M., Chakraborty, C., Workman, G., Weaver, M., Sage, E. H., Barres, B. A., & Eroglu, C. (2011). Control of excitatory CNS synaptogenesis by astrocyte-secreted proteins hevin and SPARC. *Proceedings of the National Academy of Sciences of the United States of America*, *108*(32). https://doi.org/10.1073/PNAS.1104977108

Lau, S.-F., Cao, H., Fu, A. K. Y., & Ip, N. Y. (2020). Single-nucleus transcriptome analysis reveals dysregulation of angiogenic endothelial cells and neuroprotective glia in Alzheimer's disease. *Proceedings of the National Academy of Sciences of the United States of America*, *117*(41), 25800. https://doi.org/10.1073/PNAS.2008762117

Papouin, T., Dunphy, J., Tolman, M., Foley, J. C., & Haydon, P. G. (2017). Astrocytic control of synaptic function. *Philosophical Transactions of the Royal Society B: Biological Sciences*, *372*(1715). https://doi.org/10.1098/RSTB.2016.0154

Perez-Catalan, N. A., Doe, C. Q., & Ackerman, S. D. (2021). The role of astrocyte-mediated plasticity in neural circuit development and function. *Neural Development 2021 16:1*, *16*(1), 1–14. https://doi.org/10.1186/S13064-020-00151-9

Potkin, S. G., Macciardi, F., Guffanti, G., Wang, Q., Turner, J. A., Lakatos, A., Miles, M. F., Lander, A., Vawter, M. P., & Xie, X. (2010). Identifying Gene Regulatory Networks in Schizophrenia. *NeuroImage*, *53*(3), 839. https://doi.org/10.1016/J.NEUROIMAGE.2010.06.036

Pyka, M., Wetzel, C., Aguado, A., Geissler, M., Hatt, H., & Faissner, A. (2011). Chondroitin sulfate proteoglycans regulate astrocyte-dependent synaptogenesis and modulate synaptic activity in primary embryonic hippocampal neurons. *European Journal of Neuroscience*, *33*(12), 2187–2202. https://doi.org/10.1111/J.1460-9568.2011.07690.X

Schafer, D. P., & Stevens, B. (2013). Phagocytic glial cells: sculpting synaptic circuits in the developing nervous system. *Current Opinion in Neurobiology*, *23*(6), 1034–1040. https://doi.org/10.1016/j.conb.2013.09.012

Siddiqui, T. J., Tari, P. K., Connor, S. A., Zhang, P., Dobie, F. A., She, K., Kawabe, H., Wang, Y. T., Brose, N., & Craig, A. M. (2013). An LRRTM4-HSPG Complex Mediates Excitatory Synapse Development on Dentate Gyrus Granule Cells. *Neuron*, *79*(4), 680–695. https://doi.org/10.1016/J.NEURON.2013.06.029

Singh, S. K., Stogsdill, J. A., Pulimood, N. S., Dingsdale, H., Kim, Y. H., Pilaz, L. J., Kim, I. H., Manhaes, A. C., Rodrigues, W. S., Pamukcu, A., Enustun, E., Ertuz, Z., Scheiffele, P., Soderling, S. H., Silver, D. L., Ji, R. R., Medina, A. E., & Eroglu, C. (2016a). Astrocytes Assemble Thalamocortical Synapses by Bridging NRX1?? and NL1 via Hevin. *Cell*, *164*(1–2), 183–196. https://doi.org/10.1016/j.cell.2015.11.034

Singh, S. K., Stogsdill, J. A., Pulimood, N. S., Dingsdale, H., Kim, Y. H., Pilaz, L. J., Kim, I. H., Manhaes, A. C., Rodrigues, W. S., Pamukcu, A., Enustun, E., Ertuz, Z., Scheiffele, P., Soderling, S. H., Silver, D. L., Ji, R. R., Medina, A. E., & Eroglu, C. (2016b). Astrocytes

Assemble Thalamocortical Synapses by Bridging NRX1alpha and NL1 via Hevin. *Cell*, *164*(1–2), 183–196. https://doi.org/10.1016/j.cell.2015.11.034

Sofroniew, M. v., & Vinters, H. v. (2010). Astrocytes: biology and pathology. *Acta Neuropathologica*, *119*(1), 7. https://doi.org/10.1007/S00401-009-0619-8

Song, H. H., & Filmus, J. (2002). The role of glypicans in mammalian development. *Biochimica et Biophysica Acta (BBA) - General Subjects*, *1573*(3), 241–246. https://doi.org/10.1016/S0304-4165(02)00390-2

Ullian, E. M., Sapperstein, S. K., Christopherson, K. S., & Barres, B. a. (2001). Control of synapse number by glia. *Science (New York, N.Y.)*, *291*(5504), 657–661. https://doi.org/10.1126/science.291.5504.657

Wang, K.-S., Zhang, Q., Liu, X., Wu, L., & Zeng, M. (2012). PKNOX2 is Associated with Formal Thought Disorder in Schizophrenia: a Meta-Analysis of Two Genome-wide Association Studies. *Journal of Molecular Neuroscience 2012 48:1*, *48*(1), 265–272. https://doi.org/10.1007/S12031-012-9787-4

Zhang, Y., Chen, K., Sloan, S. A., Bennett, M. L., Scholze, A. R., O'Keeffe, S., Phatnani, H. P., Guarnieri, P., Caneda, C., Ruderisch, N., Deng, S., Liddelow, S. A., Zhang, C., Daneman, R., Maniatis, T., Barres, B. A., & Wu, J. Q. (2014). An RNA-Sequencing Transcriptome and Splicing Database of Glia, Neurons, and Vascular Cells of the Cerebral Cortex. *Journal of Neuroscience*, *34*(36), 11929–11947. https://doi.org/10.1523/JNEUROSCI.1860-14.2014

2 Glypican 5 and Synaptic Composition

2.1 Introduction.

The synaptic protein composition of excitatory synapses in the binocular zone of the primary visual cortex is governed by multiple factors which impact signal transduction and circuit formation. The predominant types of excitatory synapses in V1b can be broadly broken down into two classes: intracortical and thalamocortical (Nahmani & Erisir, 2005). Within V1b, intracortical synapses outnumber thalamocortical synapses. Intracortical synapses within V1b form between cortical neurons and can be found in all layers of the cortex (Fremeau et al., 2004). Thalamocortical synapses form between presynaptic neurons from the dLGN and pyramidal and fast spiking interneurons, primarily in L4 and L1 (Kloc & Maffei, 2014). These two groups are easily distinguishable based on the presynaptic isoform of vGluT that is expressed: intracortical synapses preferentially express vGlut1, while thalamocortical synapses express vGluT2 (Fremeau et al., 2004; Kaneko & Fujiyama, 2002; Nahmani & Erisir, 2005). Gpc5 is uniformly expressed by astrocytes across L1-5 of V1b placing it in position to act at both intracortical and thalamocortical synapses (Farhy-Tselnicker et al., 2021). Additionally, astrocyte secreted factors have been shown to act differently at thalamocortical and intracortical synapses (Blanco-Suarez et al., 2018; Singh et al., 2016). As such, in this study, we utilized the distinct expression profiles of vGluT1&2 to independently analyze intracortical and thalamocortical synapses.

Excitatory synaptic signal transduction is greatly influenced by postsynaptic receptor composition. The composition of AMPARs, the main mediators of fast excitatory transmission in the CNS, is tightly regulated by multiple factors and undergoes a developmental change in the visual cortex. Early in cortical development, AMPARs are primarily GluA1 containing tetramers

which lack GluA2 subunits (Brill & Huguenard, 2008; Kumar et al., 2002). This renders the receptors permeable to calcium and inwardly rectifying, which plays an important role in early developmental plasticity (D Bowie & ML Mayer, 1995). During development, there is a tightly controlled integration of GluA2 subunits into these receptors, and the timing of this integration is dependent upon cortical layer. In the primary visual cortex, GluA2 incorporation in layer 4 occurs around P7-P8 which is prior to the incorporation in layer 2/3 which occurs around eye opening at P12-P14(Brill & Huguenard, 2008; Kumar et al., 2002). Decreased synaptic GluA2 content in the adult has been associated with increased plasticity. In this way, synaptic GluA2 content is an important indicator of synaptic maturation as well as the potential for plasticity.

The first goal of this thesis was to determine if there were any large-scale compositional changes to synapses in the absence of Gpc5. To do this we utilized immunohistochemistry to characterize the synaptic protein composition of intracortical and thalamocortical synapses both during the critical period and in the adult. We isolated thalamocortical and intracortical synapses based upon the expression of either vGluT2 or vGluT1 respectively. We also looked at AMPA subunits GluA1 and GluA2 to identify any changes in maturation or plasticity that may be present in the Gpc5 cKO mice. We discovered that there is a significant delay in the maturational incorporation of GluA2 subunits into intracortical synapses. Additionally, thalamocortical synapses show a profound presynaptic deficit during the critical period which leads to loss of thalamic axonal boutons in the adult.

2.2 Synaptic Composition during the Critical Period

Due to the role of other glypican family members (Gpc4 and Gpc6) in regulating synaptic development and the recruitment of GluA1 AMPA receptors to synapses, we first asked if Gpc5 is involved in regulating the number or AMPA receptor composition of synapses. Due to the

expression of Gpc5 being constant across upper and lower cortical layers, and being high at P28, the peak of the critical period, we interrogated both thalamocortical and intracortical synapses within V1b at this timepoint. In order to address this, we utilized immunohistochemistry to label the presynaptic markers vGlut1 and vGlut2 and the postsynaptic markers GluA1 and GluA2, visualized using confocal microscopy.

To determine intracortical synapse number and AMPA receptor composition we analyzed the colocalization of GluA1 or GluA2 with the presynaptic marker vGlut1 in layer 1 and layer 2/3 of WT and Gpc5 cKO mice (Figure 2.1, 2.2). This analysis showed a significant decrease in the colocalization of GluA2 and vGluT1 in both layer 1 (mean (colocalized puncta) ± SEM, WT=113.7 ± 7.6, cKO=101.5 ± 5.6, p=0.026) and layer 2/3 (mean (colocalized puncta) ± SEM, WT=226.4 ± 10.3, cKO=170.8 ± 7.9, p=0.0021) (Figure 2.1 E,H). Concomitantly, there is a small but significant decrease in the total amount of GluA2 in layer 1 (mean (puncta) ± SEM, WT=466.6 ± 12.6, cKO=439.9 ± 13.8, p=0.03) and a larger decrease in layer 2/3 (mean (puncta) ± SEM, WT=990.00 ± 15.9, cKO=784.2 ± 13.1, p=0.0002) (Figure 2.1 D&G). We found no significant change in the amount of vGluT1 in either layer 1 (mean (puncta) ± SEM, WT=365.8 ± 5.5, cKO=360.8 ± 3.7, p=0.6) or layer 2/3 (mean (puncta) ± SEM, WT=369.0 ± 7.3, cKO=358.2 ± 6.9, p=0.19) (Figure 2.1 C&F). In the case of GluA1, we found no difference in the number of GluA1 puncta in layer 1 (mean (puncta) ± SEM, WT=481.0 ± 5.0, cKO=447.8 ± 30.2, p=0.30) or layer 2/3 (mean (puncta) ± SEM, WT=424.4 ± 17.7, cKO=455.0 ± 20.9, p=0.18), nor in the colocalization of GluA1 and vGluT1 in layer 1 (mean (colocalized puncta) ± SEM, WT=101.4 ± 5.7, cKO=97.8 ± 1.8, p=0.62) or layer 2/3 (mean (colocalized puncta) ± SEM, WT=95.3 ± 3.8, cKO=105.0 ± 8.2, p=0.24) (Figure 2.2 A-H).

To investigate if there are alterations at thalamocortical synapses in Gpc5 cKO mice, we quantified the colocalization of the presynaptic marker vGluT2 with postsynaptic GluA1 or GluA2 in layers 1 and 4, where thalamocortical synapses predominantly form (Figure 2.3, 2.4). We found no significant difference in the colocalization between vGluT2 and GluA1 in either layer 1 (mean (colocalized puncta) ± SEM, WT=49.7 ± 6.6, cKO=48.9 ± 7.6, p=0.85) or layer 4 (mean (colocalized puncta) ± SEM, WT=35.6 ± 2.1, cKO=36.8 ± 2.5, p=0.32) (Figure 2.4 E,H). In line with our interrogation of intracortical synapses, we found no change in the total amount of GluA1 in layer 1 (mean (puncta) ± SEM, WT=457.8 ± 3.7, cKO= 434.4 ± 26.8, p=0.47) though there is a small significant decrease in layer 4 (mean (puncta) ± SEM, WT=399.2 ± 25.5, cKO=376.0 ± 22.0, p=0.003) (Figure 2.4 D,G). Interestingly, there is no difference in colocalization of vGluT2 and GluA2 in layer 1 (mean (colocalized puncta) ± SEM, WT=53.4 ± 3.8, cKO=59.4 ± 2.4, p=0.07) or layer 4 (mean (colocalized puncta) ± SEM, WT=61.2 ± 4.1, cKO=64.2 ± 5.3, p=0.65) (Figure 2.3 E,H), in contrast to the observed decrease in GluA2 observed at layer 1 and 2/3 intracortical synapses. We further found no difference in the amount of GluA2 in layer 1 (mean (puncta) ± SEM, WT=475.0 ± 20.0, cKO=467.4 ± 6.6, p=0.67) or layer 4 (mean (puncta) ± SEM, WT=475.6 ±4.8, cKO=475.4 ± 10.1, p=0.98) (Figure 2.3 D,G). The number of presynaptic boutons marked by vGluT2 in layer 1 (mean (puncta) ± SEM, WT=161.8 ± 10.6, cKO=167.4 ± 8.8, p=0.55) and layer 4 (mean (puncta) ± SEM, WT=176.2 ± 8.3, cKO=178.4 ±16.5, p=0.84) are also unchanged in the Gpc5 cKO mice (Figure 2.3 C,F). Although there is no change in the number of VGlut2 boutons between the WT and Gpc5 cKO, the boutons appear smaller in the Gpc5 cKO. Upon analysis, we found a significant decrease in the volume of the vGluT2 puncta in both layer 1 (mean (μm3) ± SEM, WT=0.173 ± 0.00803, cKO=0.117 ±

0.00843, p=0.002) and layer 4 (mean (μm3) ± SEM, WT=0.140 ± 0.0148, cKO=0.0820 ± 0.00583, p=0.018) (Figure 2.5 A-C).

2.3 Synaptic Composition in the adult

The altered synaptic AMPAR composition and presynaptic volume decrease that we observed during the critical period indicates that Gpc5 cKO mice have immature synapses at this time. To determine if these synapses are permanently altered by the absence of astrocytic Gpc5 or if the maturation of these synapses is delayed, we used immunohistochemistry to probe synapse number, presynaptic bouton size and synaptic AMPAR composition of adult (P120) Gpc5 cKO mice. We analyzed intracortical and thalamocortical synapses using the presynaptic markers vGluT1 and vGluT2 respectively and focused on the postsynaptic AMPAR subunit GluA2 due to the decreased expression we observed at P28. Investigating intracortical synapses, we observed that there is no difference in the vGluT1 levels between WT and Gpc5 cKO mice in either layer 1 (mean(puncta) ± SEM, WT=374.1 ± 15.0, cKO=368.3 ± 12.6, p=0.35) or 2/3 (mean(puncta) ± SEM, WT=369.6 ± 13.7, cKO= 357.0 ± 7.6, p=0.34) (Figure 2.6 C,F). Additionally, the levels of GluA2 in layer 1 (mean(puncta) ± SEM, WT=710.0 ± 13.0, cKO= 651.9 ± 27.7, p=0.16) and 2/3 (mean(puncta) ± SEM, WT=697.4 ± 46.0, cKO=685.2 ± 19.5, p=0.77) are now recovered to WT levels (Figure 2.6 D,G). The decreased layer 2/3 colocalization of vGluT1 and GluA2, observed at P28, is no longer present at P120 (mean (colocalized puncta) ± SEM, WT=164.4 ± 16.9, cKO=155.8 ± 3.8, p=0.25) (Figure 2.6 H). In layer 1, there remains a trend towards decreased colocalization of GluA2 and vGluT1 (mean (colocalized puncta) ± SEM, WT=162.7 ±7.6, cKO=144.4 ± 4.3, p=0.069) (Figure 2.6 E).

Turning to thalamocortical synapses, we found that in the adult Gpc5 cKO, as observed at P28, there is no significant difference in the levels of vGluT2 in layer 1(mean (puncta) ± SEM, WT=159.0 ± 3.0, cKO=155.2 ± 3.2, p=0.45) (Figure 2.7 C). There is, however, a small but significant decrease in the levels of vGluT2 in layer 4 (mean(puncta) ± SEM, WT=166.2 ± 6.3, cKO= 152.7 ± 3.7, p=0.046) (Figure 2.7 F). The levels of GluA2 in layer 1 (mean (puncta) ± SEM, WT=720.6 ± 37.3, cKO=698.2 ± 36.7, p=0.62) and layer 4 (mean (puncta) ± SEM, WT=688.7 ± 34.0, cKO=675.2 ± 37.3, p=0.16) are the same in WT and Gpc5 cKO mice (Figure 2.7 D,G). Additionally, there is no significant change in the colocalization of vGluT2 and GluA2 in either layer 1 (mean (colocalized puncta) ± SEM, WT=73.1 ± 4.7, cKO=67.5 ± 4.8, p=0.29) or 4 (mean (colocalized puncta) ± SEM, WT=76.1 ± 5.4, cKO=73.2 ± 6.7, p=0.16) (Figure 2.7 E,H). When we considered the volume of the vGluT2 puncta, we found that there is no difference between the adult WT and Gpc5 cKO mice in layer 1 (mean (μm3) ± SEM, WT=0.143 ± 0.0124, cKO=0.124 ± 0.00890, p=0.19) or layer 4 (mean (μm3) ± SEM, WT=0.103 ± 0.00968, cKO= 0.109 ± 0.00642, p=0.47), in contrast to what was observed at P28 (Figure 2.8). It is interesting to note that there is no change in the volume of thalamocortical terminals in the absence of Gpc5 between P28 and P120. The ‘recovery’ of the Gpc5 cKO thalamic boutons is due to a decrease in the size of WT boutons in the adult mice, rather than an increased in the Gpc5 cKO volume (Figure 2.9).

2.4 Discussion

This data demonstrates that intracortical and thalamocortical synapses have distinct developmental aberrations in the visual cortex of Gpc5 cKO mice during the critical period. The diminished GluA2 content of intracortical synapses indicates that the absence of astrocytic Gpc5 disrupts the postsynaptic maturational shift towards GluA2 containing receptors, which occurs prior to P28, leaving these synapses functionally less mature. Thalamocortical synapses are

compositionally intact in the absence of astrocytic Gpc5 but have a distinct presynaptic phenotype of an apparent smaller bouton, again suggestive of synaptic immaturity. Together this suggests that astrocyte expressed Gpc5 contributes to synaptic maturation in the developing visual cortex. In the adult we observe that by P120 most of the synaptic compositional aberrations detected during the critical period in the Gpc5 cKO mice have been rectified. There appear to still be subtle maturational defects in V1b of Gpc5 cKO mice as evidenced by the remaining differences in GluA2/vGluT1 colocalization in layer 1, and layer 4 vGluT2 levels being lower. All of this suggests that the absence of astrocytic Gpc5 delays, but does not completely prevent, the synapses in V1b from reaching a more mature composition.

Developmentally, thalamocortical projections in layer 4 mature prior to intracortical synapses. This is seen in the timing of GluA2 incorporation as well as in the laminar timing of binocular matching, as both processes occur at thalamocortical synapses first (Brill & Huguenard, 2008; Gu & Cang, 2016; Wang et al., 2010). As the primary input to the visual cortex, disrupting synaptic connectivity from the dLGN likely has downstream effects. It is our hypothesis that Gpc5 is not directly regulating the incorporation of GluA2 at synapses, rather impaired thalamocortical synapses are preventing the correct timing of intracortical synapse maturation. This theory is supported by the recovery of intracortical synapses in the adult, while there remains a thalamocortical impairment in the absence of Gpc5.

During the critical period, the vGluT2 puncta observed in the Gpc5 cKO mice are significantly smaller, and their size does not change in the adult (Figure 2.9). This contrasts with the WT vGluT2 puncta, which are larger during the critical period and decrease in size with age (Figure 2.9). Layer 4 thalamic boutons in the somatosensory cortex show a similar trend, in which the volume of the boutons decreases throughout development (Dufour et al., 2016). This decrease

in volume is also accompanied by an increase in the number of synaptic vesicles (Dufour et al., 2016). In the absence of Gpc5, the structural development of thalamocortical synapses is disrupted such that presynaptically, they are diminished in size. The thalamocortical phenotype that is observed in the absence of Gpc5 could be explained by decreased volume of axonal boutons and/or a diminished number of synaptic vesicles. Therefore, in the next chapter of this thesis, we sought to determine the underlying structural changes that occur in the absence of Gpc5.

2.5 Methods

Characterization of synaptic composition: Astrocyte specific gpc5 ko mice

Tissue Collection and Preparation: Mice were anesthetized with an intraperitoneal injection of 100mg/kg Ketamine (Victor Medical Company) and 20 mg/kg Xylazine (Anased) prior to intracardial perfusion. For the collection of fixed brains used for immunohistochemistry experiments, mice were transcardially perfused with 10 mls PBS followed by 10 mls 4% PFA. Collected brains were placed in 4% PFA overnight at 4°C, washed 3 times in PBS, and cryoprotected in 30% sucrose at 4°C before being embedded in TFM (General data healthcare TFM-5). Fixed embedded brains were frozen in dry ice/ethanol and stored at -80°C.

Immunohistochemistry: Littermate pairs of Gpc5 WT and KO mice were used for experiments at P28 and P120. A minimum of 5 littermate pairs and 3 sections per animal were imaged and analyzed. Coronal sections (20 µm) were cut from PFA fixed mouse brains on a cryostat, mounted on Superfrost Plus micro slides (VWR 48311-703), and immediately processed for immunohistochemistry. Sections were placed in a RT humidified chamber to be blocked and permeabilized for 1 hour in 5% goat serum and 0.3% Triton X-100 in PBS. Sections were incubated with primary antibody in a humidified chamber, overnight at 4°C. Primary antibodies were diluted in 5% goat serum, 0.3% Triton X-100, and 100 mM lysine in PBS. Primary

antibodies used: rabbit anti-GluA1 (Millipore AB1504) 1:500, rabbit anti-GluA2 (Millipore AB1768-I) 1:500, guinea pig anti-vGluT1 (Millipore AB5905) 1:1000, and guinea pig anti-vGluT2 (Millipore AB2251) 1:1000. Sections were washed 3 x 5 minutes in PBS. Sections were then incubated with secondary antibodies in a humidified chamber, at RT, for 2 hours. Secondary antibodies were diluted in 5% goat serum, 0.3% Triton X-100, and 100 mM lysine in PBS. Secondary antibodies used: goat anti-rabbit Alexa 488 (Thermo Fisher Scientific A11073) 1:500, and goat anti-guinea pig Alexa 594 (Thermo Fisher Scientific A11032) 1:500. Sections were incubated with only secondary antibodies as a negative control. Sections were washed 3 x 5 minutes with PBS. SlowFade gold antifade mountant with DAPI (Thermo Fisher Scientific S36939) was applied to each section and a coverslip (22 mm x 50 mm 1.5 thickness) was placed on top and sealed with clear nail polish. GluA1 staining was omitted for P120 mice.

Imaging: Images were acquired on a Zeiss LSM-880 as 16 bit, 1420 x 1420, 0.08 µm x 0.08 µm images with a 63x oil immersion objective. All images were acquired as a z-stack of 8 slices with a total thickness of 2.68 µm. For vGluT1 and GluA1/2 co-staining, images were taken of V1b layer I and layer II/III. For vGlut2 and GluA1/2 co-staining, images were taken of V1b layer I and layer IV. Exposure settings were determined based on the WT condition and all images were acquired in the same session for each experimental pair.

Analysis: Images were analyzed using IMARIS software (Bitplane) to determine puncta and synapse number. Each z-stack was viewed as a 3D image and a Gaussian filter of 0.0725 µm was applied to all images. Four, 25 µm x 25 µm, ROIs were selected from each image for analysis. Puncta were defined using the spots tool as spheres with a set diameter: GluA1 0.4 µm, GluA2 0.4 µm, vGluT1 0.4 µm, vGluT2 0.5 µm. Synapses were defined as colocalization of presynaptic puncta (vGluT1 and vGluT2) and postsynaptic puncta (GluA1 and GluA2) using the spots

colocalization function, measuring a distance of 0.7 μm from center to center of each spot. Volume of vGluT2 puncta was measured using the surface tool, thresholded to capture all puncta defined by the spots tool. All analysis was done blind to genotype. Statistic by T-test. 5 mice/condition.

2.6 Acknowledgements

This chapter, in part, is currently being prepared for submission for publication of the material. Bosworth, AP, Weiser Novak, S, Manor, U, Allen NJ. Astrocytic glypican 5 in the synaptic maturation and stabilization of the primary visual cortex. The dissertation author was the primary investigator and author of this material.

2.7 Figures

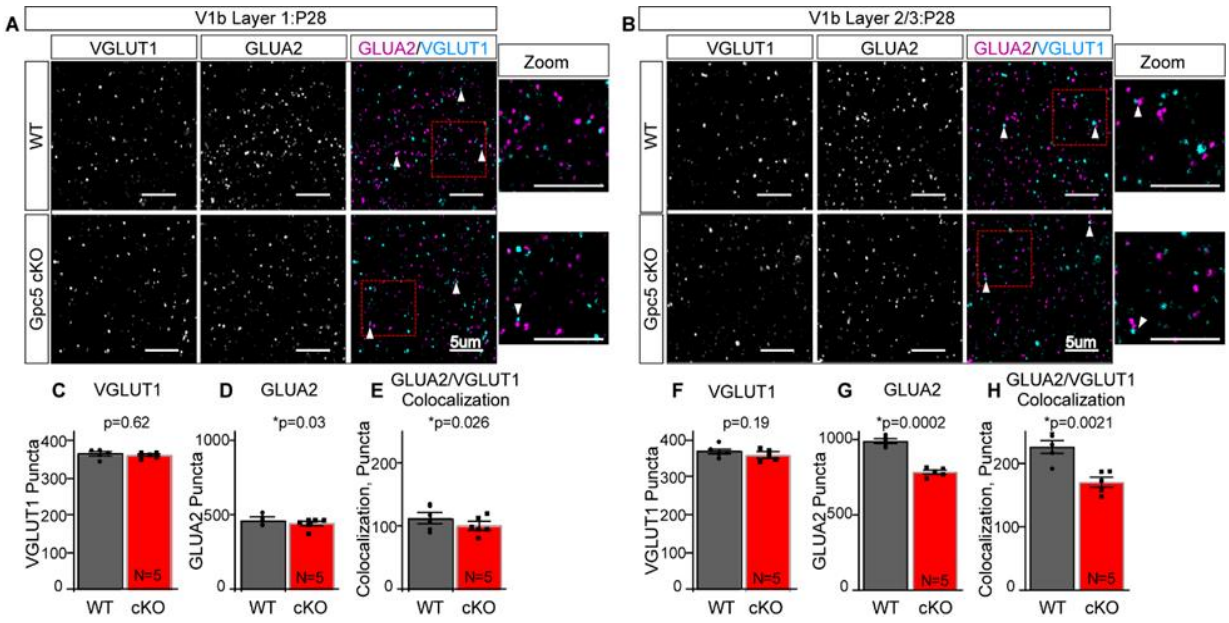

Figure 2.1: P28 synaptic composition: GluA2 containing intracortical synapses. Immunohistochemical staining shows intracortical synapses are immature in Gpc5 cKO. **A,B.** Representative images of immunostaining for intracortical presynaptic marker, vGlut1 and postsynaptic GluA2 in layers 1 (**A**) and 2/3 (**B**). **C-H.** Quantification of immunostaining, number of vGluT1 and GluA2. **C,F.** vGluT1 expression is unchanged in layers 1 and 2/3. **D,G.** GluA2 expression is decreased in layers 1 and 2/3. **E,H.** Colocalization of vGluT1 and GluA2 is decreased in layers 1 and 2/3. Scale bar in A,B: 5μM. N=5 mice/condition. Graphs show mean ± SEM. Individual data points representing mice. Statistics by T-test, significance stated on graph.

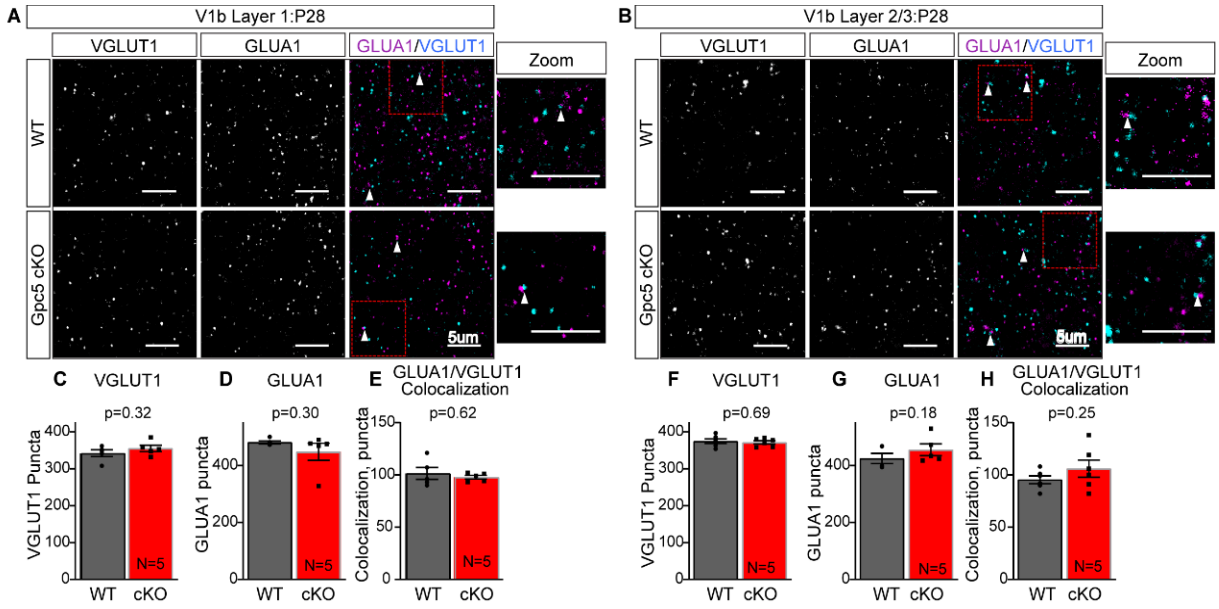

Figure 2.2: P28 synaptic composition: GluA2 lacking intracortical synapses. Immunohistochemical staining shows GluA1 content of intracortical synapses is unchanged in Gpc5 cKO. **A,B.** Representative images of immunostaining for intracortical presynaptic marker, vGlut1 and postsynaptic GluA1 in layers 1 (**A**) and 2/3 (**B**). **C-H.** Quantification of immunostaining, number of vGluT1 and GluA1. **C,F.** vGluT1 expression is unchanged in layers 1 and 2/3. **D,G.** GluA1 expression is unchanged in layers 1 and 2/3. **E,H.** Colocalization of vGluT1 and GluA1 is unchanged in layers 1 and 2/3. Scale bar in A,B: 5µM. N=5 mice/condition. Graphs show mean ± SEM. Individual data points representing mice. Statistics by T-test, significance stated on graph.

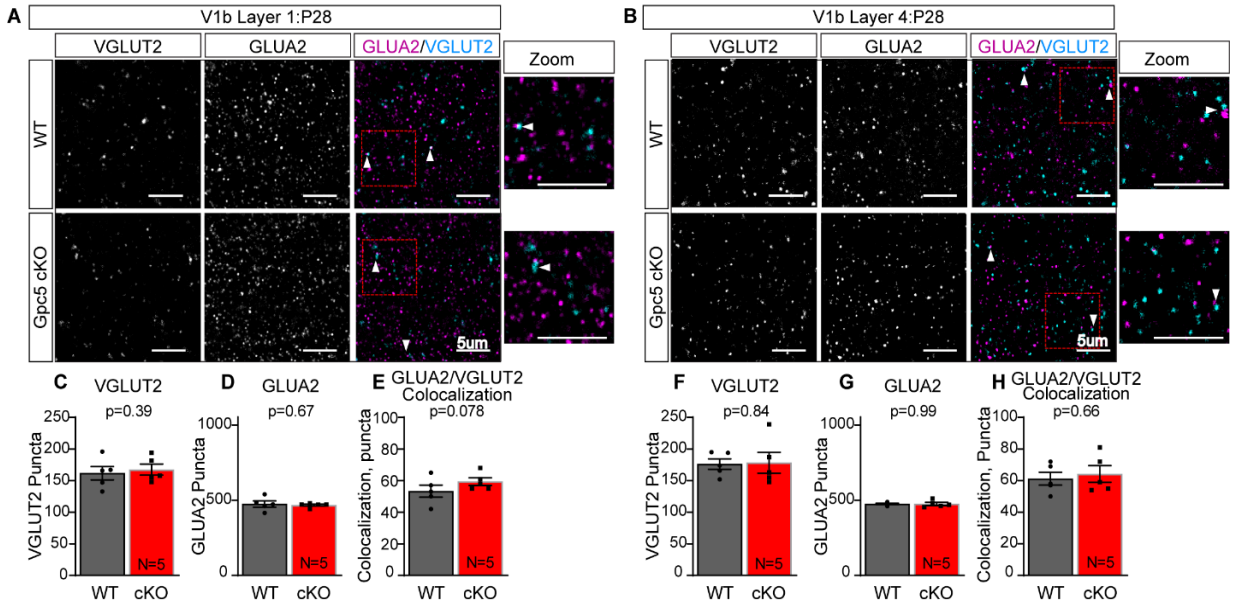

Figure 2.3: P28 synaptic composition: GluA2 containing thalamocortical synapses. Immunohistochemical staining shows thalamocortical synapses have a mature synaptic composition Gpc5 cKO. **A,B.** Representative images of immunostaining for thalamocortical presynaptic marker, vGlut2 and postsynaptic GluA2 in layers 1 (**A**) and 4 (**B**). **C-H.** Quantification of immunostaining, number of vGluT2 and GluA2. **C,F.** vGluT2 expression is unchanged in layers 1 and 4. **D,G.** GluA2 expression is unchanged in layers 1 and 4. **E,H.** Colocalization of vGluT2 and GluA2 is unchanged in layers 1 and 2/3. Scale bar in A,B: 5µM. N=5 mice/condition. Graphs show mean ± SEM. Individual data points representing mice. Statistics by T-test, significance stated on graph.

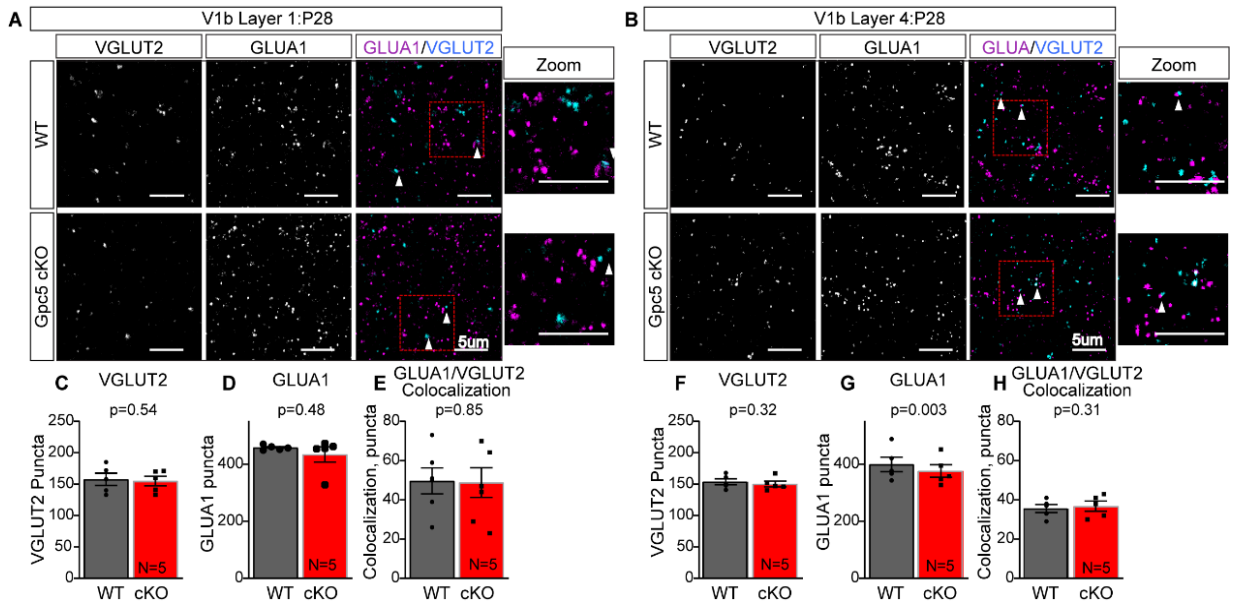

Figure 2.4: P28 synaptic composition: GluA2 lacking thalamocortical synapses. Immunohistochemical staining shows thalamocortical synapses have a mature synaptic composition Gpc5 cKO. **A,B.** Representative images of immunostaining for thalamocortical presynaptic marker, vGlut2 and postsynaptic GluA1 in layers 1 (**A**) and 4 (**B**). **C-H.** Quantification of immunostaining, number of vGluT2 and GluA1. **C,F.** vGluT2 expression is unchanged in layers 1 and 4. **D,G.** GluA1 expression is unchanged in layers 1 and 2/3. **E,H.** Colocalization of vGluT2 and GluA1 is unchanged in layers 1 and 2/3. Scale bar in A,B: 5µM. N=5 mice/condition. Graphs show mean ± SEM. Individual data points representing mice. Statistics by T-test, significance stated on graph.

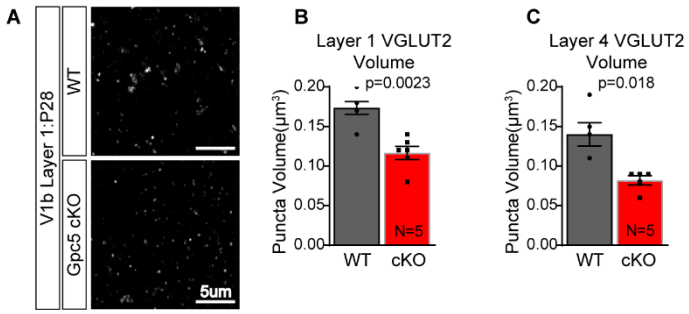

Figure 2.5: Volume of P28 presynaptic vGluT2 puncta. Volume of vGluT2 puncta is decreased in Gpc5 cKO mice. **A.** Representative images of immunostaining of thalamic presynaptic marker, vGlut2 **B.** Quantification of vGluT2 puncta volume in layer 1. **C.** Quantification of vGluT2 puncta volume in layer 4. Scale bar in A,B: 5µM. N=5 mice/condition. Graphs show mean ± SEM. Individual data points representing mice. Statistics by T-test, significance stated on graph.

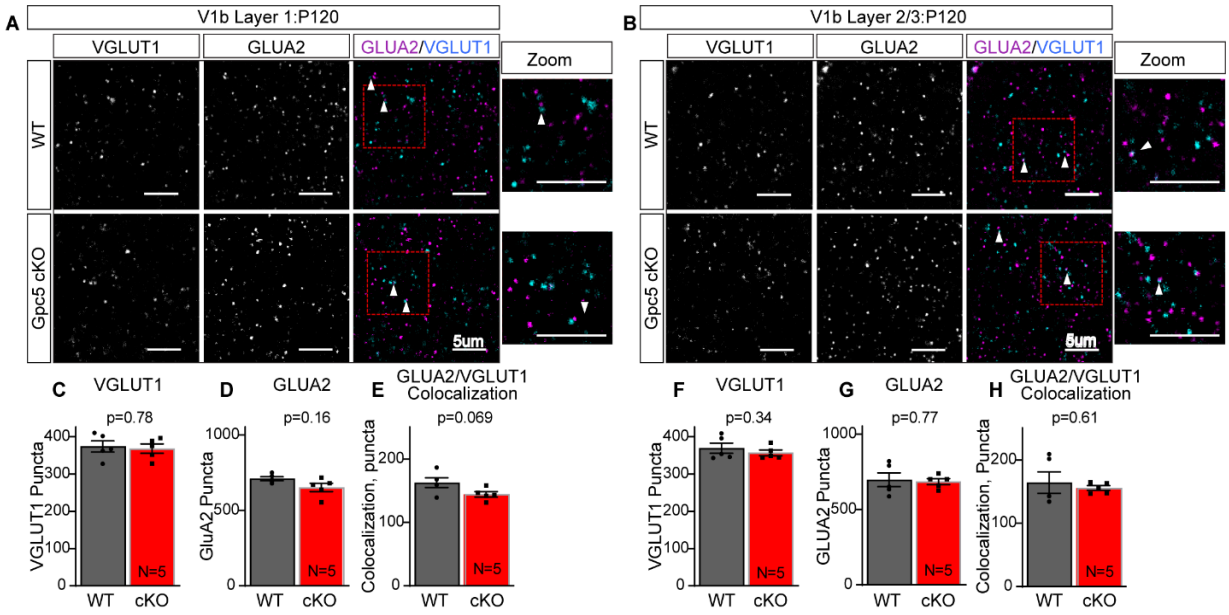

Figure 2.6: P120 synaptic composition: GluA2 containing intracortical synapses. Immunohistochemical staining shows GluA2 content of intracortical synapses is unchanged in the adult Gpc5 cKO. **A,B.** Representative images of immunostaining for intracortical presynaptic marker, vGlut1 and postsynaptic GluA2 in layers 1 (**A**) and 2/3 (**B**). **C-H.** Quantification of immunostaining, number of vGluT1 and GluA2. **C,F.** vGluT1 expression is unchanged in layers 1 and 2/3. **D,G.** GluA2 expression is unchanged in layers 1 and 2/3. **E,H.** Colocalization of vGluT1 and GluA2 is unchanged in layers 1 and 2/3. Scale bar in A,B: 5µM. N=5 mice/condition. Graphs show mean ± SEM. Individual data points representing mice. Statistics by T-test, significance stated on graph.

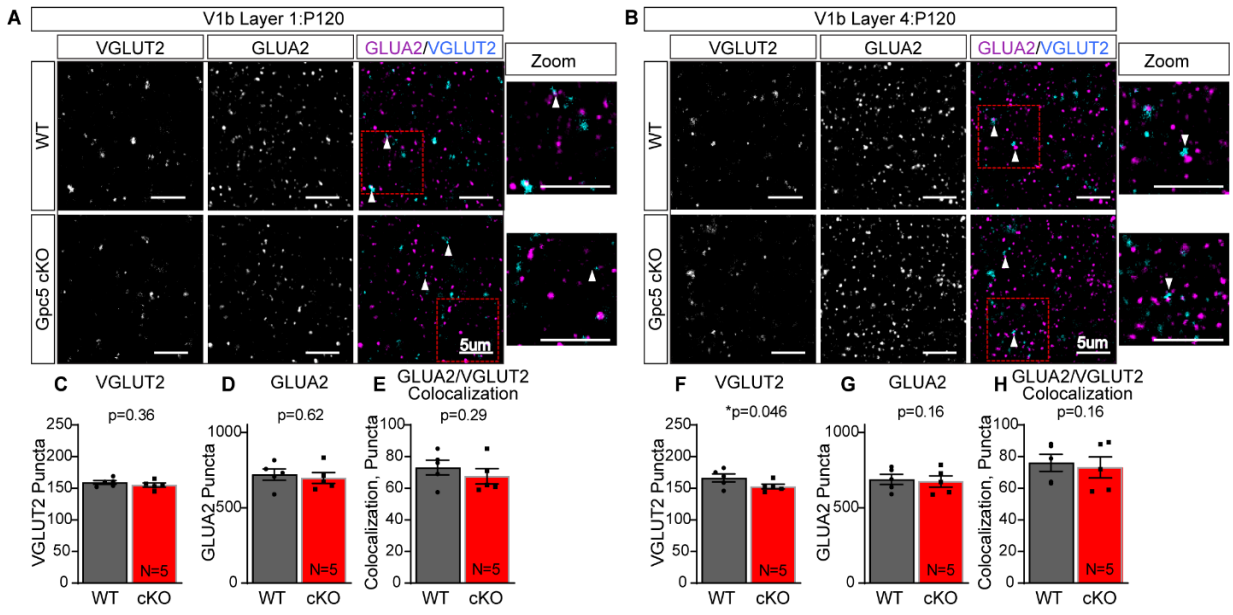

Figure 2.7: P120 synaptic composition: GluA2 containing thalamocortical synapses. Immunohistochemical staining shows GluA2 content of thalamocortical synapses is unchanged in adult Gpc5 cKO. **A,B.** Representative images of immunostaining for intracortical presynaptic marker, vGlut1 and postsynaptic GluA2 in layers 1 (**A**) and 4 (**B**). **C-H.** Quantification of immunostaining, number of vGluT1 and GluA2. **C,F.** vGluT1 expression is unchanged in layers 1 and 4. **D,G.** GluA2 expression is unchanged in layers 1 and 4. **E,H.** Colocalization of vGluT1 and GluA1 is unchanged in layers 1 and 4. Scale bar in A,B: 5µM. N=5 mice/condition. Graphs show mean ± SEM. Individual data points representing mice. Statistics by T-test, significance stated on graph.

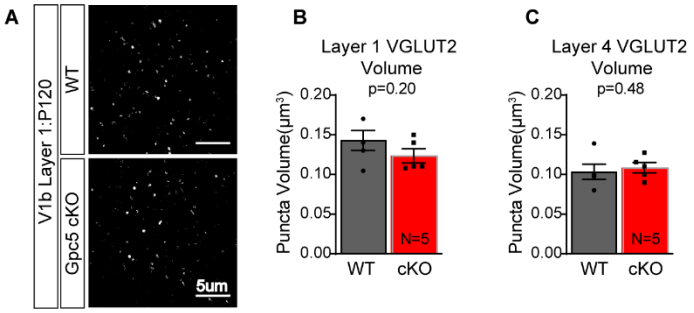

Figure 2.8: Volume of P120 presynaptic vGluT2 puncta. Volume of vGluT2 puncta is recovered in Gpc5 cKO mice. **A.** Representative images of immunostaining of thalamic presynaptic marker, vGlut2 **B.** Quantification of vGluT2 puncta volume in layer 1. **C.** Quantification of vGluT2 puncta volume in layer 4. Scale bar in A,B: 5µM. N=5 mice/condition. Graphs show mean ± SEM. Individual data points representing mice. Statistics by T-test, significance stated on graph.

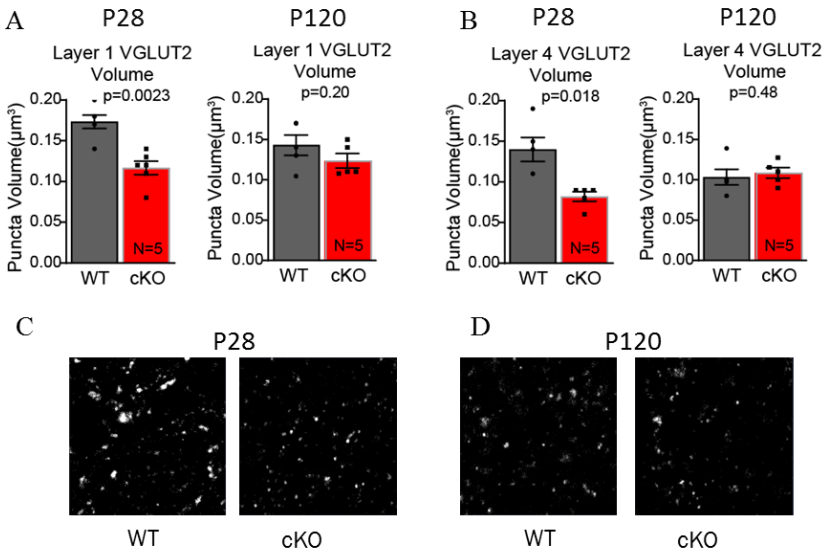

Figure 2.9: Volume of P28 vs P120 presynaptic vGluT2 puncta. [Volume of vGluT2 puncta is unchanged with aging in Gpc5 cKO mice. **A.** Quantification of vGluT2 puncta volume in layer 1 at P28 and P120. Volume of vGluT2 puncta decreases with aging in WT but not Gpc5cKO mice.**B.** Quantification of vGluT2 puncta volume in layer 4 at P28 and P120. Volume of vGluT2 puncta decreases with aging in WT but not Gpc5cKO mice. **C,D.** Representative images of vGluT2 puncta in layer 1 of P28 and P120 mice respectively. No statistics shown, data pulled from experiments above.

2.8 References

Blanco-Suarez, E., Liu, T.-F., Kopelevich, A., & Allen, N. J. (2018). Astrocyte-Secreted Chordin-like 1 Drives Synapse Maturation and Limits Plasticity by Increasing Synaptic GluA2 AMPA Receptors. *Neuron*, *100*(5), 1116-1132.e13. https://doi.org/10.1016/J.NEURON.2018.09.043

Brill, J., & Huguenard, J. R. (2008). Sequential Changes in AMPA Receptor Targeting in the Developing Neocortical Excitatory Circuit. *Journal of Neuroscience*, *28*(51). http://www.jneurosci.org/content/28/51/13918.long

D Bowie, & ML Mayer. (1995). Inward rectification of both AMPA and kainate subtype glutamate receptors generated by polyamine-mediated ion channel block. *Neuron*, *15*(2), 453–462. https://doi.org/10.1016/0896-6273(95)90049-7

Dufour, A., Rollenhagen, A., Sätzler, K., & Lübke, J. H. R. (2016). Development of Synaptic Boutons in Layer 4 of the Barrel Field of the Rat Somatosensory Cortex: A Quantitative Analysis. *Cerebral Cortex (New York, NY)*, *26*(2), 838. https://doi.org/10.1093/CERCOR/BHV270

Fremeau, R. T., Voglmaier, S., Seal, R. P., & Edwards, R. H. (2004). VGLUTs define subsets of excitatory neurons and suggest novel roles for glutamate. *Trends in Neurosciences*, *27*(2), 98–103. https://doi.org/10.1016/J.TINS.2003.11.005

Gu, Y., & Cang, J. (2016). Binocular matching of thalamocortical and intracortical circuits in the mouse visual cortex. *ELife*, *5*(DECEMBER2016). https://doi.org/10.7554/ELIFE.22032

Farhy-Tselnicker, I., Boisvert, M. M., Liu, H., Dowling, C., Erikson, G. A., Blanco-Suarez, E., Farhy, C., Shokhirev, M. N., Ecker, J. R., & Allen, N. J. (2021). Activity-dependent modulation of synapse-regulating genes in astrocytes. *ELife*, *10*. https://doi.org/10.7554/ELIFE.70514

Kaneko, T., & Fujiyama, F. (2002). Complementary distribution of vesicular glutamate transporters in the central nervous system. *Neuroscience Research*, *42*(4), 243–250. https://doi.org/10.1016/S0168-0102(02)00009-3

Kloc, M., & Maffei, A. (2014). Target-specific properties of thalamocortical synapses onto layer 4 of mouse primary visual cortex. *Journal of Neuroscience*, 34(46),15455-15465.https://doi.org/10.1523/JNEUROSCI.2595

Kumar, S. S., Bacci, A., Kharazia, V., & Huguenard, J. R. (2002). A developmental switch of AMPA receptor subunits in neocortical pyramidal neurons. *The Journal of Neuroscience: The Official Journal of the Society for Neuroscience*, *22*(8), 3005–3015. https://doi.org/20026285

Nahmani, M., & Erisir, A. (2005). VGluT2 immunochemistry identifies thalamocortical terminals in layer 4 of adult and developing visual cortex. *Journal of Comparative Neurology*, *484*(4), 458–473. https://doi.org/10.1002/CNE.20505

Singh, S. K., Stogsdill, J. A., Pulimood, N. S., Dingsdale, H., Kim, Y. H., Pilaz, L. J., Kim, I. H., Manhaes, A. C., Rodrigues, W. S., Pamukcu, A., Enustun, E., Ertuz, Z., Scheiffele, P., Soderling, S. H., Silver, D. L., Ji, R. R., Medina, A. E., & Eroglu, C. (2016). Astrocytes Assemble Thalamocortical Synapses by Bridging NRX1alpha and NL1 via Hevin. *Cell*, *164*(1–2), 183–196. https://doi.org/10.1016/j.cell.2015.11.034

Wang, B.-S., Sarnaik, R., & Cang, J. (2010). Critical Period Plasticity Matches Binocular Orientation Preference in the Visual Cortex. *Neuron*, *65*(2), 246. https://doi.org/10.1016/J.NEURON.2010.01.002

Wearne, S. L., Rodriguez, A., Ehlenberger, D. B., Rocher, A. B., Henderson, S. C., & Hof, P. R. (2005). New techniques for imaging, digitization and analysis of three-dimensional neural morphology on multiple scales. *Neuroscience*, *136*(3), 661–680. https://doi.org/10.1016/J.NEUROSCIENCE.2005.05.053

3 Glypican 5 and Synaptic Structure

3.1 Introduction

In addition to the composition of presynaptic and postsynaptic machinery, the physical structure of synapses holds many clues as to the maturational state and strength of a given synapse. Excitatory synapses primarily consist of a presynaptic axonal bouton and a post synaptic dendritic spine (Grillo et al., 2013; Jennifer N & Kristen M, 2008). The structure of these two separate compartments can tell us a great deal about the functional properties of the synapse (Arellano et al., 2007; Harris & Stevens, 1989).

Synaptic Structure

The presynaptic site of excitatory synapses is the axonal bouton. Axonal boutons are swellings of the presynaptic axon which can be en passant, consisting of a 'beads on a string' structure, or terminal boutons, occurring at the end of an axonal branch (Bopp et al., 2017; Grillo et al., 2013; Rodriguez-Moreno et al., 2018). En passant boutons are the most common class of presynaptic structure (Grillo et al., 2013). Thalamic boutons are distinct from intracortical boutons in multiple ways. Thalamic boutons can be identified by their relatively large structure as well as the increased prevalence of mitochondria within the bouton. Additionally, these boutons often receive more than one postsynaptic partner (Rodriguez-Moreno et al., 2018).

A large amount of research has been conducted interrogating the structure of post synaptic dendritic spines. Dendritic spines are small membranous protrusions on the dendritic shaft which act as the postsynaptic compartment of excitatory synapses (Nakahata & Yasuda, 2018). Spines are able to assume a variety of shapes which range from mushroom to filopodia like, each of which has unique properties. Mushroom spines, distinguished by the presence of a large head attached to the dendrite by a thin neck, are the substrate for mature, stable synapses (Berry &

Nedivi, 2017; Helm et al., 2021). Thin filopodia like spines lack a recognizable head structure and exist as more transient immature synaptic sites (Berry & Nedivi, 2017; Risher, Ustunkaya, et al., 2014). Excitatory synapses can also occur on stubby spines which lack a defined neck or directly onto dendritic shafts (Helm et al., 2021). There has long been speculation as to the functional relevance of spine structure, such as how the diameter of the neck is involved in the compartmentalization of synaptic signaling cascades or the amplification of synaptic input (Harnett et al., 2012; Jan Tønnesen et al., 2014). While the exact manner in which spine structure impacts synaptic function is not agreed upon within the scientific community, it is acknowledged that spine structure is functionally relevant and is regulated by both development and experience (Helm et al., 2021; Nakahata & Yasuda, 2018).

Interrogation of synaptic structure

The original method employed to interrogate neuronal structure was the golgi method, in which neurons were sparsely and randomly labeled with metal precipitate. This allowed researchers to observe that neurons were not directly connected and first observe the presence of axonal boutons and dendritic spines. This method continues to be useful but lacks specificity (Vints et al., 2019). Many other methods have been employed since the invention of the golgi method to interrogate neuronal morphology. This thesis employs two different methods to investigate synaptic structure in different neuronal populations, electron microscopy and fluorescent cell fills.

The invention of electron microscopy furthered our ability to investigate neuronal morphology at the level of individual synapses. The one limitation that must be overcome when employing electron microscopy, is how to identify a single subset of neurons. The goal of this project was to specifically interrogate the structure of thalamocortical synapses within layer 4 of

V1b and to do this, we utilized the genetically encoded EM probe APEX2. APEX2 is an engineered peroxidase which forms a dark precipitate, observable on electron micrographs, upon reaction with 3'3-diamino-benzidine (Lam et al., 2014). In order to directly target the thalamocortical synapses, a virus containing APEX2 targeted to mitochondria was injected into the dLGN (Figure 3.1). This allowed us to specifically identify thalamic projections in V1b by the presence of APEX2 positive mitochondria in the axon. Reconstruction of these axons allowed us to interrogate the presynaptic structure of these synapses. We were also able to reconstruct the postsynaptic partners to identify any structural changes.

In order to interrogate intracortical synapses, we chose to look at layer 2/3 pyramidal neurons, as the majority of synapses onto these neurons are intracortical in origin (Luo et al., 2017). Dendritic spines are the primary site of excitatory synapses on pyramidal neurons in the cortex (Ballesteros-Yáñez et al., 2006). As such, we are able to probe for large scale structural changes at excitatory intracortical synapses by investigating the spine structure on these layer 2/3 pyramidal neurons. To specifically target this subset of cortical neurons, we individually filled L2/3 pyramidal cells with fluorescent dye. This method has been used extensively to investigate the structure of individual neurons (Bushong et al., 2002; Han et al., 1993).

3.2 Glypican 5 and thalamocortical synapse structure

The observed decrease in vGluT2 puncta volume by light microscopy in Gpc5 cKO mice suggests a potential presynaptic structural phenotype and could be the result of a decrease in size of the presynaptic bouton, or a decreased recruitment of presynaptic vesicles containing vGlut2 to the presynaptic site. In order to specifically analyze thalamocortical synapses formed between presynaptic vGlut2 expressing neurons originating in the visual thalamus (dLGN) and layer 4 target neurons in the visual cortex, we used the genetically encoded electron microscopy (EM)

marker APEX2 to label mitochondria within these axons, enabling us to specifically analyze this sub-class of synapses by EM. To identify thalamic projections within V1b, AAV9-COX4-DAPEX2 (Zhang et al., 2019) was injected into the dLGN of littermate pairs of WT and cKO mice at P14 and brains were collected at P28. Within V1b, the APEX2 labeled mitochondria of the dLGN projections were identifiable in layers 1 and 4, where thalamic projections synapse in the visual cortex (Figure 3.1) (Nahmani & Erisir, 2005). The presence of APEX2 in the appropriate layers provided validation that thalamic axons, and not cortical axons, were targeted. Following the DAB reaction and verification of APEX2 signal, tissue was processed for TEM and blocks were made. Serial sections were cut and a ROI in layer 4 was selected based on neuron morphology and distance from the pial surface. Sections were imaged on a Zeiss Sigma VP scanning electron microscope, and then aligned to form a block of at least 2.5 µm thick.

Thalamocortical boutons were identified by the presence of DAB reacted mitochondria within the parent axon. Utilizing the APEX2 EM marker as a label for dLGN thalamic projections, we reconstructed APEX2 positive boutons (Figure 3.2). In the reconstructed boutons, we looked at bouton volume, number of postsynaptic partners, and the number of synaptic vesicles. Labeled boutons had the features of vGluT2 positive thalamic boutons, including a large volume, asymmetric synapses, and multiple synaptic contacts at some boutons. We analyzed 90 APEX2 labeled thalamic boutons in both the WT and the Gpc5 cKO. Of the analyzed boutons, in each genotype 45 had a single postsynaptic partner and were considered monosynaptic, while 45 had more than one postsynaptic partner and were considered multisynaptic (Figure 3.3 A,B). We analyzed all labeled boutons as a single group, as well as looking at monosynaptic and multisynaptic boutons individually.

In the Gpc5 cKO mice we found a significant decrease in the average volume of the boutons (mean (µm3) ± SEM, WT=0.50 ±0.026, cKO=0.41 ± 0.026, p=0.017) (Figure 3.4 C). This result is driven by a significant decrease in the volume of multisynaptic boutons (mean (µm3) ± SEM, WT=0.639 ± 0.036, cKO=0.51 ± 0.040, p=0.039), with no difference in the volume of monosynaptic boutons (mean (µm3) ± SEM, WT=0.37 ± 0.026, cKO=0.32 ± 0.027, p=0.66) (Figure 3.4 A,B,D). In WT mice there is a significant difference between the size of monosynaptic and multisynaptic boutons (mean(µm3) ± SEM, mono=0.37 ± 0.026, multi=0.639 ± 0.036, $p<0.0001$), which is also present in Gpc5 cKO mice (mean(µm3) ± SEM, mono=0.32 ± 0.027, multi=0.51 ± 0.04, p=0.0003) (Figure 3.4D). There is no significant difference in the number of synaptic vesicles within a bouton between the WT and cKO for monosynaptic (mean(vesicles)± SEM, WT=294 ± 26.66, cKO=311 ± 33.5, p=0.99) but there is for multisynaptic (mean(vesicles) ± SEM, WT=648 ± 46.6, cKO=496 ± 49.0, p=0.04) boutons which is in line with our volume data (Figure 3.4 F). Additionally, we found that the average number of postsynaptic partners at a multisynaptic bouton is higher in the Gpc5 cKO (mean(count) ± SEM, WT=2.29 ± 0.075, cKO=2.8 ± 0.14, p=0.006), and that the maximum observed number of synapses at a single bouton is also greater in the Gpc5 cKO (max number of synapses, WT=3, cKO=5) (Figure 3.5 A,B).

In order to specifically interrogate the postsynaptic structure of thalamocortical synapses, we used the dataset we generated using the genetically encoded EM marker APEX2 as described above. We reconstructed the post synaptic density (PSD) and postsynaptic partners of the labeled reconstructed boutons (Figure 3.6 A,B). The predominant post synaptic structures present at these thalamocortical synapses are dendritic spines, though synapses directly onto the dendritic shaft were occasionally observed. To characterize the postsynaptic component of these thalamocortical synapses, we measured the surface area of the PSD, and categorized spines as mushroom (mature),

thin (immature), or other based on the presence of an obvious spine head, for the 90 labeled boutons. We looked at both monosynaptic boutons, with a single postsynaptic partner, and multisynaptic boutons, with multiple postsynaptic partners. We found a significant decrease in the surface area of the PSD in Gpc5 cKO mice (mean (μm2) ± SEM, WT=0.19 ± 0.013, cKO=0.11 ± 0.007, p=<0.0001) (Figure 3.7 A,B,C). The decreased PSD surface area is seen at spines on monosynaptic boutons (mean (μm2) ± SEM, WT=0.20 ± 0.025, cKO=0.12 ± 0.013, p=0.018), as well as at spines on multisynaptic boutons (mean (μm2) ± SEM, WT=0.18 ± 0.016, cKO=0.11 ± 0.009, p=0.0001) (Figure 3.7 D). Given the decreased size of the PSD, we next asked if the structure of the postsynaptic spine is shifted to a more immature phenotype. In the Gpc5 cKO we found a trend towards an increase in the number of thin spines (fraction of total spines, WT=0.29, cKO=0.42) and a decrease in the number of mushroom spines (fraction of total spines, WT=0.64, cKO=0.53) relative to WT mice($\chi 2$=0.15) (Figure 3.6 C). This trend held when we separately analyzed spines opposing monosynaptic and multisynaptic boutons but was primarily driven by monosynaptic boutons. For monosynaptic boutons we found an increase in the fraction of thin spines (Fraction of spines, WT=0.25, cKO=0.48) and a decrease in the fraction of mushroom spines (Fraction of spines, WT=0.64, cKO=0.55) in the Gpc5 cKO ($\chi 2$=0.0018). At multisynaptic boutons there is a non-significant trend towards an increase in the fraction of thin spines (Fraction of spines, WT=0.25, cKO=0.33) and a decrease in the fraction of mushroom spines (Fraction of spines, WT=0.69, cKO=0.59) relative to WT ($\chi 2$=0.39) (Figure 3.6 D).

3.3 Glypican 5 and L2/3 synapse structure

Given the decreased GluA2 levels that we observed at layer 2/3 intracortical synapses in the P28 Gpc5 cKO mice, we next asked if there was a concurrent shift towards a more immature dendritic spine structure in this layer, which consists of predominantly intracortical synapses. To

investigate this, we used sharp electrodes filled with fluorescent dye (AF488) to label individual layer 2/3 pyramidal neurons within V1b in acute brain sections of P28 WT and Gpc5 cKO mice. Sections were then fixed with PFA and cells imaged using confocal microscopy (Figure 3.8 A). Using NeuronStudio, we quantified spine density, spine length, spine head diameter, and head/neck ratio of spines located on secondary apical and basal dendrites. We found no significant difference in the average spine density for secondary apical (mean (spines/μm) ± SEM, WT=1.25 ± 0.035, cKO=1.18 ± 0.044, p=0.31) or basal (mean (spines/μm) ± SEM, WT=1.13 ± 0.069, cKO=1.18 ± 0.073, p=0.27) dendrites (Figure 3.8 D,E). There is a small trend towards increased average spine length of apical (mean (μm) ± SEM, WT=1.29 ± 0.015, cKO=1.36 ± 0.023, p=0.059) but not basal (mean (μm) ± SEM, WT=1.14 ± 0.02, cKO=1.21 ± 0.10, p=0.58) spines located on secondary dendrites in Gpc5 cKO mice (Figure 3.8 F,G). Additionally, there is no change in the head diameter of either apical (mean (μm) ± SEM, WT=0.35 ± 0.012, cKO=0.35 ± 0.0068, p=0.76) or basal (mean (μm) ± SEM, WT=0.34 ± 0.0082, cKO=0.32 ± 0.0073, p=0.20) dendritic spines in Gpc5 cKO mice (Figure 3.8 F,G). Further, the head to neck ratio is also unchanged for both apical (mean ± SEM, WT=4.11 ± 0.12, cKO=4.12 ±0.11, p=0.96) and basal (mean ± SEM, WT=4.73 ± 0.34, cKO=4.28 ± 0.61, p=0.55) spines (Figure 3.8 H,I). These spine parameters were also used to designate spines as either mushroom, thin, or stubby. The categorization of spine structure in the Gpc5 cKO mice showed that there is no difference in the prevalence of mushroom (Fraction of total spines ± SEM, WT=0.29 ± 0.025, cKO=0.33 ± 0.045, p=0.90), thin (Fraction of total spines ± SEM, WT=0.61± 0.039, cKO=0.61 ± 0.029, p=>0.99), or stubby (Fraction of total spines ± SEM, WT=0.066 ± 0.0077, cKO=0.056 ± 0.010, p=0.99) spines, among secondary apical dendrites in layer 2/3 neurons (Figure 3.8 B). The same observation holds when considering the prevalence of mushroom (Fraction of total spines ± SEM, WT=0.35 ± 0.053,

cKO=0.29 ± 0.020, p=0.97), thin (Fraction of total spines ± SEM, WT=0.55 ± .056, cKO=0.60 ± 0.069, p=0.98), or stubby (Fraction of total spines ± SEM, WT=0.099 ± 0.0062, cKO=0.10 ± 0.078, p=>0.99) spines among secondary basal dendrites in layer 2/3 neurons (Figure 3.8 C). Overall, we did not observe any gross changes in the structure of spines on dendrites of layer 2/3 neurons in Gpc5 cKO mice.

3.4 Discussion

Within this chapter, we interrogated the role of astrocytic Gpc5 on synaptic structure in V1b. Utilizing APEX2, we generated a novel dataset interrogating the structure of thalamocortical synapses in V1b. The specificity of our approach was supported by the laminar expression of APEX2 as well as the structural properties of the reconstructed boutons. Qualitatively, thalamic boutons are large and can receive multiple synaptic partners, which we observed in our data. The measured volume of WT boutons agrees with published data on thalamic boutons in the motor and somatosensory cortices (Bopp et al., 2017; Risher, et al., 2014; Rodriguez-Moreno et al., 2018). Additionally, the size of the vesicular cloud and surface are of the PSDs also correspond to previous EM studies of other thalamic projections (Bopp et al., 2017; Rodriguez-Moreno et al., 2018; Singh et al., 2016). The agreement between our WT data and previously published studies validates our experimental approach and allows us to make comparisons with the Gpc5 cKO animal.

Overall, our data demonstrates that multisynaptic thalamocortical boutons are structurally altered in the absence of astrocytic Gpc5. There is an overall decrease in the size of the axonal boutons, an effect which is primarily driven by multisynaptic boutons. This in conjunction with the decreased number of synaptic vesicles, likely explains the decreased vGluT2 puncta volume that was observed in our immunohistochemical experiments. A decreased number of vGluT2

positive vesicles clustered in a smaller area could lead to immunohistochemical puncta appearing visibly smaller. The number of vesicles within a bouton, as well as the volume of a bouton, are indicators of the strength of a synapse, with smaller vesicle clouds and boutons indicating weaker synapses (Arellano et al., 2007; Harris & Stevens, 1989; Knott et al., 2006; Ofer et al., 2021). The presynaptic properties of the thalamocortical synapses in the Gpc5 cKO, including the smaller bouton size and smaller vesicle cloud suggests that the absence of astrocytic Gpc5 renders thalamocortical synapses weaker. The decreased PSD surface area at thalamocortical synapses in the Gpc5 cKO also indicates that the strength of these thalamocortical synapses are diminished (Arellano et al., 2007; Harris & Stevens, 1989). The large effect seen at multisynaptic boutons indicates that the developmental role of astrocytic Gpc5 may involve the refinement of multisynaptic thalamic boutons. During development, synapses undergo a period of robust synaptic growth, followed by refinement in which appropriate synapses are strengthened and stabilized while others are pruned away (Allen, 2013; Kano & Watanabe, 2019; Yoshihara et al., 2009). The large number of immature postsynaptic partners in the Gpc5 cKO may be an indication that this process of stabilization and pruning is not occurring. It is not immediately clear whether Gpc5 is necessary for the stabilization of certain synapses or for the pruning process.

We observed that in the adult Gpc5 cKO mice, there is a loss of vGluT2 positive terminals in layer 4. This would suggest that Gpc5 is necessary for stability and maintenance of synapses rather than pruning. If Gpc5 is involved in pruning, it is more likely that we would see an abundance of synapses, rather than a loss of axonal boutons. This is also supported by the observation that large thalamic boutons are lost during normal aging (Grillo et al., 2013). As the Gpc5 cKO does not have large, stabilized boutons, instead of seeing a loss of large boutons, we see a loss of boutons in general. This could have implications for the stability of cortical circuits,

as connections may be lost randomly instead of preferentially. As a heparan sulfate proteoglycan, Gpc5 has long heparan sulfate chains which are ideally structured to interact with multiple proteins simultaneously (Kamimura & Maeda, 2021). This provides the potential for Gpc5 to be involved in the formation of trans synaptic complexes which could stabilize synapses.

An alternative hypothesis is that Gpc5 actively prevents excessive synapse formation. Astrocyte secreted hevin expression peaks during the same time period as Gpc5 and is responsible for the assembly of thalamocortical synapses by bridging Nrx1a and NL1(Singh et al., 2016). It is possible that Gpc5 has an opposing role to the action of a factor such as hevin and prevents the formation of inappropriate synaptic connections similar to the action of SPARC (Kucukdereli et al., 2011). Heparan sulfate proteoglycans have been shown to bind cell adhesion receptors and Gpc5 may inhibit axo-dendritic interactions by competing at one of these receptors (Sarrazin et al., 2011).

Overall, the immature postsynaptic phenotype, along with the smaller and less refined thalamic axonal boutons described above, indicate that the absence of astrocytic Gpc5 significantly disrupted the maturation of thalamocortical synapses, leaving them weaker and less refined at P28. However, postsynaptic structural perturbations were not observed on L2/3 pyramidal neurons in spite of the observed immature synaptic composition of intracortical synapses at this time point. The multitude of structural changes at thalamocortical synapses, but not intracortical synapses, suggests that the primary target of astrocytic Gpc5 is thalamocortical synapses. As layer 4 neurons project directly to layer 2/3 neurons, we hypothesize that these immature unrefined thalamocortical synapses have downstream effects that impact the AMPAR maturation-state of intracortical synapses.

3.5 Methods

Characterization of thalamocortical synapse structure: Astrocyte specific Gpc5 ko mice

Intracranial viral injection: To label thalamocortical projections for EM reconstruction, AAV9-COX4-APEX2 was injected into the dLGN of WT and KO littermate pairs at P14. Mice were anesthetized with oxygenated isoflurane (2-3%) and injection was done with a Nanoject pressure injection system ($3x10^{12}$ vg/nl). Virus was injected at coordinates 2.0 mm posterior from bregma, 1.9 mm lateral from the midline, and 2.9 mm below the pia. A total of 150 nL of virus was delivered at a rate of 2 nl per second. Following 2 weeks of expression, mice were collected at P28, and the brain was processed as described in Zhang et al. 2019.

Tissue collection: P28 mice were anesthetized with an intraperitoneal injection of 100mg/kg Ketamine (Victor Medical Company) and 20 mg/kg Xylazine (Anased) prior to intracardial perfusion.

Tissue processing: Briefly, animals were transcardially perfused with a modified oxygenated Ringer's solution containing heparin followed by a buffered aldehyde fixative solution (2% paraformaldehyde, 2.5% glutaraldehyde in 4mM, in buffer with 0.15M sodium cacodylate, 4mM $CaCl_2$), both maintained at 40°C in a water bath to ensure that perfusate was delivered to the animal at approximately body temperature. The brain was carefully removed and left in fresh ice-cold fixative at 4°C. All steps were performed at ice cold temperatures unless otherwise indicated.

After overnight post-fixation, brains were washed three times in buffer (0.15M sodium cacodylate, 4mM $CaCl_2$; cacodylate buffer). The brain was carefully mounted on a Leica VT1000S vibrating microtome in cacodylate buffer, and 100µm coronal sections containing the primary visual cortex were collected in 6 well plates and washed 2x10 minutes in cacodylate buffer supplemented with 50mM glycine, followed by 1x10 minutes in cacodylate buffer. A 10X

diaminobenzidine (DAB) tetrahydrochloride solution was freshly prepared by dissolving 50mg of DAB in 0.1 M HCl at room temperature prior to tissue processing. Sections were then incubated in DAB solution (final concentration of 0.3 mg/mL DAB in cacodylate buffer) for 30 minutes in the dark. After 30 minutes, 10µL/mL of cacodylate supplemented with 0.3% H_2O_2 was added directly to the DAB solution (final H_2O_2 concentration of 0.003%) and swirled extensively to initiate the peroxidase reaction which was allowed to proceed for 1 hour in the dark. Slices were washed 3x10 minutes in cacodylate buffer and then further post-fixed in cacodylate buffer with 3% glutaraldehyde.

The following day, sections were rinsed 2x10 minutes in cacodylate buffer with 50mM glycine followed by 1x10 minutes in cacodylate buffer. Sections containing DAB reaction product were carefully transferred to a petri dish filled with ice cold cacodylate buffer for photography and microdissection, whereby 2mm wide strips containing reaction product and spanning from the cortical surface to the corpus collosum were collected into scintillation vials for further processing.

Samples were stained with reduced osmium (1% osmium tetroxide and 1.5% potassium ferrocyanide in cacodylate buffer) for 1h at room temperature. Samples were then gently rinsed 5x3 minutes with ice cold water and left in 1% aqueous uranyl acetate at 4°C overnight.

Samples were then serially dehydrated in ice cold aqueous ethanol solutions of ascending concentrations before 3x10 minute incubations with absolute ethanol at room temperature. Samples were then infiltrated with ascending concentrations of Durcupan resin in absolute ethanol at room temperature (3:1, 4h; 1:1, 4h; 1:3, overnight) before 2x4h incubations in pure resin. Samples were embedded with fresh resin and paper labels in silicon molds, with the tissue oriented *en face* to the block face and polymerized for 60h at 65°C in a small oven.

Serial sections were collected onto silicon wafers as described elsewhere (Horstmann, 2012) with some modifications. Briefly, the block was trimmed using a 90° diamond trimming knife (Diatome) on an ultramicrotome (Leica UC7) to a trapezoidal frustum of 150x400µm which included the region from the cortical surface to deep cortical layers. A silicon chip (35x7mm; University Wafer, Boston, MA) was hydrophilized in a plasma cleaner (Harrick) immediately preceding partial immersion in a Diatome Histo knife mounted on the ultramicrotome. Ribbons of 150-200 serial sections of thicknesses between 50-60nm were cut using with 4 drops of pure ethanol in the water boat and the ionizing gun (Leica) activated and oriented towards the cutting edge of the knife. When ribbons of sufficient quality and length were generated, they were released from the knife edge using a single-eyelash brush and carefully positioned over the chip. The water level was then slowly lowered and sections were allowed to dry down on the silicon substrate. Chips were dried on a hot plate set to 60°C and immediately labeled with a diamond scribe to indicate animal ID and nominal section thickness.

Imaging: Chips were mounted on aluminum stubs using carbon sticky tabs and loaded into a scanning electron microscope (SEM; Zeiss Sigma VP) equipped with a sensitive backscatter detector (Gatan), as well as extended rastering capabilities and a control system designed for serial section imaging workflows (ATLAS5, FIBICS). Low resolution image maps of the ribbon(s) of serial sections were collected, and a mid-resolution map of a central section was generated for reference. From this map, a region of interest (ROI) of 50x50µm was selected from between 250-350µm from the cortical surface that [1] had DAB+ terminals; [2] was not obstructed by blood vessels or somata; [3] was free from obvious debris throughout the series as assessed from the low resolution map. This region was identified at one end of the ribbon of sections, and the ROI

was imaged at high resolution (pixel size: 2nm; dwell time: 6µs; EHT: 3kV; working distance: 8-9mm) on every section in the ribbon.

Image Analysis: Image stacks were collated and rigidly aligned using TrakEM2 in Fiji (https://journals.plos.org/plosone/article?id=10.1371/journal.pone.0038011) and cropped to a minimum continuous cube of roughly aligned data with minimal padding. Fine stack alignment was accomplished using SWiFT-IR (https://ieeexplore.ieee.org/document/8010595) as deployed on 3DEM.org using the TACC compute resource Stampede 2 (https://doi.org/10.1523/JNEUROSCI.1169-19.2019). The well aligned data was then imported into VAST Lite (VAST) for annotation and analysis (Wearne et al., 2005).

Briefly, axons with DAB+ mitochondria and their corresponding postsynaptic partners were identified and segmented in VAST. Volume of terminals, vesicle cloud size, and PSD surface area were determined by individually segmenting structures and using VASTTOOLS Matlab script. To categorize post synaptic targets, all post synaptic structures synapsing with a target axonal terminal were segmented. 3D reconstructions of the segmented post synaptic structures were then determined to be either mushroom, thin, stubby, or shaft. Mushroom spines were identified by the presence of a defined head and neck, thin spines were categorized as long filopodia like structures with no defined head, stubby spines were identified as short structures with no definable neck, and shaft synapses occurred directly on the dendritic shaft.

Characterization of L2/3 spine structure: Astrocyte specific Gpc5 ko mice

Tissue collection: P28 mice were anesthetized with an intraperitoneal injection of 100mg/kg Ketamine (Victor Medical Company) and 20 mg/kg Xylazine (Anased) prior to intracardial perfusion. For cell fill experiments, mice were transcardially perfused with oxygenated aCSF (in mM: NaCl 126, $NaHCO_3$ 26, Glucose 10, KCl 2.5, $MgCl_2$ 2, NaH_2PO_4 1.25, $CaCl_2$ 2, pH 7.4) at

34°C for 30 seconds followed by 34°C 4% PFA for 15 minutes. Brains were collected and immediately sectioned on vibratome in PBS.

Cell fills: Littermate pairs of Gpc5 WT and KO mice were used for experiments at P28. Coronal sections (200 µm), of lightly fixed tissue, were cut on a vibratome in ice cold PBS and stored in 4°C PBS for up to 48 hours. Slices were placed in a still RT PBS bath and pyramidal neurons in V1b layer II/III were filled. Identified pyramidal soma were impaled with a sharp micropipette (100-400 MΩ) backfilled with 10 mM Alexa 488 (Thermo Fisher A10436) in 200 mM KCl. Dye was injected by applying a 1.5 V negative current pulse for 5-10 minutes until cell was filled. Multiple cells were filled in each slice. After filling, slices were placed in 4°C 4% PFA for 30 minutes. Slices were mounted on slides with SlowFade gold antifade mountant with DAPI (Thermo Fisher Scientific S36939) and coverslips (22 mm x 50 mm 1.5 thickness) were placed on top and sealed with clear nail polish. Slides were prepped for slices by applying a thick clear nail polish boundary to prevent coverslips from crushing slices.

Imaging: Images were acquired on a Zeiss LSM-880 as 16-bit, 1548 x 1548, 0.08 µm x 0.08 µm images with a 63x oil immersion objective. Exposure parameters were established based on WT samples and all sections were imaged in a single session. A z-stack (0.19 µm slices), spanning the depth of the dendrite was taken for each cell, both basal and apical dendrites were imaged. A minimum of 3 littermate pairs and 3 cells per animal were imaged.

Analysis: Spine analysis was performed using NeuronStudio software (Wearne et al., 2005). A 15um segment of secondary apical or basal dendrite was selected and the number of spines, spine neck length and spine head diameter were measured and classified according to Risher et al. 2014b. Head diameter for mushroom spines was decreased to 0.35µm.

3.6 Acknowledgements

This chapter, in part, is currently being prepared for submission for publication of the material. Bosworth, AP, Weiser Novak, S, Manor, U, Allen NJ. Astrocytic glypican 5 in the synaptic maturation and stabilization of the primary visual cortex. The dissertation author was the primary investigator and author of this material.

3.7 Figures

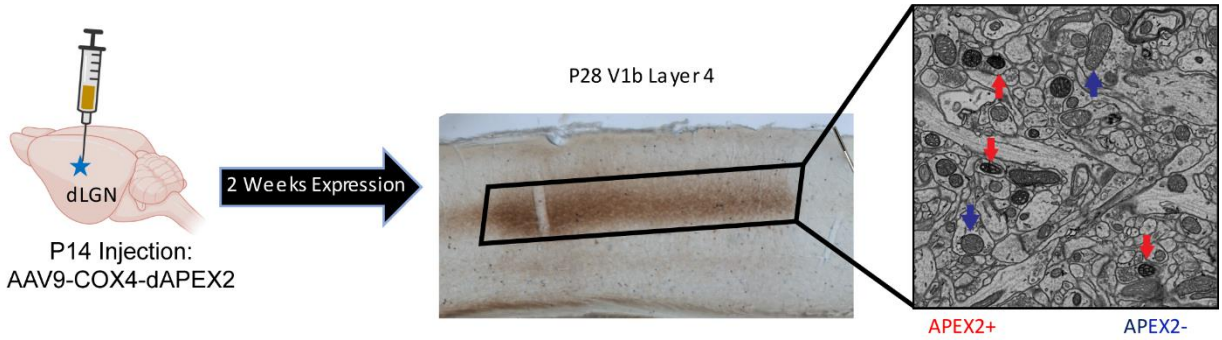

Figure 3.1: Schematic of targeting thalamocortical synapses with APEX2. Genetically encoded EM marker APEX2 was used to selectively identify thalamocortical axons within V1b. **A.** Schematic of experimental design. Mice were injected with AAV9-COX4-DAPEX2 at P14 and collected at P28. Sections of V1b underwent a DAB reaction and were processed for TEM. A ROI in layer 4 was selected based on morphological cell markers, distance from pial surface, and presence of DAB reacted mitochondria. APEX2+ mitochondria indicated by red arrows, APEX2- mitochondria indicated by blue arrows.

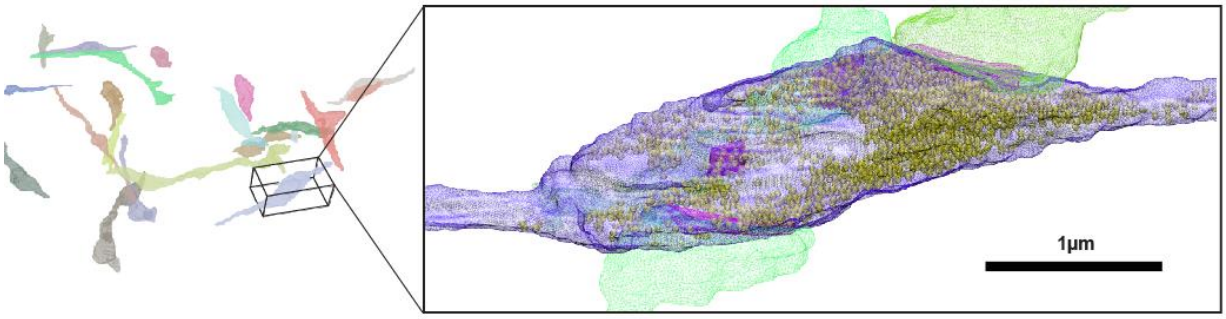

Figure 3.2: 3D reconstruction of APEX2 positive thalamic boutons. Representative reconstruction of a thalamic bouton containing and APEX2 positive mitochondria. Axon in blue, vesicles in yellow, PSD in pink, dendritic spines in green. Scale bar 1µm.

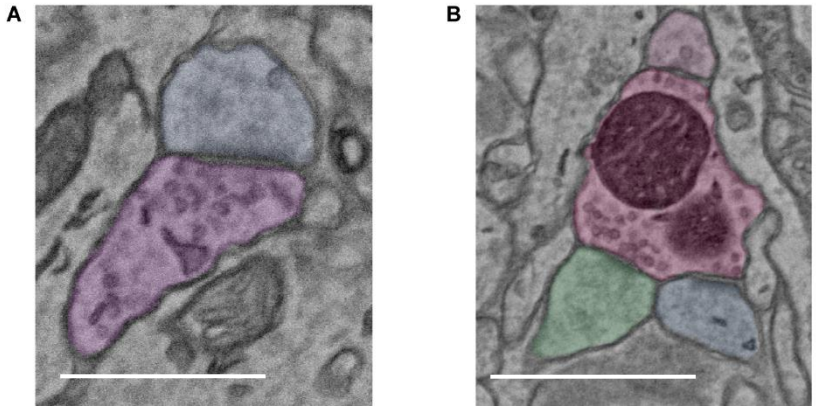

Figure 3.3: Monosynaptic and multisynaptic thalamic boutons. Thalamic boutons receive can have a single postsynaptic partner or multiple postsynaptic partners. **A.** Representative electron micrograph of a monosynaptic thalamic bouton. **B.** Example electron micrograph of a multisynaptic thalamic bouton. Scale bar 1µm.

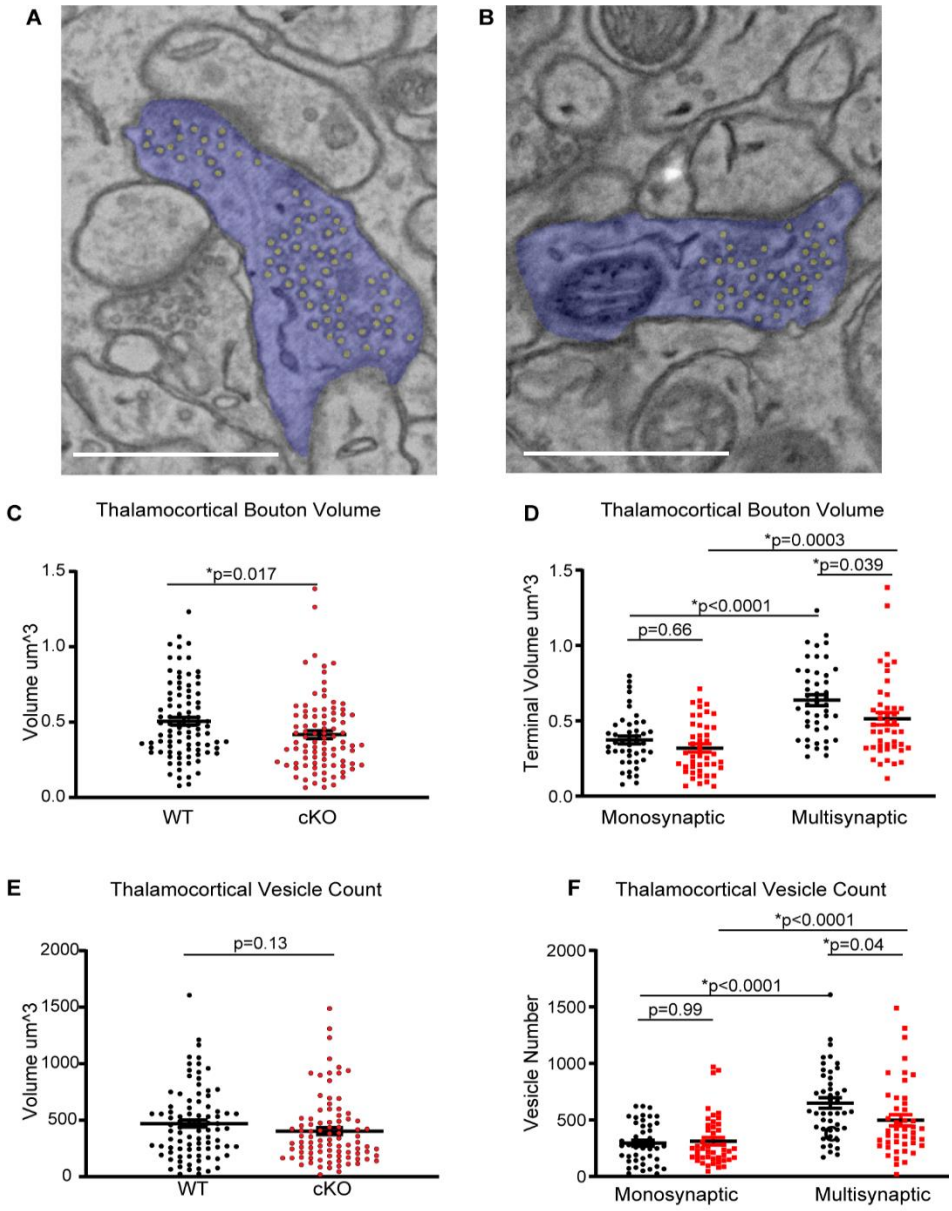

Figure 3.4: Thalamocortical synapses are presynaptically weaker in Gpc5 cKO mice. **A.** Representative electron micrograph of WT thalamic bouton. Vesicles marked in yellow, bouton marked in purple. **B.** Representative electron micrograph of cKO thalamic bouton. Vesicles marked in yellow, axon marked in purple. **C.** Average volume of thalamic boutons is decreased in Gpc5 cKO mice. N=90 boutons/2 mice. **D.** Volume of multisynaptic, but not monosynaptic, axonal boutons is decreased in Gpc5 cKO mice. There is a significant difference in the volume of monosynaptic and multisynaptic boutons in both WT and cKO mice. **E.** Average number of synaptic vesicles is unchanged in Gpc5 cKO mice. N=90 boutons/2 mice. **F.** The number of synaptic vesicles in multisynaptic axonal boutons is significantly decreased in cKO mice. There is a significant difference in the number of vesicles present within monosynaptic and multisynaptic axonal boutons in both WT and cKO mice. N=45 boutons/2 mice. Graphs show mean ± SEM. Individual data points represent boutons. C,E Statistics by T test. D,F statistics by two way ANOVA. Significance stated on graph. Scale bar 1µm.

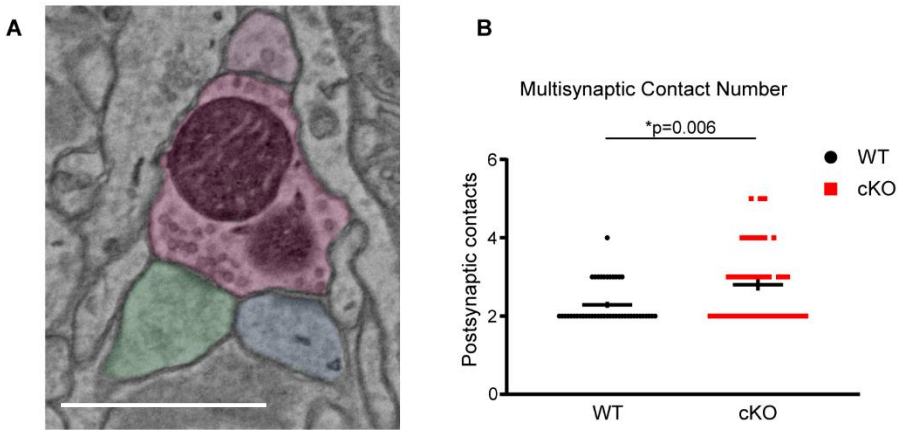

Figure 3.5: Multisynaptic thalamic boutons have a greater number of postsynaptic partners in Gpc5 cKO. **A.** Representative electron micrograph of multisynaptic thalamic bouton. **B.** The number of postsynaptic contacts at multisynaptic boutons is increased in Gpc5 cKO mice. The maximum number of postsynaptic partners is also greater in Gpc5 cKO mice. N=45 boutons/2 mice. Graphs show mean ± SEM. Individual data points represent boutons. Statistics by Mann-Whitney. Significance stated on graph. Scale bar 1µm.

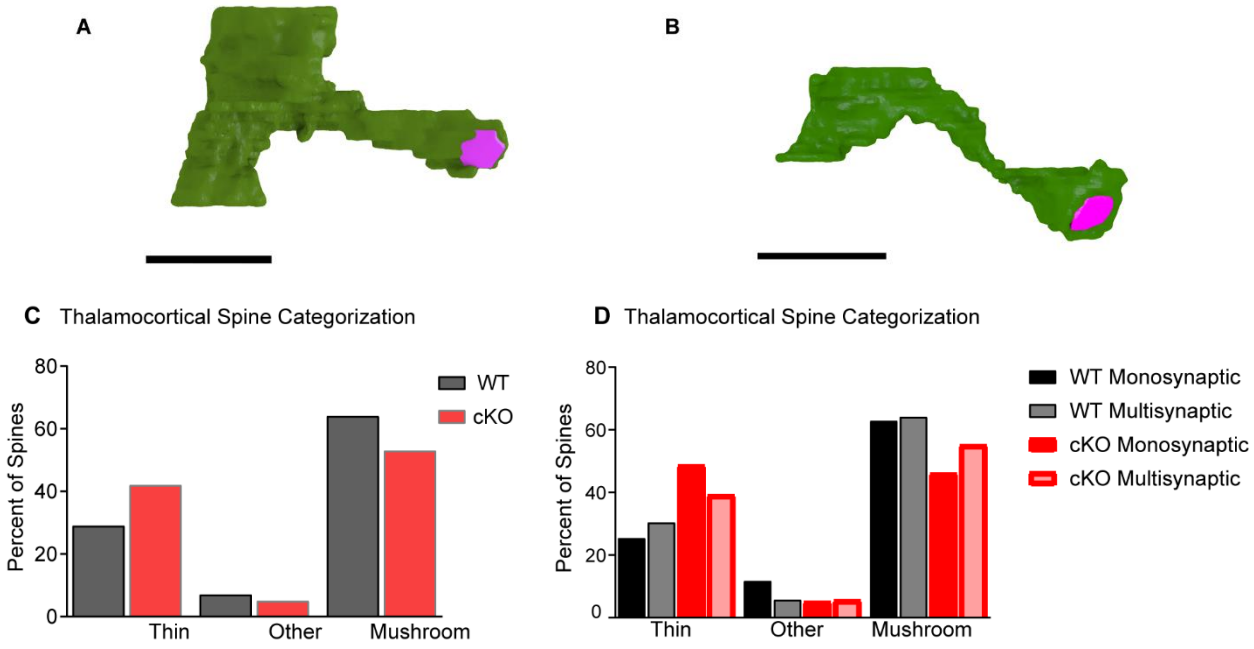

Figure 3.6: Thalamocortical dendritic spines have altered structure in Gpc5 cKO mice. **A**. Example image of reconstructed thin filopodia-like dendritic spine. **B**. Example image of reconstructed mature mushroom dendritic spine. **C.** Dendritic spine structure is shifted to more immature state in cKO mice. N=90 boutons/2mice **D.** Dendritic spine structure is shifted towards a more immature state in both monosynaptic and multisynaptic boutons. Prevalence of thin spines is increased, and prevalence of mushroom spines is decreased at both monosynaptic and multisynaptic APEX2 positive synapses. Other category includes stubby spines and synapses directly onto the dendritic shaft. Spines were reconstructed from N=90 boutons/2 mice. Scale bar 1 µm.

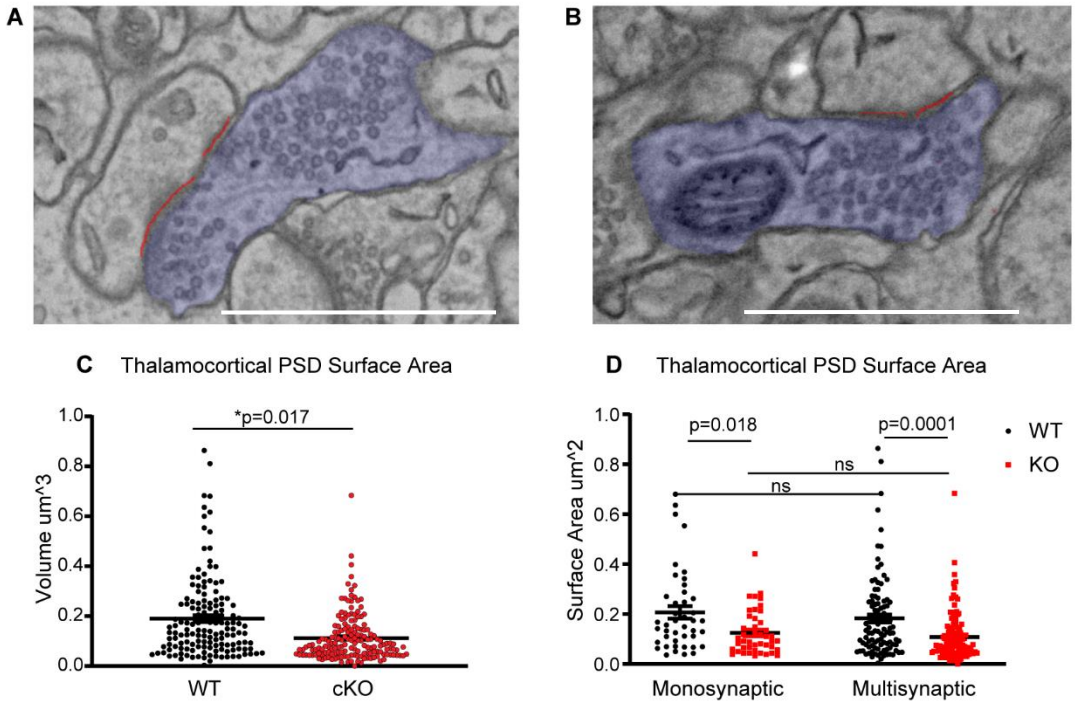

Figure 3.7: Thalamocortical synapses are postsynaptically weaker in Gpc5 cKO mice. **A.** Example Image of WT PSD. PSD marked in red, axon marked in purple. **B.** Example image of cKO PSD. PSD marked in red, axon in purple. **C.** The surface area of the PSD at APEX2 positive thalamocortical synapses is decreased in Gpc5 cKO mice. N=90 boutons/2 mice. **D.** The surface area of the PSD is decreased for both monosynaptic and multisynaptic boutons in Gpc5 cKO mice. N=45 boutons/2 mice. Graphs show mean ± SEM. Individual data points represent boutons. Statistics by two-way ANOVA. Significance stated on graph. Scale bar 1 µm.

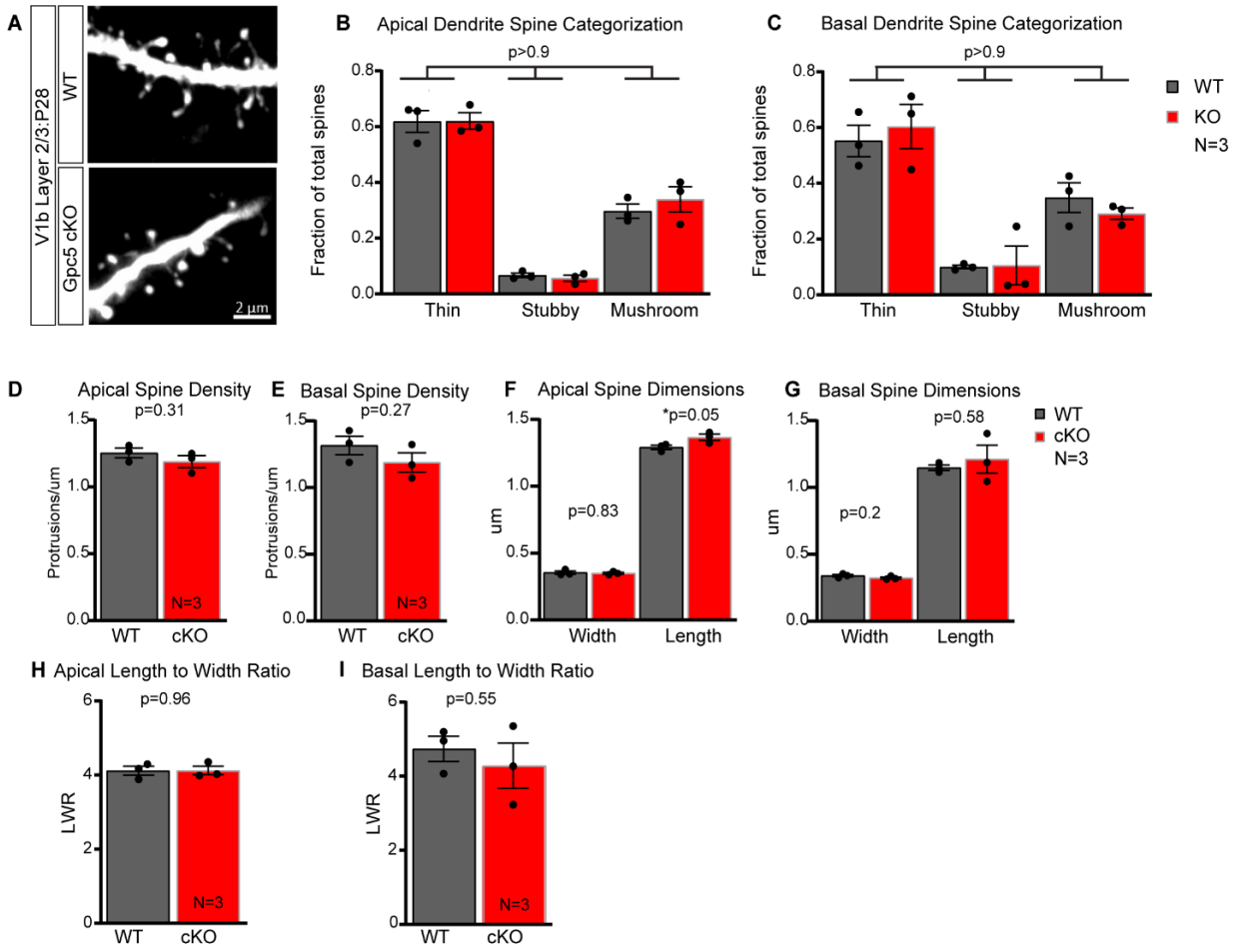

Figure 3.8: Layer 2/3 excitatory synapses are structurally intact in Gpc5 cKO. Layer 2/3 pyramidal neurons were filled with fluorescent dye AF488 to asses structural postsynaptic changes in Gpc5 cKO mice. Spine structure was assessed on secondary basal and apical dendrites **A.** Representative images of layer 2/3 pyramidal cell fills. **B,C.** Categorization of spine shape on apical and basal dendrites. There is no shift in the spine shape in Gpc5 cKO mice at these synapses. Spine shape was determined based off of Risher et al., 2014. **D,E.** Quantification of spine density from A for apical and basal dendrites respectively. **F,G.** Quantification of spine length and diameter from A for apical and basal dendrites respectively. **H,I.** Ratio of spine neck length to spine head width from A for apical and basal dendrites. N=3 mice. Graphs show mean ± SEM. Individual data points represent mice. B-I: Statistics by T-test. Significance shown on graph.

3.8 References

Allen, N. J. (2013). Role of glia in developmental synapse formation. In *Current Opinion in Neurobiology* (Vol. 23, Issue 6, pp. 1027–1033). https://doi.org/10.1016/j.conb.2013.06.004

Arellano, J. I., Benavides-Piccione, R., DeFelipe, J., & Yuste, R. (2007). Ultrastructure of Dendritic Spines: Correlation Between Synaptic and Spine Morphologies. *Frontiers in Neuroscience*, *1*(1), 131. https://doi.org/10.3389/NEURO.01.1.1.010.2007

Ballesteros-Yáñez, I., Benavides-Piccione, R., Elston, G. N., Yuste, R., & DeFelipe, J. (2006). Density and morphology of dendritic spines in mouse neocortex. *Neuroscience*, *138*(2), 403–409. https://doi.org/10.1016/J.NEUROSCIENCE.2005.11.038

Berry, K. P., & Nedivi, E. (2017). Spine dynamics: Are they all the same? *Neuron*, *96*(1), 43. https://doi.org/10.1016/J.NEURON.2017.08.008

Bopp, R., Holler-Rickauer, S., Martin, K. A. C., & Schuhknecht, G. F. P. (2017). An Ultrastructural Study of the Thalamic Input to Layer 4 of Primary Motor and Primary Somatosensory Cortex in the Mouse. *The Journal of Neuroscience*, *37*(9), 2435. https://doi.org/10.1523/JNEUROSCI.2557-16.2017

Bushong, E. A., Martone, M. E., Jones, Y. Z., & Ellisman, M. H. (2002). Protoplasmic Astrocytes in CA1 Stratum Radiatum Occupy Separate Anatomical Domains. *Journal of Neuroscience*, *22*(1), 183–192. https://doi.org/10.1523/JNEUROSCI.22-01-00183.2002

Grillo, F. W., Song, S., Teles-Grilo Ruivo, L. M., Huang, L., Gao, G., Knott, G. W., MacO, B., Ferretti, V., Thompson, D., Little, G. E., & de Paola, V. (2013). Increased axonal bouton dynamics in the aging mouse cortex. *Proceedings of the National Academy of Sciences of the United States of America*, *110*(16). https://doi.org/10.1073/PNAS.1218731110

Han, Z.-S., Buhl, E. H., Lörinczi, Z., & Somogyi, P. (1993). A High Degree of Spatial Selectivity in the Axonal and Dendritic Domains of Physiologically Identified Local-circuit Neurons in the Dentate Gyms of the Rat Hippocampus. *European Journal of Neuroscience*, *5*(5), 395–410. https://doi.org/10.1111/J.1460-9568.1993.TB00507.X

Harnett, M. T., Makara, J. K., Spruston, N., Kath, W. L., & Magee, J. C. (2012). Synaptic amplification by dendritic spines enhances input cooperativity. *Nature*, *491*(7425), 599. https://doi.org/10.1038/NATURE11554

Harris, K. M., & Stevens, J. K. (1989). Dendritic spines of CA 1 pyramidal cells in the rat hippocampus: serial electron microscopy with reference to their biophysical characteristics. *Journal of Neuroscience*, *9*(8), 2982–2997. https://doi.org/10.1523/JNEUROSCI.09-08-02982.1989

Helm, M. S., Dankovich, T. M., Mandad, S., Rammner, B., Jähne, S., Salimi, V., Koerbs, C., Leibrandt, R., Urlaub, H., Schikorski, T., & Rizzoli, S. O. (2021). A large-scale nanoscopy

and biochemistry analysis of postsynaptic dendritic spines. *Nature Neuroscience 2021 24:8*, *24*(8), 1151–1162. https://doi.org/10.1038/s41593-021-00874-w

Jan Tønnesen, Gergely Katona, Balazs Rózsa, & U Valentin Nägerl. (2014). Spine neck plasticity regulates compartmentalization of synapses. *Nature Neuroscience*, *17*(5), 678–685. https://doi.org/10.1038/NN.3682

Jennifer N, B., & Kristen M, H. (2008). Balancing structure and function at hippocampal dendritic spines. *Annual Review of Neuroscience*, *31*, 47–67. https://doi.org/10.1146/ANNUREV.NEURO.31.060407.125646

Kamimura, K., & Maeda, N. (2021). Glypicans and Heparan Sulfate in Synaptic Development, Neural Plasticity, and Neurological Disorders. *Frontiers in Neural Circuits*, *0*, 2. https://doi.org/10.3389/FNCIR.2021.595596

Kano, M., & Watanabe, T. (2019). Developmental synapse remodeling in the cerebellum and visual thalamus. *F1000Research*, *8*. https://doi.org/10.12688/F1000RESEARCH.18903.1

Knott, G. W., Holtmaat, A., Wilbrecht, L., Welker, E., & Svoboda, K. (2006). Spine growth precedes synapse formation in the adult neocortex in vivo. *Nature Neuroscience 2006 9:9*, *9*(9), 1117–1124. https://doi.org/10.1038/nn1747

Kucukdereli, H., Allen, N. J., Lee, A. T., Feng, A., Ozlu, M. I., Conatser, L. M., Chakraborty, C., Workman, G., Weaver, M., Sage, E. H., Barres, B. A., & Eroglu, C. (2011). Control of excitatory CNS synaptogenesis by astrocyte-secreted proteins hevin and SPARC. *Proceedings of the National Academy of Sciences of the United States of America*, *108*(32). https://doi.org/10.1073/PNAS.1104977108

Lam, S. S., Martell, J. D., Kamer, K. J., Deerinck, T. J., Ellisman, M. H., Mootha, V. K., & Ting, A. Y. (2014). Directed evolution of APEX2 for electron microscopy and proximity labeling. *Nature Methods 2014 12:1*, *12*(1), 51–54. https://doi.org/10.1038/nmeth.3179

Luo, H., Hasegawa, K., Liu, M., & Song, W.-J. (2017). Comparison of the Upper Marginal Neurons of Cortical Layer 2 with Layer 2/3 Pyramidal Neurons in Mouse Temporal Cortex. *Frontiers in Neuroanatomy*, *0*, 115. https://doi.org/10.3389/FNANA.2017.00115

Nahmani, M., & Erisir, AVGluT2 immunochemistry identifies thalamocortical terminals in layer 4 of adult and developing visual cortex. *Journal of Comparative Neurology*, *484*(4), 458–473. https://doi.org/10.1002/CNE.20505

Nakahata, Y., & Yasuda, R. (2018). Plasticity of Spine Structure: Local Signaling, Translation and Cytoskeletal Reorganization. *Frontiers in Synaptic Neuroscience*, *10*(AUG), 29. https://doi.org/10.3389/FNSYN.2018.00029

Ofer, N., Berger, D. R., Kasthuri, N., Lichtman, J. W., & Yuste, R. (2021). Ultrastructural analysis of dendritic spine necks reveals a continuum of spine morphologies. *Developmental Neurobiology*, *81*(5), 746–757. https://doi.org/10.1002/DNEU.22829

Risher, W. C., Patel, S., Kim, I. H. wan, Uezu, A., Bhagat, S., Wilton, D. K., Pilaz, L. J., Singh Alvarado, J., Calhan, O. Y., Silver, D. L., Stevens, B., Calakos, N., Soderling, S. H., & Eroglu, C. (2014). Astrocytes refine cortical connectivity at dendritic spines. *ELife*, *3*. https://doi.org/10.7554/eLife.04047

Risher, W. C., Ustunkaya, T., Singh Alvarado, J., & Eroglu, C. (2014). Rapid Golgi Analysis Method for Efficient and Unbiased Classification of Dendritic Spines. *PLoS ONE*, *9*(9), e107591. https://doi.org/10.1371/journal.pone.0107591

Rodriguez-Moreno, J., Rollenhagen, A., Arlandis, J., Santuy, A., Merchan-Pérez, A., DeFelipe, J., Lübke, J. H. R., & Clasca, F. (2018). Quantitative 3D Ultrastructure of Thalamocortical Synapses from the "Lemniscal" Ventral Posteromedial Nucleus in Mouse Barrel Cortex. *Cerebral Cortex (New York, NY)*, *28*(9), 3159. https://doi.org/10.1093/CERCOR/BHX187

Sarrazin, S., Lamanna, W. C., & Esko, J. D. (2011). Heparan Sulfate Proteoglycans. *Cold Spring Harbor Perspectives in Biology*, *3*(7), 1–33. https://doi.org/10.1101/CSHPERSPECT.A004952

Singh, S. K., Stogsdill, J. A., Pulimood, N. S., Dingsdale, H., Kim, Y. H., Pilaz, L. J., Kim, I. H., Manhaes, A. C., Rodrigues, W. S., Pamukcu, A., Enustun, E., Ertuz, Z., Scheiffele, P., Soderling, S. H., Silver, D. L., Ji, R. R., Medina, A. E., & Eroglu, C. (2016). Astrocytes Assemble Thalamocortical Synapses by Bridging NRX1?? and NL1 via Hevin. *Cell*, *164*(1–2), 183–196. https://doi.org/10.1016/j.cell.2015.11.034

Vints, K., Vandael, D., Baatsen, P., Pavie, B., Vernaillen, F., Corthout, N., Rybakin, V., Munck, S., & Gounko, N. v. (2019). Modernization of Golgi staining techniques for high-resolution, 3-dimensional imaging of individual neurons. *Scientific Reports 2019 9:1*, *9*(1), 1–14. https://doi.org/10.1038/s41598-018-37377-x

Yoshihara, Y., de Roo, M., & Muller, D. (2009). Dendritic spine formation and stabilization. *Current Opinion in Neurobiology*, *19*(2), 146–153. https://doi.org/10.1016/J.CONB.2009.05.013

Zhang, Q., Lee, W.-C. A., Paul, D. L., & Ginty, D. D. (2019). Multiplexed peroxidase-based electron microscopy labeling enables simultaneous visualization of multiple cell types. *Nature Neuroscience 2019 22:5*, *22*(5), 828–839. https://doi.org/10.1038/s41593-019-0358-7

4 Glypican 5 and Ocular Dominance Plasticity

4.1 Introduction

During the critical period there is a high level of plasticity within the visual cortex, and brief periods of sensory deprivation are sufficient to alter the neural connectivity within the binocular zone. Binocular neurons in the mouse visual cortex receive information from both eyes, and exhibit ocular dominance (OD), responding predominantly to either ipsilateral or contralateral visual inputs. This OD is organized by competition between inputs from the two eyes. The synaptic connections are stable early in life and adulthood but in between experience a period of enhanced activity-dependent plasticity known as a critical period (Grutzendler et al., 2002). The visual critical period in the mouse opens around P21, after eye opening, and closes near P35 (Espinosa & Stryker, 2012). The critical period typically studied in the visual system refers to the period of increased OD plasticity during which monocular deprivation can rapidly and significantly alter the ocular dominance of the cortical neurons (Berardi et al., 2000). After this time, the binocular cortical circuitry is mature and the amount of observed OD plasticity is greatly diminished (Yu et al., 2012). There is also an age dependent decrease in structural and functional plasticity, and in the adult visual cortex, the majority of synaptic connections remain stable for more than a year (Gilbert & Li, 2012; Grutzendler et al., 2002; Levy et al., 2014).

The cortical response to monocular deprivation in adults differs from that of juveniles. Prior to the closing of the critical period, 3 days of monocular deprivation causes a rapid decrease in the response to the deprived eye (2days) and a slower increase in the response to the non-deprived eye (5 days) (Hübener & Bonhoeffer, 2014). This alters the ratio of contralateral vs. ipsilateral response strength and constitutes an OD shift. In the adult, prolonged monocular deprivation (7 days) is required to induce an OD shift which is the result of a slow increase in

response to the non-deprived eye (Gilbert & Li, 2012). It is interesting to note that in the absence of the rapid depression of responses to the deprived eye (2 days), the necessary monocular deprivation reflects the time course of the slower potentiation of responses to the non-deprived eye (7 days). In addition to requiring a longer monocular deprivation protocol to yield an OD shift, the magnitude of the shift is diminished relative to juvenile animals (He et al., 2006; Sato & Stryker, 2008a; Yoshimura et al., 2003).

There are synaptic features which are associated with a more plastic state, two of which are decreased synaptic GluA2 content and immature synaptic structure (Blanco-Suarez et al., 2018). The Gpc5 cKO mice have decreased GluA2 content at intracortical synapses as well as immature synapse structure at thalamocortical synapses, including fewer mushroom spines and increased number of synaptic contacts at multisynaptic boutons. This led us to ask whether the Gpc5 cKO mice would show enhanced experience dependent plasticity in the visual cortex during the critical period and in adulthood.

4.2 Glypican 5 and ocular dominance plasticity during the critical period

Monocular enucleation at the peak of the critical period induces ocular dominance plasticity and causes a shift in the synaptic responsiveness of neurons in the binocular zone away from the deprived eye and towards the nondeprived eye. To assess this, mice were monocularly deprived by removing one eye during peak critical period (P28). Following enucleation, mice were returned to their cage for 12hrs or 5 days after which they were exposed to 30 minutes of bright light. This brief period of light stimulation is sufficient to induce the expression of the immediate early gene Arc in the activated neurons of the primary visual cortex, including the binocular zone (Figure 4.1 A). Following light exposure, the brains were collected, and we performed smFISH to visualize Arc expression i.e. activated neurons in the binocular zone. The

width of the Arc signal provides a readout of the size of the binocular zone innervated by the intact eye and expansion of the Arc signal, following monocular enucleation, provides a measurement of the induced ocular dominance plasticity. We found that the size of V1b following 12hrs of deprivation, a period insufficient to induce remodeling, is unchanged in the Gpc5 cKO mice (mean(μm) ± SEM, WT=1012 ± 19.94, cKO=1036 ± 10.46, p=0.11) indicating that the absence of astrocytic Gpc5 does not alter baseline connectivity in V1b (Figure 4.1 C). In both the WT and Gpc5 cKO mice, 5 days of monocular deprivation is sufficient to significantly increase the width of the Arc signal (Average increase(μm), WT=369, WT 12Hr vs. WT 5D p=<0.0001, cKO=338.2, cKO 12Hr vs cKO 5D p=<0.0001) indicating remodeling of V1b activated by input from the intact eye. Furthermore, we found no significant difference between WT and Gpc5 cKO mice in the width of the Arc signal following 5 days of deprivation (mean(μm) ± SEM, WT=1381 ± 15.63, cKO=1374 ± 8.412, p=0.70) (Figure 4.1 C).

These experiments demonstrate that lack of Gpc5 in astrocytes does not affect large scale sensory remodeling during the critical period. It is possible that astrocyte Gpc5 does regulate some aspects of plasticity during the critical period, but the extensive amount of plasticity inherent to the critical period occludes any effect. As Gpc5 remains highly expressed in the adult brain, when plasticity is lower, this led us to ask if adult mice lacking Gpc5 show differences in plasticity in response to monocular deprivation.

4.3 Glypican 5 and ocular dominance plasticity in the adult

In adulthood, the high level of experience dependent plasticity present during the critical period is lost, and brief periods of sensory deprivation are insufficient to induce remodeling in the binocular zone. Although the composition of the V1b intracortical and thalamocortical synapses in adult Gpc5 cKO mice suggests that these synapses have matured, there remains a persistent

diminishment of the layer 1 colocalization of GluA2 and vGluT1, and decreased number of vGluT2 boutons in layer 4. This, combined with the observation that Gpc5 expression by astrocytes remains high in the adult brain, led us to ask if there is increased ocular dominance plasticity as a result of incomplete synaptic maturation in Gpc5 cKO mice.

To assess this, we again performed the Arc FISH assay to probe for changes in V1b neural connectivity following a brief period of monocular enucleation in adult P120 mice. Mice were monocularly enucleated and returned to their home cage for 12 hrs or 5 days after which they were subjected to 30 minutes of bright light. Upon collection, we performed FISH and measured the width of the Arc signal in the binocular zone (Figure 4.2 A). Once again, we found no difference in the width of the Arc signal between the WT and cKO mice following 12 hrs of deprivation (mean(μm) ± SEM, WT=1093 ± 9.65, cKO=1077 ± 9.83, p=0.16), indicating no baseline changes in cortical connectivity in the Gpc5 cKO mice at P120 (Figure 4.2 C). After 5 days of deprivation, we found a significant increase in the width of the Arc signal in the Gpc5 cKO mice but not in the WT mice (Increase(μm), WT=54.1, WT 12Hr vs WT 5D p=0.91, cKO=163.9, cKO 12Hr vs cKO 5D p=<0.0001). The total width of the V1b Arc signal is also significantly increased in the cKO mice following 5 days of deprivation (mean(μm) ± SEM, WT=1147 ± 15.04, cKO=1241 ± 27.57, p=0.005) (Figure 4.2 C).

In light of the large developmental deficit observed in the Gpc5 cKO mice, we wanted to determine if the enhanced plasticity in the adult was the result of incomplete synaptic maturation or a true indication of an ongoing role of Gpc5 in the adult mouse. In order to do this, we generated an astrocyte specific inducible knock out mouse. We accomplished this by crossing floxed-Gpc5 mice (Gpc5tm1c(KOMP)Wtsi) to an astrocyte specific Aldh1l1 inducible cre recombinase line (B6N.FVB-Tg(Aldh1l1-cre/ERT2)1Khakh/J), and compared Gpc5fl/fl cre negative (WT) and

Gpc5fl/fl cre positive (cKO) littermate pairs for all experiments. All mice were treated with tamoxifen for 5 days at P21 to induce the recombination Gpc5 and were collected at P120. To determine if Gpc5 expression, in the inducible cKO line, has been reduced in astrocytes across layers 1-6, we used smFISH (RNAscope). The V1b of WT and cKO littermate pairs at P120 was probed for Gpc5 mRNA, along with an astrocyte probe, Glast (Slc1a3). Gpc5 expression was analyzed within the boundary of Glast positive cells. In inducible cKO mice, Gpc5 expression is decreased in astrocytes (Threshold area (μm2) ± SEM, WT=6.4 ± 0.3, cKO=5.7 ± 1.1, p=0.38). demonstrating the efficacy of the approach (Figure 4.3 A). Inducible cKO mice retain a significant amount of Gpc5 due to incomplete astrocytic recombination and OPC expression.

To assess plasticity in the adult inducible KO mice, we again performed the Arc FISH assay to probe for changes in V1b neural connectivity following a brief period of monocular enucleation in adult P120 mice. Mice were monocularly enucleated and returned to their home cage for 5 days, after which they were subjected to 30 minutes of bright light. Upon collection, we performed FISH and measured the width of the Arc signal in the binocular zone (Figure 4.2 A). In preliminary experiments, we discovered, after 5 days of deprivation, the total width of the V1b Arc signal is significantly increased in the inducible KO mice compared to WT (mean(μm) ± SEM, WT=1043 ± 1 cKO=1140 ± 25, p=0.0029) (Figure 4.3 B).

Although the extent of V1b expansion in the Gpc5 cKO adult is not as large as during the critical period, the significant increase in Arc signal indicates that the absence of astrocytic Gpc5 is sufficient to allow cortical remodeling in the adult. The preliminary evidence of cortical remodeling in the inducible Gpc5 cKO is evidence that Gpc5 is directly repressing plasticity in the adult and not simply the result of incomplete maturation or development. The presence of remodeling in the adult Gpc5 cKO supports the hypothesis that the plasticity enhancing effects of

removing Gpc5 may have been occluded when the levels of plasticity were probed during the critical period.

4.4 Discussion

During the critical period, there is a plethora of mechanisms underlying the large-scale plasticity that is occurring (Espinosa & Stryker, 2012). Visual experience such as monocular deprivation or binocular deprivation is sufficient to induce changes in excitability as well as remodeling of thalamocortical synapses (Coleman et al., 2010; Maffei et al., 2004). Additionally, these visual interventions alter the binocular matching of thalamocortical synapses (Wang et al., 2010). These changes are the result of the addition and removal of thalamocortical synapses, in addition to strengthening and weaking of existing synapses. As Gpc5 appears to have a role in the structure and strength of thalamocortical synapses, it is conceivable that it also plays a role in controlling plasticity within V1b. The absence of plasticity phenotype in the Gpc5 cKO mice during the critical period does not necessarily mean that Gpc5 is not playing a role. It is conceivable that the enhanced plasticity resulting from the removal of Gpc5 is occluded by the large amount of plasticity that is present. This hypothesis is supported by the enhanced plasticity observed in the adult Gpc5 cKO mice. Adult mice have minimal plasticity and therefore the effect of Gpc5 removal can be observed. The presence of enhanced plasticity in the inducible astrocytic Gpc5 KO also indicates that Gpc5 is indeed involved in the repression of plasticity in the adult.

In adult mice, sensory deprivation leads to a decrease in the range of axonal bouton sizes and fewer large and small boutons are observed (Sammons et al., 2018). As bouton volume can be measured as a proxy for synaptic strength, this indicates that synapses trend towards a homeostatic median strength (Knott et al., 2006; Sammons et al., 2018). As axonal bouton size moves towards the mean, the potential for synapses weakening and strengthening increases and

synapses effectively increase their functional range. Gpc5 cKO mice, with their unrefined and weakened thalamocortical synapses, may initially have a larger functional range than WT mice. This possibility is particularly intriguing when we consider that OD shifts in adult animals are driven by the potentiation of remaining visual input (Sato & Stryker, 2008b). In this way, Gpc5 could be repressing plasticity in the adult through the stabilization of mature, persistent synapses. Further support that astrocytic Gpc5 acts as a synaptic stabilizer, rather than being involved in the formation of synapses is that MD during the critical period induces transient changes in the density of dendritic spines in L2/3 and 5 but not in layer 4 (Montey & Quinlan, 2011). As thalamocortical terminals in layer 4 appear to be a primary target of astrocytic Gpc5, it is unlikely that it is involved in spine formation or pruning. Astrocytic Gpc5 as a thalamocortical stabilization factor would agree with both the developmental synaptic weakness and instability as well as the enhanced adult plasticity observed in the cKO.

4.5 Methods

Astrocyte specific inducible knock out mice: In order to selectively remove Gpc5 from astrocytes, homozygous Gpc5 floxed mice were crossed to the astrocyte specific Aldh1l1 inducible cre recombinase line, B6N.FVB-Tg(Aldh1l1-cre/ERT2)1Khakh/J. Gpc5 floxed mice were generated by KOMP/MMRRC/EUCOMM as conditional ready mice. Gpc5 strain was received as the tm1a allele (C57BL/6N-Atm1Brd Gpc5tm1a(KOMP)Wtsi/, MMRRC Stock #: 047921-UCD) and crossed with mice expressing the Flp recombinase (B6.129S4-Gt(ROSA)26Sortm1(FLP1)Dym/RainJ , Jax stock number 009086) to generate Gpc5tm1c(KOMP)Wtsi (UC Davis KOMP repository, project ID CSD76974) in which exon 3 is floxed. Upon exposure to cre recombinase, exon 3 is excised, causing a frameshift and premature stop codon, leading to a nonsense mediated decay of the mRNA. All experiments were performed

using cre negative WT and cre positive cKO littermate pairs. Tamoxifen was administered to induce recombination at P21. 5 days of IP tamoxifen administration, 75mg/kg tamoxifen diluted in corn oil at 20 mg/ml. Mice of both genders were used.

Characterization of ocular dominance plasticity: Astrocyte specific Gpc5 ko mice

Monocular enucleation: Littermate pairs of Gpc5 WT and KO mice were used for experiments during the critical period at P28 and after the critical period at P120. Mice were anesthetized with 2% isoflurane in oxygen and the right eye was removed via transection of the optic nerve. The empty ocular cavity was filled with Gelfoam (Pfizer 031508) and eyelid was sutured closed with 6-0 silk sutures (Henry Schein 101-2636). Erthromycin 0.5% and lidocaine 2% were applied to sutured eyelid. Normal reared, control mice, were collected 12 hours later. Monocularly deprived mice were collected after 5 days of 12 hour light/12 hour dark cycle. Mice were collected at the end of a 12 hour dark cycle and subjected to 30 mins of light to trigger Arc expression in the visual cortex.

Tissue Collection:

Fluorescent *in situ* hybridization: Littermate mice (GFAP Cre x Gpc5 fl/fl WT and KO) were used at ages P28 and P120 to analyze Arc expression following monocular expression. Fresh frozen, 18 µm coronal sections (3.4 mm posterior to Bregma) were collected using a cryostat (Hacker Industries OTF5000). Fluorescent (FISH) (ACDbio 320850) *in situ* hybridization was performed following manufacturer's instructions for fresh frozen tissue. Slides were briefly frozen at -20C for 20 minutes, followed by 15 minutes in PFA at 4C. Sections then underwent dehydration via 5 minute washes in 50%, 75%, and 100% (x2) ethanol. Following dehydration, sections were incubated with Protease 3 (P28) or Protease 4 (P120) for 15 minutes at room temperature and then washed 2 times in PBS. Slides were incubated with target probes for 2 hours

at 40C followed by 3 amplification steps and 1 detection step with RNAscope wash buffer rinses between each step. Sections were mounted with SlowFade gold antifade with DAPI (ThermoFisher Scientific S36939) and applied coverslip (22 mm x 50 mm, 1.5 thickness) was sealed with clear nail polish. Slides were imaged within 1 day or stored at -20C. A single probe was used: Arc (ACDbio 316911). A negative 3-plex probe (ACDbio 320871) was used to determine background signal.

Imaging: Arc was imaged in channel 550. The entire coronal section was imaged at 10X, as 16-bit images, on a Zeiss Axio Imager.Z2 fluorescent microscope with 10% tile overlap. In all experiments, a minimum of 5 littermate pairs and 4 sections per animal were imaged.

Analysis: Arc analysis was performed using the Zen blue edition software (Zeiss) distance tool. The width of the activated binocular zone was measured as the width of the Arc signal in V1b layer IV contralateral to the deprived eye. A minimum of 5 littermate pairs and 4 sections per animal were used for each condition.

4.6 Acknowledgements

This chapter, in part, is currently being prepared for submission for publication of the material. Bosworth, AP, Weiser Novak, S, Manor, U, Allen NJ. Astrocytic glypican 5 in the synaptic maturation and stabilization of the primary visual cortex. The dissertation author was the primary investigator and author of this material.

4.7 Figures

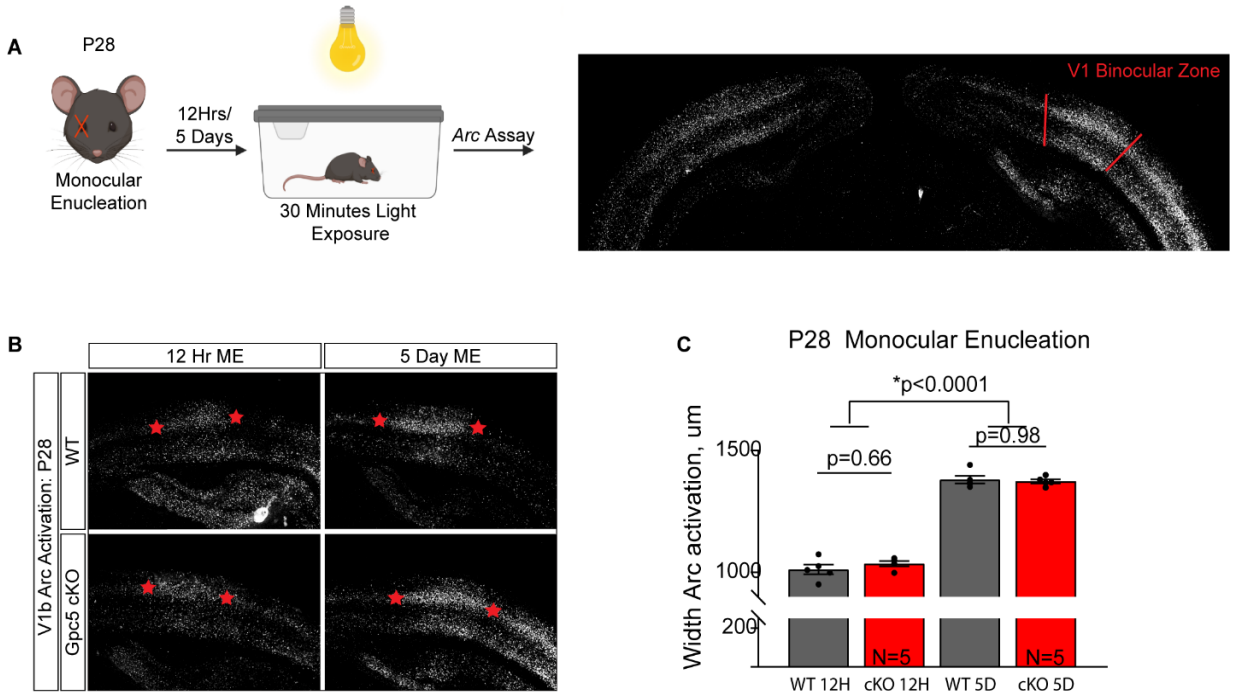

Figure 4.1: Ocular dominance plasticity is unchanged during the critical period. **A.** Schematic of experiment. P28 WT and cKO mice were enucleated and collected after 12hrs or 5 days. Sections of VC were probed for Arc expression. **B**. Representative images of Arc expression in V1b ipsilateral to nondeprived eye 12hrs or 5days after enucleation. **C.** Ocular dominance plasticity is unchanged in P28 Gpc5 cKO mice. Quantification of B. N=5 mice/condition. Graphs show mean ± SEM. Individual data points representing mice. Statistics by two-way ANOVA, significance stated on graph.

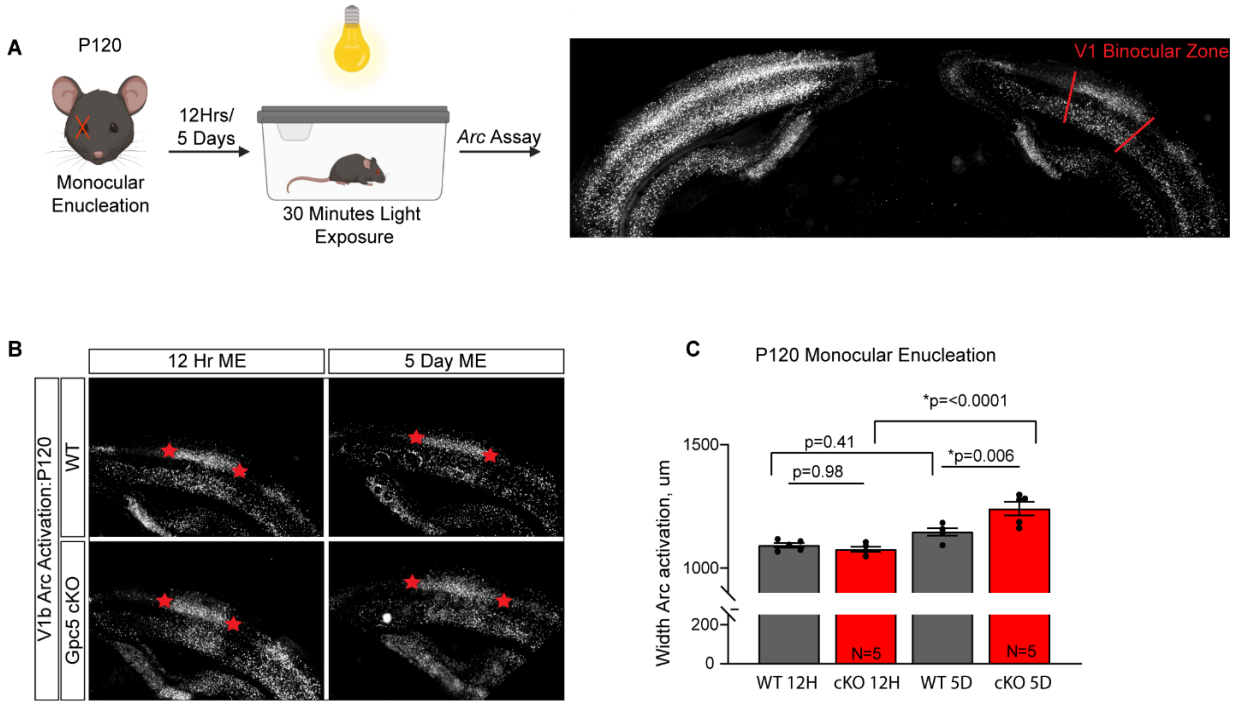

Figure 4.2: Ocular dominance plasticity is enhanced in adult Gpc5 cKO mice. A. Schematic of experiment. P120 WT and cKO mice were enucleated and collected after 12hrs or 5 days. Sections of VC were probed for Arc expression. B. Representative images of Arc expression in V1b ipsilateral to nondeprived eye 12hrs or 5days after enucleation. C. Ocular dominance plasticity is enhanced in P120 Gpc5 cKO mice. Quantification of B. N=5 mice/condition. Graphs show mean ± SEM. Individual data points representing mice. Statistics by two-way ANOVA, significance stated on graph.

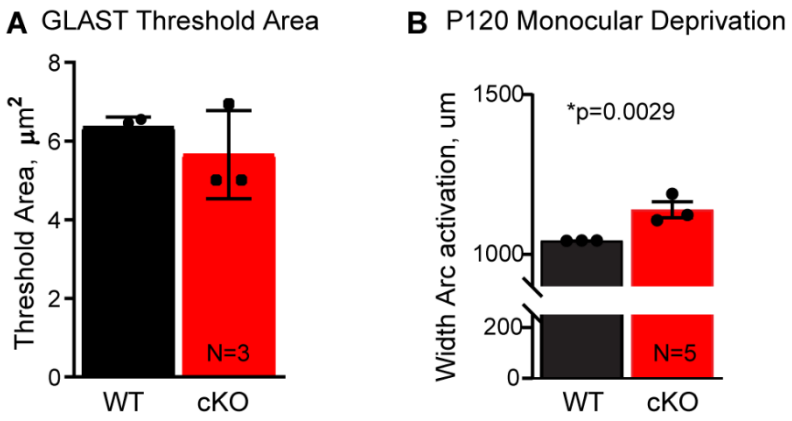

Figure 4.3: Ocular dominance plasticity is enhanced in adult inducible Gpc5 cKO. Preliminary data. **A.** Gpc5 expression is decreased 12% in astrocytes at P120. Recombination induced at P21 through Tamoxifen administration. **B**. Ocular dominance plasticity is enhanced in P120 inducible Gpc5 cKO mice. N=3 mice/condition. Graphs show mean ± SEM. Individual data points representing mice. Statistics by t-test, significance stated on graph.

4.8 References

Berardi, N., Pizzorusso, T., & Maffei, L. (2000). Critical periods during sensory development. *Current Opinion in Neurobiology*, *10*(1), 138–145. https://doi.org/10.1016/S0959-4388(99)00047-1

Coleman, J. E., Nahmani, M., Gavornik, J. P., Haslinger, R., Heynen, A. J., Erisir, A., & Bear, M. F. (2010). Rapid structural remodeling of thalamocortical synapses parallels experience-dependent functional plasticity in mouse primary visual cortex. *Journal of Neuroscience*, *30*(29), 9670–9682. https://doi.org/10.1523/JNEUROSCI.1248-10.2010

Espinosa, J. S., & Stryker, M. P. (2012). Development and plasticity of the primary visual cortex. *Neuron*, *75*(2), 230–249. https://doi.org/10.1016/j.neuron.2012.06.009

Gilbert, C. D., & Li, W. (2012). Adult visual cortical plasticity. *Neuron*, *75*(2), 250–264. https://doi.org/10.1016/j.neuron.2012.06.030

Grutzendler, J., Kasthuri, N., & Gan, W.-B. (2002). Long-term dendritic spine stability in the adult cortex. *Nature 2003 420:6917*, *420*(6917), 812–816. https://doi.org/10.1038/nature01276

He, H.-Y., Hodos, W., & Quinlan, E. M. (2006). Visual Deprivation Reactivates Rapid Ocular Dominance Plasticity in Adult Visual Cortex. *The Journal of Neuroscience*, *26*(11), 2951. https://doi.org/10.1523/JNEUROSCI.5554-05.2006

Hübener, M., & Bonhoeffer, T. (2014). Neuronal Plasticity: Beyond the Critical Period. *Cell*, *159*(4), 727–737. https://doi.org/10.1016/J.CELL.2014.10.035

Knott, G. W., Holtmaat, A., Wilbrecht, L., Welker, E., & Svoboda, K. (2006). Spine growth precedes synapse formation in the adult neocortex in vivo. *Nature Neuroscience 2006 9:9*, *9*(9), 1117–1124. https://doi.org/10.1038/nn1747

Levy, A. D., Omar, M. H., & Koleske, A. J. (2014). Extracellular matrix control of dendritic spine and synapse structure and plasticity in adulthood. *Frontiers in Neuroanatomy*, *8*(OCT). https://doi.org/10.3389/FNANA.2014.00116

Maffei, A., Nelson, S. B., & Turrigiano, G. G. (2004). Selective reconfiguration of layer 4 visual cortical circuitry by visual deprivation. *Nature Neuroscience*, *7*(12), 1353–1359. https://doi.org/10.1038/nn1351

Montey, K. L., & Quinlan, E. M. (2011). Reactivation of thalamocortical plasticity by dark exposure during recovery from chronic monocular deprivation. *Nature Communications*, *2*(1), 317. https://doi.org/10.1038/NCOMMS1312

Sammons, R. P., Clopath, C., & Barnes, S. J. (2018). Size-Dependent Axonal Bouton Dynamics following Visual Deprivation In Vivo. *Cell Reports*, *22*(3), 576. https://doi.org/10.1016/J.CELREP.2017.12.065

Sato, M., & Stryker, M. P. (2008a). Distinctive features of adult ocular dominance plasticity. *The Journal of Neuroscience : The Official Journal of the Society for Neuroscience*, *28*(41), 10278–10286. https://doi.org/10.1523/JNEUROSCI.2451-08.2008

Sato, M., & Stryker, M. P. (2008b). Distinctive features of adult ocular dominance plasticity. *The Journal of Neuroscience : The Official Journal of the Society for Neuroscience*, *28*(41), 10278–10286. https://doi.org/10.1523/JNEUROSCI.2451-08.2008

Wang, B.-S., Sarnaik, R., & Cang, J. (2010). Critical Period Plasticity Matches Binocular Orientation Preference in the Visual Cortex. *Neuron*, *65*(2), 246. https://doi.org/10.1016/J.NEURON.2010.01.002

Yoshimura, Y., Ohmura, T., & Komatsu, Y. (2003). Two Forms of Synaptic Plasticity with Distinct Dependence on Age, Experience, and NMDA Receptor Subtype in Rat Visual Cortex. *The Journal of Neuroscience*, *23*(16), 6557. https://doi.org/10.1523/JNEUROSCI.23-16-06557.2003

Yu, X., Chung, S., Chen, D.-Y., Wang, S., Dodd, S., Walters, J., Isaac, J., & Koretsky, A. (2012). Thalamocortical Inputs Show Post-Critical Period Plasticity. *Neuron*, *74*(4), 731. https://doi.org/10.1016/J.NEURON.2012.04.024

5 Conclusion

5.1 Introduction

In this study, we have demonstrated that astrocytic Gpc5 is involved in synapse stabilization and the timing of excitatory synapse maturation within the visual cortex. The absence of astrocytic Gpc5 is sufficient to reduce the expression of GluA2 at intracortical synapses during the critical period as well as decrease the strength and refinement of thalamocortical synapses. While adult cKO mice recover a mature synaptic AMPA receptor composition, the observed increase in adult OD plasticity provides an intriguing indication that Gpc5 is involved in the repression of plasticity in the adult brain. It is important to note that these effects are observed in the presence of unaltered Gpc5 expression in OPCs, so there are still significant levels of Gpc5 present in the visual cortex.

5.2 Glypican 5 and synaptic structure

Gpc5 is homogenously expressed throughout the cortical layers in the visual cortex and yet the major structural phenotype that we discovered associated with Gpc5 cKO mice was mainly observed at thalamocortical connections. At these terminals we discovered multiple indications of weakened synapses including smaller bouton size, fewer vesicles, and smaller PSD surface area (Harris & Stevens, 1989; Knott et al., 2006). The presence of weakened synapses in conjunction with the larger number of postsynaptic partners suggests that these synapses are not undergoing the maturational process whereby some synapses are strengthened while others are pruned (Allen, 2013; Dufour et al., 2016). During development, axonal bouton volume decreases while vesicle number increases at thalamocortical synapses (Dufour et al., 2016). Gpc5 cKO mice show a deficit in the number of synaptic vesicles at thalamocortical boutons, this deficit may result in premature shrinkage of the axonal boutons, leading to the observed phenotype. A deficit in the number of

synaptic vesicles may be the result of impaired vesicular recruitment or a failure of synapses to stabilize and strengthen. In light of the timing of peak Gpc5 expression during a period of synaptic maturation, it is likely that this factor is necessary for the stabilization of appropriate synapses following excessive synapse formation. In the absence of this strengthening, pruning may be interrupted leading to excessive weaker synaptic connectivity (Allen, 2013; Arellano et al., 2007; Pchitskaya & Bezprozvanny, 2020). Weaker synapses with more immature dendritic spine structure are indicative of a less stable synaptic connection (Harris & Stevens, 1989). In the adult, destabilized axonal boutons have been associated with cognitive decline (Grillo et al., 2013). Interestingly, aged astrocytes have also been shown to have deleterious effects on the size of the neuronal readily releasable pool (Kawano et al., 2012). This is of particular interest as decreased Gpc5 expression has been associated with Alzheimer's disease (Grubman et al., 2019; Lau et al., 2020). Diminished Gpc5 expression may contribute to synaptic loss via the destabilization of axonal boutons and the size of their vesicle clouds. This possibility is supported by the observed decrease in vGluT2 presynaptic sites in adult Gpc5 cKO mice.

It is also possible that Gpc5 is not involved in regulating the stability of thalamocortical axonal boutons and is instead involved in the process of binocular matching. Within the binocular zone of V1, retinogeniculate thalamic inputs from both retinae converge on individual neurons within layer 4 which renders them binocularly responsive. The binocular matching of thalamic inputs is strengthened during the critical period and is weaker in young mice (P15-P21) (Gu & Cang, 2016; Wang et al., 2010). Thalamocortical synapses are refined as layer 4 neurons are tuned to respond to the same orientation selectivity in both eyes. Gpc5 expression peaks just prior to this process of binocular matching and the increased number of postsynaptic targets in cKO mice suggests that thalamocortical synapses are unrefined.

Identifying the mechanism of how astrocytic Gpc5 regulates thalamocortical synapses would elucidate whether the lack of thalamocortical refinement is the result of diminished pruning, aberrant synapse formation, or inhibition of synaptic strengthening and stabilization.

5.3 Glypican 5 and synaptic plasticity

It has been shown that astrocytes secrete multiple factors that are able to either enhance or repress plasticity within the primary visual cortex. We have shown that in the absence of Gpc5, brief visual deprivation is sufficient to increase plasticity in the adult, but not during the critical period. This suggests that Gpc5 may be involved in actively repressing plasticity after the close of the critical period. Astrocyte secreted factors, such as Chrdl1, have been shown to repress plasticity through the recruitment of GluA2 AMPAR subunits (Blanco-Suarez et al., 2018). Although Gpc5 cKO mice have reduced synaptic GluA2 during the critical period, they appear to have recovered GluA2 levels in the adult at most synapses, so it is unlikely that this is the mechanism through which Gpc5 represses plasticity. There is, however, a small reduction in GluA2 in layer 1 where synaptic connections from all cortical layers occur. The neuronal factor PirB also represses plasticity and increased spine density has been seen in these KO mice (Bochner et al., 2014). This is of interest due to the increased spine density observed at thalamocortical boutons in Gpc5 cKO mice during the critical period. Decreased vGluT2 levels in the adult Gpc5 cKO also suggests a stabilization deficit which could increase plasticity. An alternative possibility is that Gpc5 is involved in the recruitment of synaptic vesicles. We have shown that there is a decrease in the number of vesicles within a single thalamic bouton in the absence of Gpc5, which could be the result of impaired vesicular recruitment during development. Recruitment of synaptic vesicles to the readily releasable pool is important for activity dependent plasticity (Wesseling, 2019). If this recruitment process is impaired in the absence of Gpc5, this could alter the

propensity of these thalamocortical synapses to undergo activity dependent plasticity. If the basal size of the readily releasable pool is diminished in the absence of Gpc5, there may be greater potential for plasticity. In the future it will be important to determine if Gpc5 is actively repressing plasticity through the direct regulation of AMPAR subunit composition, synaptic stabilization, or vesicular recruitment. Preliminary evidence from inducible KO mice indicates that the increased plasticity observed in the absence of Gpc5 is not the result of incomplete maturation or an incomplete closure of the critical period in Gpc5 cKO mice. These experiments indicate that Gpc5 is indeed involved with the direct repression of plasticity in the adult and should be pursued further.

5.4 Glypican 5 and synaptic composition

We have shown that the absence of astrocytic Gpc5 delays the normal maturation of intracortical excitatory synapses within the visual cortex, evidenced as a decrease in GluA2 content. The developmental switch to GluA2 containing receptors in layer 2/3 occurs around P12-14 which is when we begin to see an increase in Gpc5 expression (Brill & Huguenard, 2008). This is in contrast to layer 4 which undergoes the developmental switch at P7, potentially explaining why we see a GluA2 deficit in layer 2/3 but not layer 4 (Brill & Huguenard, 2008). Astrocytic involvement in the composition of AMPARs has been shown in multiple studies. Gpc4 and 6 have been found to induce nascent synapse formation via clustering of GluA1 AMPARs, while Chrdl1 and SPARC regulate GluA2 incorporation at synaptic sites (Blanco-Suarez et al., 2018; Farhy-Tselnicker et al., 2017; Jones et al., 2011). These factors are evidence that astrocytes secrete multiple synaptogenic molecules which are involved in shaping the composition of glutamatergic receptors, and we now identify Gpc5 as an additional signal. Alternatively, as thalamorecipient neurons in layer 4 feed directly onto layer 2/3 intracortical neurons, another explanation is that

the AMPAR maturational delay observed at intracortical synapses is the downstream result of unrefined thalamocortical connectivity, which will require further experimentation to resolve.

5.5 Mechanisms of glypican function

While the exact mechanism of Gpc5 action remains to be determined, research regarding other glypicans and HSPGs, suggests that Gpc5 is possibly involved in the formation of trans-synaptic complexes which are integral for the synaptic composition and stabilization of synapses. Additionally, astrocytic Gpc4 acts via Ptprd to induce the presynaptic release of NP1, leading to the clustering of GluA1 AMPARs at the synapse (Farhy-Tselnicker et al., 2017). Neuronal Gpc4 has been shown to bind with the postsynaptic receptor GPR158 to induce presynaptic differentiation (Condomitti et al., 2018). Loss of GPR158 leads to increased synaptic density, with altered dendritic bouton morphology, impaired PSD ultrastructure, and weakened synapses which is very similar to the thalamocortical phenotype in Gpc5 cKO mice (Condomitti et al., 2018). Neuronal Gpc4 also induces synapse formation through the binding of post synaptic LRRTM4(Wit et al., 2013). The postsynaptic LRRTM4 is necessary for synapses development and function and has been shown to bind Gpc1, 3, and 5, in addition to Gpc4(Siddiqui et al., 2013; Wit et al., 2013). Astrocytic Gpc3 has been shown to be sufficient to induce both excitatory and inhibitory synapses when overexpressed in vitro (Yu et al., 2020). Additionally, mice lacking Ext1, the enzyme necessary for heparan sulfate chain elongation, show decreased expression of GluA2 at synapses. Ext1, like Gpcs, has also been implicated in ASD (Irie et al., 2012). The unique actions of neuronal versus astrocytic Gpc4 demonstrate the observation that Gpcs which have been cleaved from the cell surface are involved in synaptogenesis through different mechanisms than Gpcs which are uncleaved. The long heparan sulfate chains of glypicans, make them ideal candidates for forming these trans-synaptic complexes, as their length and number provides a

substrate for interacting with multiple proteins at the same time. Typically it is uncleaved Gpcs, existing on the cell surface, which are involved in the formation of transsynaptic complexes (Kamimura & Maeda, 2021). It is possible that astrocytic Gpc5 may play a completely unique role from OPC Gpc5 in this way. Astrocytic Gpc5 appears to be involved in the stabilization of thalamocortical synapses, which would suggest that it could be carrying out this role through the formation of or interaction with stabilizing transsynaptic complexes. Given the distance of astrocytic processes from the synaptic cleft, it is likely that, if uncleaved, Gpc5 is interacting with an extrasynaptic receptor. If Gpc5 exists on the surface of astrocytes, while being cleaved from the surface of OPCs, or vice versa, this could explain the Gpc5 cKO phenotype despite the significant amount of Gpc5 expression remaining in OPCs. Future studies should investigate whether astrocytic Gpc5 is interacting with one of these receptors, or known pathways (including Ptpr), involved in the formation of trans synaptic complexes, or if there is a unique mechanism through which it is acting. Given the wide range of effects of glypicans on synaptic function, it is no surprise that many of them have been implicated in disorders associated with aberrant glutamatergic signaling such as neuroticism, schizophrenia, and Alzheimer's.

Overall, this study identifies Gpc5 from astrocytes as playing an important role in the timing of synapse maturation and stabilization within the visual cortex. We show that Gpc5 is necessary for the refinement and strengthening of thalamocortical synapses which has implications for the reliability of thalamic input to the visual cortex and intracortical circuit maturation. The impact of astrocytic Gpc5 on adult plasticity and the stabilization of thalamocortical synaptic connections may provide insight into the observed link with Alzheimer's disease.

5.6 Acknowledgements

This chapter, in part, is currently being prepared for submission for publication of the material. Bosworth, AP, Weiser Novak, S, Manor, U, Allen NJ. Astrocytic glypican 5 in the synaptic maturation and stabilization of the primary visual cortex. The dissertation author was the primary investigator and author of this material.

5.7 References

Allen, N. J. (2013). Role of glia in developmental synapse formation. In *Current Opinion in Neurobiology* (Vol. 23, Issue 6, pp. 1027–1033). https://doi.org/10.1016/j.conb.2013.06.004

Arellano, J. I., Benavides-Piccione, R., DeFelipe, J., & Yuste, R. (2007). Ultrastructure of Dendritic Spines: Correlation Between Synaptic and Spine Morphologies. *Frontiers in Neuroscience*, *1*(1), 131. https://doi.org/10.3389/NEURO.01.1.1.010.2007

Blanco-Suarez, E., Liu, T.-F., Kopelevich, A., & Allen, N. J. (2018). Astrocyte-Secreted Chordin-like 1 Drives Synapse Maturation and Limits Plasticity by Increasing Synaptic GluA2 AMPA Receptors. *Neuron*, *100*(5), 1116-1132.e13. https://doi.org/10.1016/J.NEURON.2018.09.043

Bochner, D. N., Sapp, R. W., Adelson, J. D., Zhang, S., Lee, H., Djurisic, M., Syken, J., Dan, Y., & Shatz, C. J. (2014). Blocking PirB up-regulates spines and functional synapses to unlock visual cortical plasticity and facilitate recovery from amblyopia. *Science Translational Medicine*, *6*(258), 258ra140. https://doi.org/10.1126/scitranslmed.3010157

Brill, J., & Huguenard, J. R. (2008). Sequential Changes in AMPA Receptor Targeting in the Developing Neocortical Excitatory Circuit. *Journal of Neuroscience*, *28*(51). http://www.jneurosci.org/content/28/51/13918.long

Condomitti, G., Wierda, K. D., Schroeder, A., Rubio, S. E., Vennekens, K. M., Orlandi, C., Martemyanov, K. A., Gounko, N. v., Savas, J. N., & Wit, J. de. (2018). An input-specific orphan receptor GPR158-HSPG interaction organizes hippocampal mossy fiber-CA3 synapses. *Neuron*, *100*(1), 201. https://doi.org/10.1016/J.NEURON.2018.08.038

Dufour, A., Rollenhagen, A., Sätzler, K., & Lübke, J. H. R. (2016). Development of Synaptic Boutons in Layer 4 of the Barrel Field of the Rat Somatosensory Cortex: A Quantitative Analysis. *Cerebral Cortex (New York, NY)*, *26*(2), 838. https://doi.org/10.1093/CERCOR/BHV270

Farhy-Tselnicker, I., van Casteren, A. C. M., Lee, A., Chang, V. T., Aricescu, A. R., & Allen, N. J. (2017). Astrocyte-Secreted Glypican 4 Regulates Release of Neuronal Pentraxin 1 from Axons to Induce Functional Synapse Formation. *Neuron*, *96*(2), 428-445.e13. https://doi.org/10.1016/j.neuron.2017.09.053

Grillo, F. W., Song, S., Teles-Grilo Ruivo, L. M., Huang, L., Gao, G., Knott, G. W., MacO, B., Ferretti, V., Thompson, D., Little, G. E., & de Paola, V. (2013). Increased axonal bouton dynamics in the aging mouse cortex. *Proceedings of the National Academy of Sciences of the United States of America*, *110*(16). https://doi.org/10.1073/PNAS.1218731110

Grubman, A., Chew, G., Ouyang, J. F., Sun, G., Choo, X. Y., McLean, C., Simmons, R. K., Buckberry, S., Vargas-Landin, D. B., Poppe, D., Pflueger, J., Lister, R., Rackham, O. J. L., Petretto, E., & Polo, J. M. (2019). A single-cell atlas of entorhinal cortex from individuals

with Alzheimer's disease reveals cell-type-specific gene expression regulation. *Nature Neuroscience 2019 22:12*, *22*(12), 2087–2097. https://doi.org/10.1038/s41593-019-0539-4

Gu, Y., & Cang, J. (2016). Binocular matching of thalamocortical and intracortical circuits in the mouse visual cortex. *ELife*, *5*(DECEMBER2016). https://doi.org/10.7554/ELIFE.22032

Harris, K. M., & Stevens, J. K. (1989). Dendritic spines of CA 1 pyramidal cells in the rat hippocampus: serial electron microscopy with reference to their biophysical characteristics. *Journal of Neuroscience*, *9*(8), 2982–2997. https://doi.org/10.1523/JNEUROSCI.09-08-02982.1989

Irie, F., Badie-Mahdavi, H., & Yamaguchi, Y. (2012). Autism-like socio-communicative deficits and stereotypies in mice lacking heparan sulfate. *Proceedings of the National Academy of Sciences of the United States of America*, *109*(13), 5052. https://doi.org/10.1073/PNAS.1117881109

Jones, E. v., Bernardinelli, Y., Tse, Y. C., Chierzi, S., Wong, T. P., & Murai, K. K. (2011). Astrocytes Control Glutamate Receptor Levels at Developing Synapses through SPARC–β-Integrin Interactions. *The Journal of Neuroscience*, *31*(11), 4154. https://doi.org/10.1523/JNEUROSCI.4757-10.2011

Kamimura, K., & Maeda, N. (2021). Glypicans and Heparan Sulfate in Synaptic Development, Neural Plasticity, and Neurological Disorders. *Frontiers in Neural Circuits*, *0*, 2. https://doi.org/10.3389/FNCIR.2021.595596

Kawano, H., Katsurabayashi, S., Kakazu, Y., Yamashita, Y., Kubo, N., Kubo, M., Okuda, H., Takasaki, K., Kubota, K., Mishima, K., Fujiwara, M., Harata, N. C., & Iwasaki, K. (2012). Long-Term Culture of Astrocytes Attenuates the Readily Releasable Pool of Synaptic Vesicles. *PLOS ONE*, *7*(10), e48034. https://doi.org/10.1371/JOURNAL.PONE.0048034

Knott, G. W., Holtmaat, A., Wilbrecht, L., Welker, E., & Svoboda, K. (2006). Spine growth precedes synapse formation in the adult neocortex in vivo. *Nature Neuroscience 2006 9:9*, *9*(9), 1117–1124. https://doi.org/10.1038/nn1747

Lau, S.-F., Cao, H., Fu, A. K. Y., & Ip, N. Y. (2020). Single-nucleus transcriptome analysis reveals dysregulation of angiogenic endothelial cells and neuroprotective glia in Alzheimer's disease. *Proceedings of the National Academy of Sciences of the United States of America*, *117*(41), 25800. https://doi.org/10.1073/PNAS.2008762117

Pchitskaya, E., & Bezprozvanny, I. (2020). Dendritic Spines Shape Analysis—Classification or Clusterization? Perspective. *Frontiers in Synaptic Neuroscience*, *0*, 31. https://doi.org/10.3389/FNSYN.2020.00031

Siddiqui, T. J., Tari, P. K., Connor, S. A., Zhang, P., Dobie, F. A., She, K., Kawabe, H., Wang, Y. T., Brose, N., & Craig, A. M. (2013). An LRRTM4-HSPG Complex Mediates Excitatory Synapse Development on Dentate Gyrus Granule Cells. *Neuron*, *79*(4), 680–695. https://doi.org/10.1016/J.NEURON.2013.06.029

Wang, B.-S., Sarnaik, R., & Cang, J. (2010). Critical Period Plasticity Matches Binocular Orientation Preference in the Visual Cortex. *Neuron*, *65*(2), 246. https://doi.org/10.1016/J.NEURON.2010.01.002

Wesseling, J. F. (2019). Considerations for Measuring Activity-Dependence of Recruitment of Synaptic Vesicles to the Readily Releasable Pool. *Frontiers in Synaptic Neuroscience*, *0*, 32. https://doi.org/10.3389/FNSYN.2019.00032

Wit, J. de, O'Sullivan, M. L., Savas, J. N., Condomitti, G., Caccese, M. C., Vennekens, K. M., Yates, J. R., III, & Ghosh, A. (2013). Unbiased Discovery of Glypican as a Novel Receptor for LRRTM4 in Regulating Excitatory Synapse Development. *Neuron*, *79*(4), 696. https://doi.org/10.1016/J.NEURON.2013.06.049

Yu, K., Lin, C.-C. J., Hatcher, A., Lozzi, B., Kong, K., Huang-Hobbs, E., Cheng, Y.-T., Beechar, V. B., Zhu, W., Zhang, Y., Chen, F., Mills, G. B., Mohila, C. A., Creighton, C. J., Noebels, J. L., Scott, K. L., & Deneen, B. (2020). PIK3CA variants selectively initiate brain hyperactivity during gliomagenesis. *Nature 2020 578:7793*, *578*(7793), 166–171. https://doi.org/10.1038/s41586-020-1952-2